R-13-11

Quality control of GPS deformation data from Forsmark and analysis of crustal deformation in the local scale

Lennart Ekman, Mats Ekman
LE Geokonsult AB

March 2013

Svensk Kärnbränslehantering AB
Swedish Nuclear Fuel
and Waste Management Co

Box 250, SE-101 24 Stockholm
Phone +46 8 459 84 00

ISSN 1402-3091
SKB R-13-11
ID 1392463

Quality control of GPS deformation data from Forsmark and analysis of crustal deformation in the local scale

Lennart Ekman, Mats Ekman
LE Geokonsult AB

March 2013

Abstract

A network comprising seven GPS stations was established at Forsmark, Sweden, within about 10 km radius from the centre of the investigation area for a final repository for spent nuclear fuel with the purpose of monitoring slow rock motion. During the period November 2005 to December 2009, GPS data were collected in eighteen intermittent measurement campaigns, each with a duration of between three and seven days.

As shown in Gustafson and Ljungberg (2010), the data expose a considerable scatter, indicating a non-linear variability of the GPS baseline velocities. However, the commission narrated in Gustafson and Ljungberg (2010) was restricted to account only for the field performance of the GPS measurement campaign and to present the resulting measurement data per se, merely supplemented with a linear regression solution for the baseline motions.

The preliminary interpretation of GPS data in Gustafson and Ljungberg (2010) was in the present report followed by a closer examination where the non-linear variability is modelled as sinusoidal. Evidence for sinusoidal variations were also found in resulting data from GPS measurements at the Äspö/Laxemar area at Oskarshamn (Sjöberg et al. 2004), as well as in GPS data from several sites in western, middle and north-eastern Finland (Ollikainen et al. 2004, Ahola et al. 2008, Poutanen et al. 2010).

We here postulate that the baseline velocities are characterized by a long-term linear drift superposed by a non-linear sinusoidal motion. This was modelled in two steps. Initially an Auto Regressive (AR) model was applied and the linear trends between the GPS stations were estimated. In a second step, an Auto Regressive Moving Average (ARMA) model was estimated for (almost) all baselines. The residuals between the original data and the one-step predictor for the ARMA model were then used to estimate new linear trends for the baselines.

Our analysis of the Forsmark GPS data indicates relative motions more than 10 times slower than those presented in Gustafson and Ljungberg (2010), which is in line with findings in Finland (Satakunta, Olkiluoto, Kivetty, Romuvaara) as well as with many of the baselines in the measurements at Oskarshamn (Äspö/Laxemar).

We recommend that the GPS measurements proceed for a number of years, preferably as continuous measurements rather than intermittent campaigns. The advantages with continuous measurements are that they enable identification of slow as well as rapid periodical changes, and also counteract the aliasing effect.

Sammanfattning

Ett nätverk bestående av sju GPS-stationer etablerades i Forsmark inom en radie av ca 10 km från centrum av undersökningsområdet för lokalisering av ett slutförvar för använt kärnbränsle med syftet att monitera långsamma berggrundsrörelser. Under perioden november 2005 till och med december 2009 insamlades GPS-data inom ramen för 18 intermittenta mätkampanjer, var och en pågående under tre till sju dagar.

Som framgår av Gustafson och Ljungberg (2010) uppvisar data en betydande spridning, vilket indikerar en icke-linjär variabilitet hos baslinjernas rörelser. Det uppdrag som redovisas i Gustafson och Ljungberg (2010) var emellertid begränsat till en beskrivning av mätutförandet i fält och till att presentera resulterande data utan annan tolkning än tillämpning av linjär regression.

Den preliminära tolkningen i Gustafson och Ljungberg (2010) följdes senare upp med en fördjupad dataanalys vars resultat presenteras i föreliggande rapport. Den icke-linjära variabilitet som identifierades i Gustafson och Ljungberg (2010) har här modellerats som sinusformad. Liknande variationsmönster kännetecknar även GPS-data från Äspö-/Laxemarområdet i Oskarshamns kommun (Sjöberg et al. 2004) liksom data från områden i västra, mellersta och nord-östra Finland där GPS-mätningar utförts (Ollikainen et al. 2004, Ahola et al. 2008, Poutanen et al. 2010).

Den studie som presenteras i denna rapport indikerar att baslinjerörelserna karaktäriseras av en linjär långtidstrend, som emellertid överlagras av en icke-linjär, sinusformad variabilitet. Den sinusformade variabiliteten modellerades i två steg. För det första tillämpades en AR (*Auto Regressive)*-modell på de flesta av baslinjerna. I anslutning till modelleringen uppskattades de linjära trenderna mellan basstationerna. I steg två applicerades en ARMA (*Auto Regressive Moving Average)*-modell, gemensam för (nästan) alla baslinjer. Residualerna mellan ursprungsdata och en-stegsprediktorn för ARMA-modellen användes därefter för att estimera nya linjära trender för respektive baslinje.

Efter modelleringen och efterföljande förnyade skattningar av linjära trender indikerar resultaten berggrundsrörelser som är mer än 10 gånger långsammare än de resultat som presenteras i Gustafson and Ljungberg (2010). Dessa resultat ligger i linje med vad som uppnåtts i de finska GPS-mätningarna (Satakunta, Olkiluoto, Kivetty, Romuvaara), liksom med många av baslinjerna i Oskarshamnsmätningarna (Äspö/Laxemar).

Vi rekommenderar att GPS-mätningarna fortsätter under ytterligare ett antal år. I stället för som hittills i intermittenta mätkampanjer bör dock mätningarna utföras kontinuerligt. Fördelarna med kontinuerliga mätningar är att de möjliggör identifiering av såväl långsamma som snabba periodiska förändringar, samt att de dessutom motverkar aliasing-effekten.

Contents

1 Introduction

1.1 Site investigations at Forsmark

Geological and ecological site investigations were performed by the Swedish Nuclear Fuel and Waste Management Company (SKB) at Forsmark, northern Uppland, Sweden, during the period 2002–2007 with the purpose to localize and characterize a site for construction and operation of a final repository for spent nuclear fuel. The Forsmark site with surroundings is displayed in Figure 1-1, which also presents the boundaries of the candidate area for the repository, as well as the borders defined for the regional and local model areas considered when processing data from the site investigation.

1.2 Monitoring within the Forsmark site investigation area

Besides a large number of investigations of once-for-all character during the site investigation period, a variety of measuring equipment was installed within the investigation area in order to enable long-term observations, in this report referred to as "monitoring", of a selection of geoscientific and ecological parameters. The extent and application of the monitoring programme performed at the Forsmark site is presented in SKB (2007). The long-term observations are continuing also after completed site investigations, however with some up-dates and modifications in relation to the original programme.

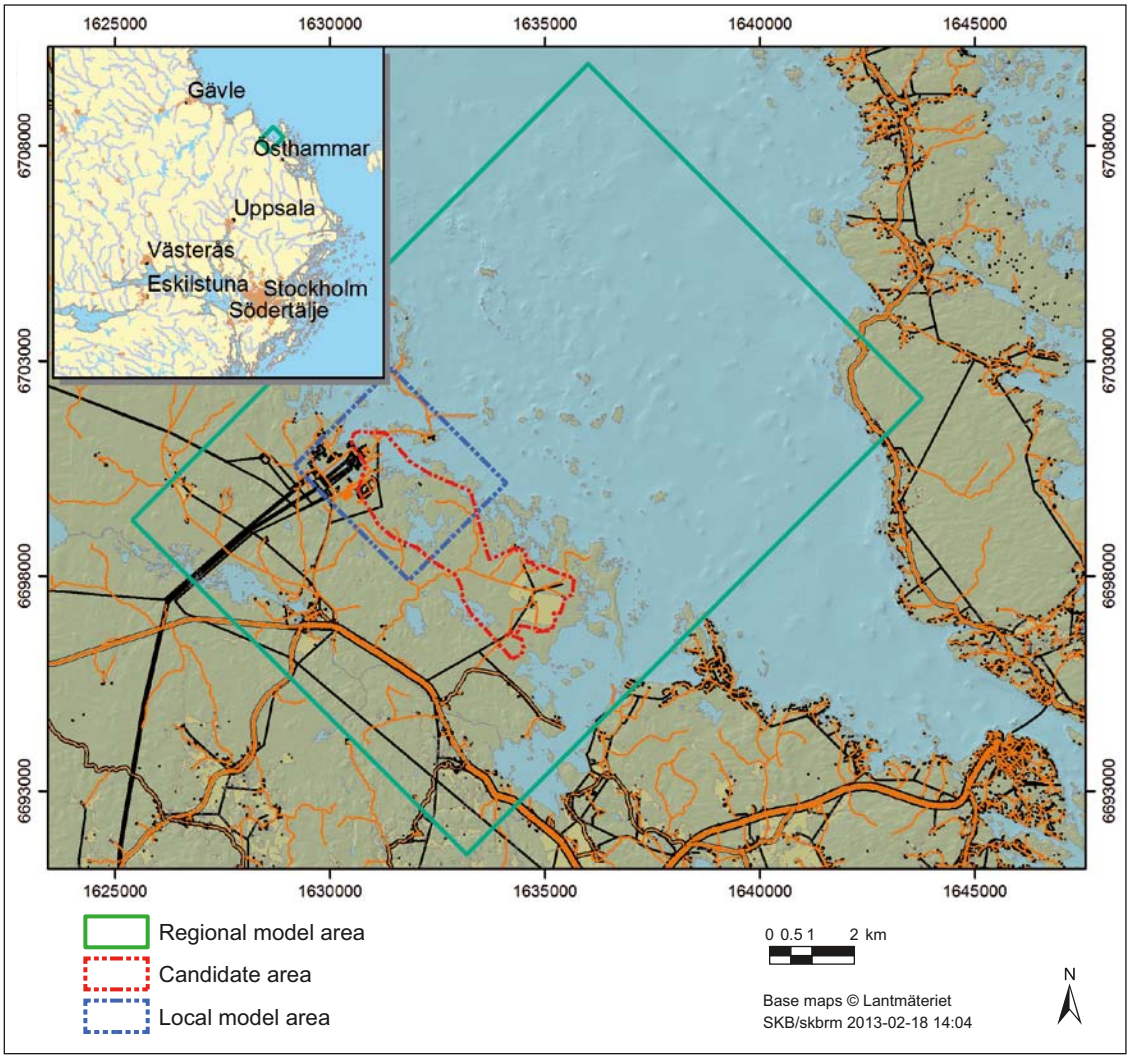

Figure 1-1. *The Forsmark investigation area with environs. The extents of the regional (green) and local (blue) model areas as well as of the candidate area (red) are outlined in the map.*

Many of the monitored parameters are related to the subjects of meteorology, hydrology, hydrogeology, hydrochemistry and ecology, but also instrumentation aimed for monitoring of seismic events and crustal deformation was installed. Seismic events have been recorded since 2002 within the frame of the Swedish National Seismic Network (SNSN), which includes a seismic station located within the Forsmark investigation area and operative since 2004. Another monitoring activity has been registration of horizontal and vertical bedrock motions by GNSS (*Global Navigation Satellite System)* technique. The specific system employed was the GPS (*Global Positioning System)*, which at the measurement period 2005–2009 was the only fully developed and maintained GNSS-system. Today also the GLONASS-system is available, see Chapter 7. Furthermore, the Galileo-system is under development, but not yet (March 2013) fully operational.

The measurements were started in November 2005. During the following years the measurement performance was presented in annual reports (Gustafson and Ljungberg 2007, 2008, 2009). The GPS monitoring continued until December 2009, after which the survey was interrupted for evaluation of the so far collected data. The results of this evaluation was presented in a summary report (Gustafson and Ljungberg 2010), where the measurement performance is accounted for, along with an analysis of the validity of data from the entire four-year period of data collection. Resulting data show a complex variability with time, indicating a need for a deeper data analysis. The specific commission presented in Gustafson and Ljungberg (2010) did, however, not include a comprehensive data analysis, and the data presentation was therefore only supplemented with an interpretation of the long-term baseline motions based on standard linear regression methodology. This solution should be regarded as preliminary.

The results from Forsmark presented in Gustafson and Ljungberg (2010) were later compared to results from corresponding GPS measurements in some other areas of similar geologic-tectonic character, which highlighted issues about data significance and reliability of the Forsmark results. This motivated the here presented assessment of the Forsmark GPS measurements in terms of data quality, analysis and conclusions.

Raw data from the GPS monitoring at Forsmark, resulting data for the long-term bedrock motions from Gustafson and Ljungberg (2010), as well as new bedrock motion data ensuing the analysis and modelling of the GPS data presented in this report are stored in SKB's database Sicada.

1.3 Report structure

In Chapter 2 the background for the decision to include GPS monitoring in the monitoring activities is explained along with a description of the design of the GPS monitoring system at Forsmark. GPS monitoring in areas outside Forsmark are also briefly commented on in this chapter.

The objectives for deepening the data analysis with the results in Gustafson and Ljungberg (2010) as a starting point are presented in Chapter 3, whereas a brief summary of the performance and results of the GPS monitoring 2005–2009 at Forsmark presented in Gustafson and Ljungberg (2010) is given in Chapter 4.

Methods applied for the new quality check of the Forsmark GPS data, as well as of the analysis of crustal deformation within the Forsmark investigation area, are provided in Chapter 5. Performance and results of these exercises are exposed in Chapter 6, in which also questions about data quality and reliability of the results are brought up to discussion.

Finally, in Chapter 7 a brief outline is given of the new results obtained, together with a comparison with the results presented in Gustafson and Ljungberg (2010). In this last chapter, also a summing-up is made of the most important conclusions of the analyses performed in the current report. Based on that, some recommendations are given, aiming at improving results of future GNSS campaigns.

The report also includes six appendices, primarily with diagrams illustrating results of the different analyses, but also with a table and some comments on the data analysed. Each appendix is presented in the text below.

2 Background for and design of the GPS monitoring system at Forsmark and comparison with GPS monitoring at other sites

2.1 Crustal deformation and GPS monitoring

The Eurasian shield is subject to strains emanating from tectonic crustal shortening and glacioisostatic recovery after the retreat of, mainly, the Weichselian continental ice sheet. Ever since the bedrock was first segmented by large-scaled orogenies and rifting events, strains have been increasingly localized to deformation zones. Such deformation zones occur at all scales, ranging in size from hundreds of km to mesoscale fractures, and constitute boundaries of less deformed rock blocks.

The imposed strain is dissipated along the zones as either seismic events, i.e. earthquakes, as aseismic slip along zones in which the stick-slip mechanism is less pronounced or, to a lesser extent, as plastic deformation of the blocks.

For nuclear waste disposal, it is of outmost importance to understand, characterize and, if possible, quantify the amount of strain and in particular the strain rate, that is the velocity with which the rock is deformed. This enables a long-term estimation of the stresses necessary to generate earthquakes and earthquake recurrence times.

As mentioned in Section 1.2, GPS measurements were performed at Forsmark during a period of four years within the frame of a comprehensive programme for monitoring geoscientific parameters. GNSS technique, where GPS is one of a couple of presently existing systems, may for several reasons ideally offer an excellent and accurate tool for crustal deformation studies. For example, distances between data sampling stations are not limited to the local scale, there is no need for inter-station visibility, and accuracies are normally superior to those of traditional methods (Poutanen et al. 2010). Nevertheless, the GPS technique is bothered with some limitations in accuracy due to observation errors. Some of the GPS errors are random, others are more systematic. Much of the efforts during analysis and evaluation of GPS measurements is therefore aiming at avoiding pitfalls that these errors may be the cause of.

The main purpose of the GPS campaign at Forsmark was to measure relative movement of larger rock blocks to, thereby, indirectly estimate the long-term slip of their boundaries, in other words the deformation zones. However, intraplate strain rates are very low and, therefore, very difficult to measure. Intraplate strain rate estimates range between roughly 10^{-12} per year (Andersson 1986, Muir-Wood 1995) and $1.5 \cdot 10^{-9}$ per year (Slunga 1991, Sandiford et al. 2004, Scherneck et al. 2010). However, Slunga (1991) argues that most of the strain energy is continuously released aseismically, meaning that only a fraction of the tectonic strain would be effective for accumulating energy and restoring stresses. This implies that the strain rate effective for local stress regeneration is much lower than the large-scale strain rate across the Fennoscandian Shield.

2.2 Design of the GPS monitoring system at Forsmark

As described above, GPS monitoring is a method for accurate measuring of bedrock motions appearing as extremely tardy dislocations of major blocks in relation to adjacent blocks. By positioning a GPS network such that individual sampling stations straddle major deformation zones, the crustal deformation along these can ideally be recorded with sufficient precision. However, the vertical accuracy is degraded by the fact that observing satellites are above, never below the horizon. This results in a known geometrical dilution of the accuracy for any specific satellite constellation (Harte and Levitan 2009). Averaged over all orbits (which is done by considering a period of 24 hours), the error is approximately a factor 1.5 larger in the vertical direction than in the horizontal plane near the equator. The horizontal directions at the latitude of Forsmark are also degraded due to satellite orbital inclinations of 55 degrees for all modern GPS satellites. Every other error source in practice affects all directions the same, since multipath and antenna phase center effects are eliminated in the post-processing. As a result, the accuracy is best in Easting, lower in Northing (although some satellites can be tracked over the pole), while the vertical is the least accurate.

A network of seven GPS sampling stations were established at Forsmark, on three rock blocks, explicitly on different sides of the three major deformation zones that intersect the Forsmark region in a northwest-southeast direction, namely Singö DZ, Eckarfjärden DZ and Forsmark DZ, see Figure 2-1, and GPS monitoring was initiated, performed as intermittent measurement campaigns with a duration of 3–7 days per campaign. A close-up of one of the data sampling stations is shown in Figure 2-2.

2.3 GPS monitoring at other sites

Deformation measurements by applying GPS technique have been made at several other sites, within as well as outside Sweden. After that the results of the GPS measurements at Forsmark had been presented, the indicated crustal motions were compared to the results from corresponding GPS surveys performed during the period 2000–2004 within SKB's site investigation area at Äspö/Laxemar in the municipality of Oskarshamn, Sweden (Sjöberg et al. 2004), and with GPS measurements carried out by Posiva at Olkiluoto, Kivetty and Rumovaara, Finland, reported in several annual reports, e.g. Ollikainen et al. (2004) and Ahola et al. (2008), as well as within a larger area in the Satakunta region, Finland (Poutanen et al. 2010). The comparison of the results is of a special interest due to the fact that these sites are situated relatively close to each other (in a global perspective), within similar geologic-tectonic environments.

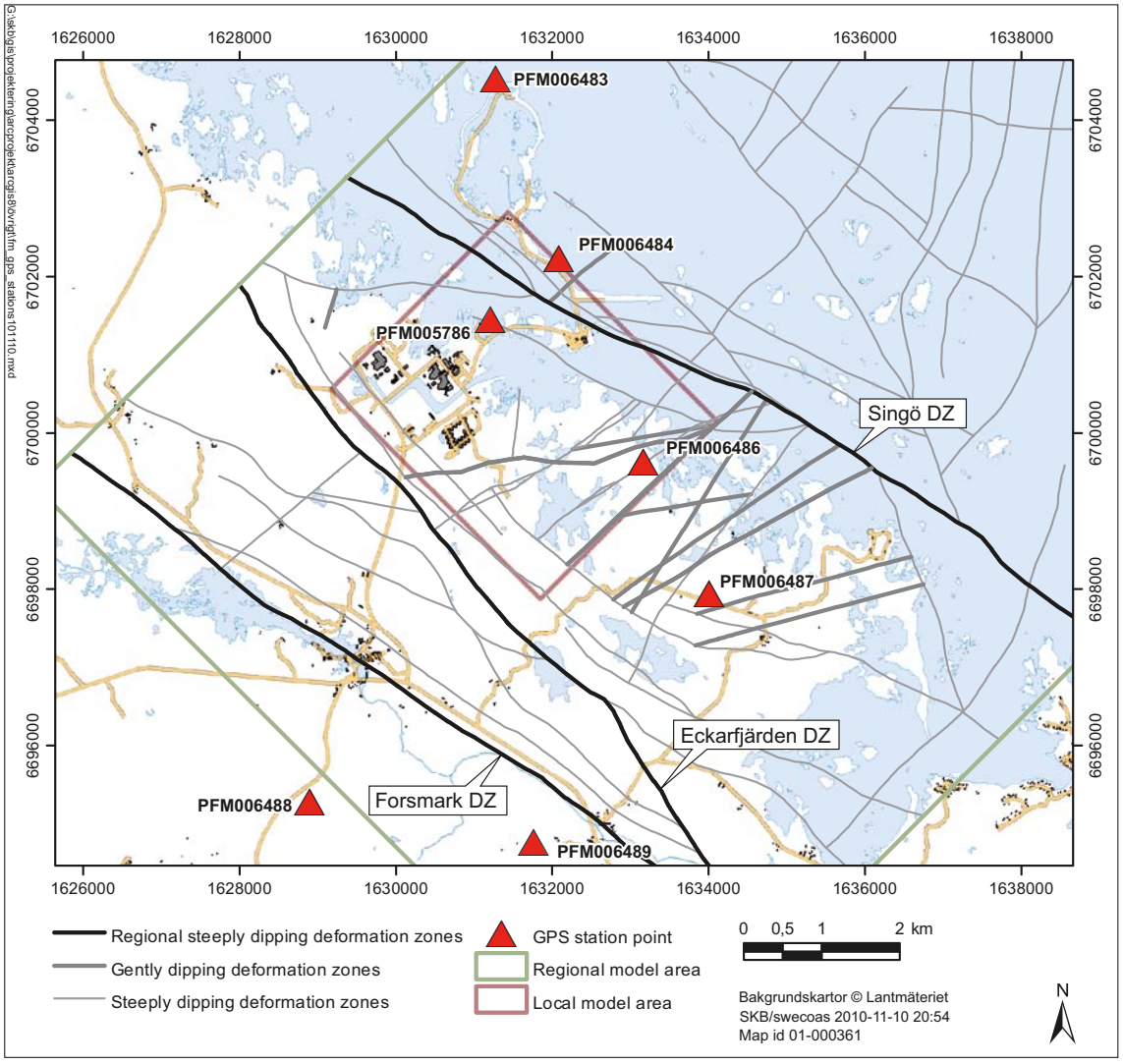

Figure 2-1. *General overview of the Forsmark site investigation area with the seven GPS sampling stations. From Gustafson and Ljungberg (2010, Figure 1-1).*

Figure 2-2. *Sampling station at Forsmark with a choke ring antenna and GPS receiver mounted to the lower left. All stations are attached to a short steel rod anchored to the rock for good mechanical and thermal stability. From Gustafson and Ljungberg (2010, Figure 3-1).*

The GPS surveys compared have in all cases been performed as intermittent campaigns. However, the execution of the measurements has not been identical regarding number of sampling stations, distance between GPS stations (in this report referred to as baseline lengths) or concerning number and duration of measurement periods. Also the data analysis has varied slightly between the different campaigns. Due to these and other differences in prerequisites, the degree of reliability of the results of the GPS monitoring may possibly differ between the sites. Table 2-1 presents some basic facts about the design of the measurement nets and of the periods of performance at the different sites.

Table 2-1. Measurement design and periods of performance of GPS-measurements at Forsmark, Äspö/Laxemar, Olkiluoto, Kivetty, Rumovaara and Satakunta.

Site	Number of sampling stations	Baseline lengths (range) [km]	Measurement period	Number of measurement campaigns	Duration of measurement campaigns [days]
Forsmark	7	1.2–9.8	2005–2009	18	3–7
Äspö/Laxemar	10	0.6–5.7	2000–2004	11	3–5
Olkiluoto	10	0.5–3.6	1995–2008	24	2–3
Kivetty	7	0.7–2.8	1996–2007	16	1
Romuvaara	7	0.5–1.9	1996–2007	16	1
Satakunta	15	5.2–42.8	2003–2008	18	2–5

2.4 GPS results from Forsmark in relation to results from other sites

The results presented in Gustafson and Ljungberg (2010) indicate bedrock motion rates within the Forsmark GPS network in the range of 0.3–2.5 mm/year, expressed as distance changes per year between the seven GPS stations (baseline length changes). This is in the same order of magnitude as observed for some of the baselines in the GPS network at Äspö/Laxemar (Sjöberg et al. 2004). However, the observed and statistically significant deformation rates at Olkiluoto, Kivetty and Rumovaara, as well as in the Satakunta area, are about one order of magnitude lower than those at Forsmark (Ollikainen et al. 2004, Ahola et al. 2008, Poutanen et al. 2010). It should however be noted that for a majority of the sampling stations the deformation rates derived from the Satakunta GPS measurements are assessed as statistically non-significant, mainly due to too short time series (Poutanen et al. 2010).

As observed, the GPS measurements at Forsmark and Äspö/Laxemar indicate essentially larger deformation rates than those at Olkiluoto, Kivetty, Rumovaara and Satakunta sites. Furthermore, the Forsmark results are characterized by pronounced variances. With that as a background, it was judged as of interest to scrutinize the collected GPS data from Forsmark in order to, hopefully, better assess to which degree these data can be trusted and to reduce uncertainties in the results. It is worth pointing out that the analyses of the Forsmark GPS data presented in this report are of strictly mathematical/statistical character. Technical or physical causes to possible systematic measurement errors or possible physical explanations to the observed oscillatory behaviour of the measurement data have not been explored. However, some possible sources of error referred to in the literature are briefly discussed in Chapter 3.

3 Objectives

As emphasized in Section 2.4, the results of the GPS measurements at Forsmark presented in Gustafson and Ljungberg (2010) indicate deformation rates which, especially in comparison with GPS results from Olkiluoto, Kivetty, Rumovaara and Satakunta, Finland, may be regarded as unexpectedly large. The Forsmark results also demonstrate a pronounced data variability. With this background in mind, together with the known error sources involved in GPS-measurements and the delicate post-processing procedures imposed, it was assessed as motivated to perform a renewed quality control of the GPS results from Forsmark and a strict mathematical/statistical evaluation of resulting data in order to further test the statistical significance.

However, not only the GPS measurements at Forsmark, but also those at Äspö/Laxemar and the GPS measurements in Finland mentioned above, indicate a sinusoidal variability, which so far is not unambiguously explained. This variability, the magnitude of which differs somewhat between the different sites, could possibly be due to some modelling shortcomings in the GPS solutions, and in that case not represent true changes of the baseline lengths.

Another possibility, suggested by Ollikainen et al. (2004), is that at least small variations may be explained by time-dependent, more or less cyclic meteorological and hydrological changes like variations in air pressure, snow cover, soil moisture and ocean water level. These factors may be regarded as a loading – unloading effect with a permanent but varying influence on the earth's crust. Also cyclic gravitational forces caused by the moon, the sun and some other planets, primarily Venus and Jupiter, exert an influence on the earth, and clear effects of these forces are observed as for example small variations (tidal effects) in groundwater levels in many boreholes at Forsmark, see e.g. Gokall-Norman and Ludvigson (2007). If the impact of these fluctuating stresses on the earth's crust at Forsmark is detectable by GPS technique is, however, a question not yet thoroughly answered.

Based on this, the working hypothesis in this report is that the baseline velocities are characterized by a long-term linear drift, however superposed by a non-linear sinusoidal motion of an origin not fully understood. This is a major challenge in the data analysis, which complicates the estimation of the long-term linear motions, especially if there is a shortage of data (see below). The main strategy in this report is to model both the linear and the non-linear behaviour of the baseline velocities. In order to overcome data shortages, the non-linear model is utilized to reduce the variance of the long-term linear trend estimates, thereby increasing reliability of the long-term bedrock motion assessments.

The differences in results of crustal deformation between the sites compared in this report, along with the statement in Poutanen et al. (2010) that repeatability of observations is judged to be essential for a high degree of accuracy, gave at the beginning of this commission rise to the hypothesis that the GPS data series from Forsmark is in fact too short to provide reliable estimates of the linear trends, especially if only standard linear regression is applied. This hypothesis is tested in the report. The result of this test and a general analysis of the data quality have served as the basis for some recommendations regarding future GPS monitoring at Forsmark.

4 A brief summary of GPS-monitoring at Forsmark

4.1 GPS stations

The selection of the GPS sampling sites at Forsmark was based on geological assessments as well as on considerations about sky visibility, nearby natural or man-made reflectors, and on the prospect to attain a firm anchorage of the stations to the bedrock. The seven stations were installed on the selected sites in August 2005 and their positions surveyed (Gustafson and Ljungberg 2010).

4.2 Data sampling and data handling/-processing

Dual frequency (L1 and L2 bands) GPS code- and carrier-phase raw data were collected for quality assurance and deformation evaluations in 18 discrete campaigns, each with the duration 3–7 days, between November 2005 and December 2009. The data collected during each campaign were processed and evaluated for quality and self-consistency by applying the Bernese post-processing software package (AIUB 2012). The Bernese software is developed by the astronomical institute at the University of Bern, Switzerland. The package performs ranging data differencing to minimize or eliminate the dominating ranging errors, which is a standard technique used in all high precision GPS work.

The data analysis also included to relate possibly recorded motions between the GPS stations to the larger scale motion of the surrounding area, using data from existing GPS stations operated by SWEPOS, which is a national network of fixed GPS reference stations operated by Lantmäteriet (the National Land Survey of Sweden).

Raw GPS data (code and carrier phase in the L1-band and carrier phase from the L2-band, along with "housekeeping data" on satellite functions and the GPS receivers) were collected directly by onboard controllers sealed inside the GPS receiver box. The onboard controller stores data at one-second intervals on a 128 MB internal and similarly sealed solid-state flash memory chip rated for "industrial" use.

After retrieval of the GPS receivers, their data were uploaded to a computer and processed for quality control using the Bernese software package, which was applied also for calculation of coordinates for three separate periods of 24 hours and for self-consistency. Precise ephemerides (trajectories of the satellites) were applied to post-process data at the highest accuracy. The precise ephemerides were available approximately two weeks after the measurements.

After post-processing, a network adjustment was made with the ADDNEQ routine in the software package in which the known distances between the stations are used to increase the accuracy. The stations in the network are related to three SWEPOS stations with stable fundaments at Lovö, Uppsala, and Mårtsbo, Gävle, by including them in the network. Coordinate conversions from ECEF system (earth-centered earth-fixed) Cartesian coordinates (geocentric coordinates) to the Swedish grid RT90-RHB70 coordinates were made in two steps: from earth-centered coordinates to WGS 84 in Geotrans V2.2.3 by the US Army Topographic Engineering center (Geospatial Information Division and National Imagery and Mapping Agency Exploitation Tools Division) and from WGS 84 to RT90 2.5 G W and RHB70 in G-trans 3.1, upgraded in 2007 to G-trans 3.6 by the National Land Survey of Sweden. In the present report as well as in Gustafson and Ljungberg (2010) the baseline lengths are calculated as the Euclidian distances in the geocentric coordinate system.

The results were entered into an "EG180 – Point surveying Session" file and delivered to the SKB Sicada database. All raw files and results were also saved both by SKB and Caliterra AB (Gustafson and Ljungberg 2010).

4.3 Results

The low frequency motions of all stations were modelled as linear displacements to estimate the motion of the reference point and therefore the entire system. A network adjustment was made to distribute all deviations from linear motion across the network and across the entire measurement period of more than four years. This function is not included in the Bernese software, and an external

program was therefore written in order to calculate residuals. The network was then adjusted until a minimum was reached in the sum of the squares of all deviations from a linear motion. This resulted in a motion of the reference point (PFM006484) that had been held stationary of dX = 0.7 mm/year, dY = –0.3 mm/year, and dZ = 0.3 mm/year for a total displacement of 0.82 mm/year. The adjustment reduced the sum of the residuals by a little over 2%. Table 4-1 gives the resulting linear velocity components for all points except PFM006485 which was replaced by point PFM005786 after the first few campaigns.

Table 4-2 lists all calculated baseline lengths between successive stations, together with the estimated changes. These changes are also presented in the map in Figure 4-1. Figures A1-1–A1-21 in Appendix 1 are graphical presentations of the baseline changes for all 21 baselines between the seven stations. Also displayed is the linear regression line, the parameters of which are given in Table 4-2. Figures A1-1–A1-21 are the same as Figures 6-2a–6-2u in Gustafson and Ljungberg (2010).

Although the fluctuations are considerable in the plots of the baselines (Figures A1-1–A1-21 in Appendix 1), the interpretation in Gustafson and Ljungberg (2010) is that the general trend indicates a decreasing length of the baselines. This "contraction" is particularly prominent along e.g. PFM006483–PFM006486, PFM006483–PFM006487, and PFM006486–PFM005786 (Figure A1-2, A1-3, and A1-15 in Appendix 1). Furthermore, some of the baselines, e.g. PFM006484–PFM005786 (Figure A1-11 in Appendix 1) and PFM6487–PFM005786 (Figure A1-18 in Appendix 1), indicate a nonlinear variation in length.

Table 4-1. Estimated linear velocity components for the seven GPS stations (sampling stations) at Forsmark. The coordinate axes are in the ECEF system. From Gustafson and Ljungberg (2010, Table 6-1).

GPS station	dX [mm/yr]	dY [mm/yr]	dZ [mm/yr]
PFM006483	1.116	0.576	–0.864
PFM006484	0.684	–0.288	–0.288
PFM006486	–1.080	–0.972	–1.656
PFM006487	0.288	–0.864	1.404
PFM006488	0.504	0.972	0.540
PFM006489	–0.828	–0.072	–0.360
PFM005786	0.576	1.044	2.340

Table 4-2. Baseline lengths and linear regression parameters (R^2=regression sum of squares/ total sum of squares). From Gustafson and Ljungberg (2010, Table 6-2).

From station	To station	Baseline length at first campaign [m]	Baseline change [mm/yr]	R^2
PFM006483	PFM006484	2,429.7806	–1.1	0.250
PFM006483	PFM006486	5,243.2741	–2.3	0.646
PFM006483	PFM006487	7,121.4999	–2.5	0.454
PFM006483	PFM006488	9,539.1960	–2.0	0.289
PFM006483	PFM006489	9,776.4689	–2.1	0.247
PFM006483	PFM005786	3,079.6614	–1.7	0.269
PFM006484	PFM006486	2,815.4548	–1.2	0.347
PFM006484	PFM006487	4,697.3130	–1.4	0.278
PFM006484	PFM006488	7,640.2039	–1.7	0.282
PFM006484	PFM006489	7,478.9470	–1.3	0.173
PFM006484	PFM005786	1,174.9330	–1.9	0.291
PFM006486	PFM006487	1,884.7595	–0.3	0.024
PFM006486	PFM006488	6,084.6024	–1.1	0.193
PFM006486	PFM006489	5,067.7066	–0.3	0.014
PFM006486	PFM005786	2,663.9278	–2.3	0.670
PFM006487	PFM006488	5,755.2821	–1.9	0.322
PFM006487	PFM006489	3,895.9832	–0.6	0.055
PFM006487	PFM005786	4,478.5431	–1.8	0.303
PFM006488	PFM006489	2,909.1961	–1.1	0.402
PFM006488	PFM005786	6,578.1313	–0.3	0.011
PFM006489	PFM005786	6,708.2742	–0.6	0.045

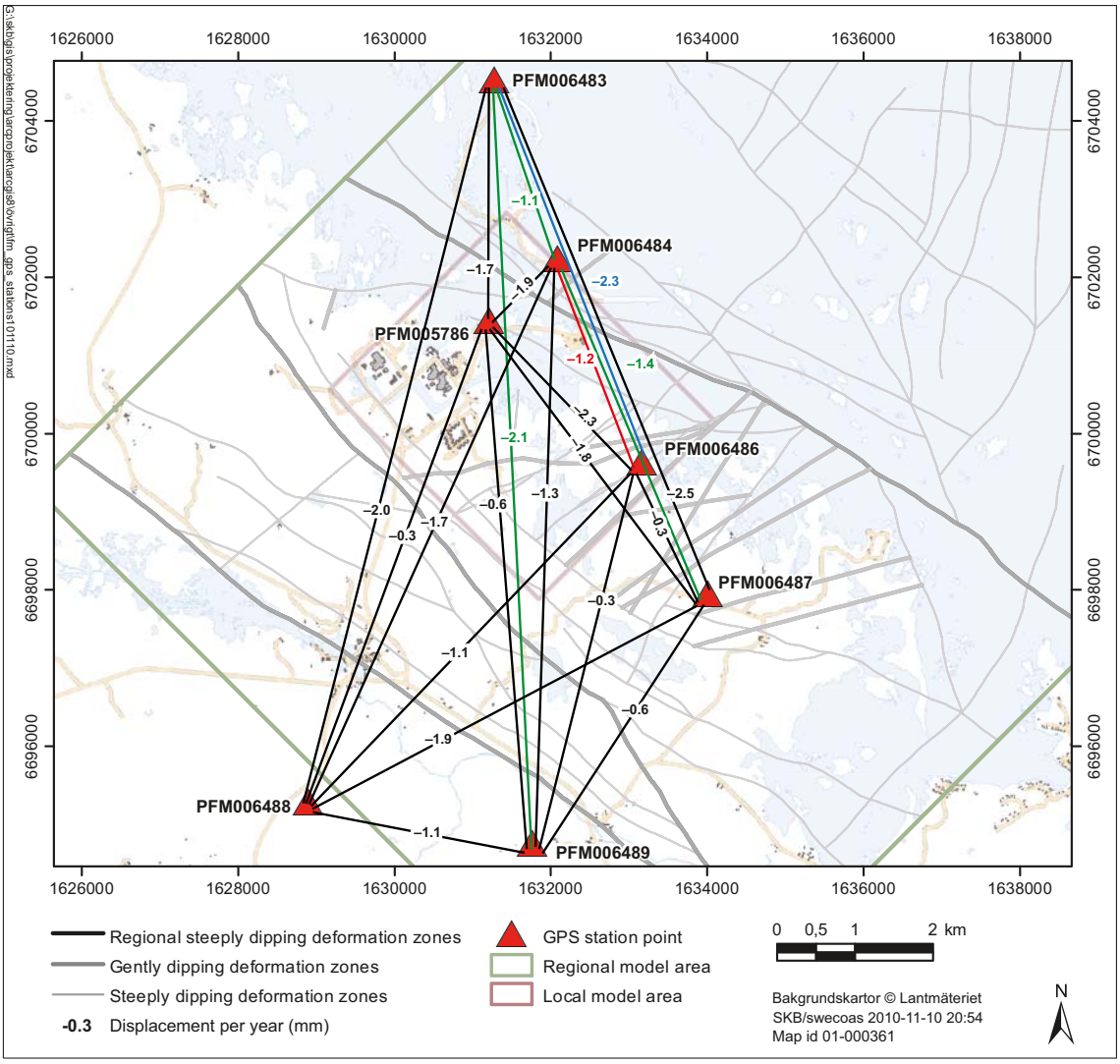

Figure 4-1. *Graphical presentation of the estimated annual changes of the baseline lengths according to Table 4-2. From Gustafson and Ljungberg (2010, Figure 6-1). Green, blue and red colours are used for some baselines in order to help the reader to visualize these lines and separate them from closely situated black baselines.*

5 Methods applied for evaluation of GPS data from the Forsmark site investigation area

This chapter provides a description of the different statistical and mathematical tools utilized for the evaluation of the Forsmark GPS data. In Section 5.1 focus is directed towards the linear regression, or more precisely, the linear curve fitting of the GPS position data from the sampling stations presented in Table 4-1. The linear regression is based on the methods of least squares (LS). However, if prior information about the variances of the different position estimates is available, this information should also be considered in the linear curve fitting. This leads to the method of best linear unbiased estimate (BLUE), which is further explained in this chapter. Moreover, methods for inferences based on the LS estimation as well as correlation analysis, including analysis of variances, are also illustrated (Section 5.2). The last section (Section 5.3) describes a method of modelling the non-linear behaviour of the baseline motions. The method is based on black-box modelling, and the approach can be considered as an attempt to capture the unexplained dynamics remaining after the linear regression. The different methods presented in this chapter are mainly directed towards the specific application in this report, but are sometimes described in more general terms.

5.1 Linear regression

The parametric model for the linear regression can, in the general scalar case, be written as:

$$y(t) = \varphi^T(t)\theta, \tag{5-1}$$

where $y(t)$ is the measurable scalar quantity, $\varphi(t)$ is a vector of known quantity, and θ is the vector of unknown parameters (T = transponate). This expression can further be formulated in a matrix notation if the quantities in (5-1) are written as follows:

$$Y = (y(1)...y(n))^T,\ \Phi = (\varphi^T(1)...\varphi^T(n))^T, \tag{5-2}$$

where n is the number of measurements. The equation in (5-1) can then be written in matrix notation as:

$$Y = \Phi\theta. \tag{5-3}$$

The LS estimate is then obtained by minimizing the function:

$$L(\theta) = \frac{1}{2}(Y - \Phi\theta)^T(Y - \Phi\theta). \tag{5-4}$$

A unique solution to (5-4) is given by

$$\hat{\theta} = (\Phi^T\Phi)^{-1}\Phi Y. \tag{5-5}$$

The estimate in (5-5) is unbiased if the equation error, ε, (or residual)

$$\varepsilon = Y - \Phi\theta \tag{5-6}$$

is white noise. However, if the equation error in (5-6) is correlated and given by:

$$E\varepsilon\varepsilon^T = P, \tag{5-7}$$

then the BLUE is given by:

$$\hat{\theta} = (P^{-1}\Phi(\Phi^T P^{-1}\Phi)^{-1})^T Y. \tag{5-8}$$

The linear curve fitting used in Sections 5.1 and 5.2 is a special case of linear regression, where the parametric model is given by:

$$y(t_i) = a + bt_i + e(t_i). \tag{5-9}$$

The measurable quantity in (5-9) depends on the variable *t*. In this report this variable is time. The variable $e(t_i)$ in (5-9) is the error, corresponding to ε in (5-6), which should be independent normally distributed random variables having zero means, i.e. white noise. The estimates of *a* and *b* in (5-9) are obviously given in (5-5). However, in order to simplify the notation in the next section, another expression of the general solution in (5-5) is introduced, which is based on the so-called normal equations. Defining

$$S_{tt} = \sum_{i=1}^{n} (t_i - \bar{t})^2, \qquad S_{yy} = \sum_{i=1}^{n} (y(t_i) - \bar{y})^2, \qquad S_{ty} = \sum_{i=1}^{n} (t_i - \bar{t})(y(t_i) - \bar{y}), \tag{5-10}$$

the estimates can be written as:

$$\hat{b} = S_{ty} \Big/ S_{tt}, \qquad \hat{a} = \bar{y} - \hat{b}\bar{t}, \tag{5-11}$$

where $\bar{y}$ and $\bar{t}$ are the means of the *t*'s and *y(t)*'s, respectively. It is straightforward to derive a solution corresponding to the BLUE in (5-8), based on the notation in (5-10). Moreover, the inference methods in the next section will make use of the notation in (5-10).

5.2 Statistical analysis and inferences concerning curve fitting

5.2.1 Inferences based on the LS estimation

It is assumed that the variables $e(t_i)$ in (5-9) are independent normally distributed random variables with zero means (white noise) and the common variance σ^2. An estimate of σ^2 is given by:

$$s_e^2 = \frac{S_{yy} - S_{ty}^2 / S_{tt}}{n-2}. \tag{5-12}$$

s_e is often referred to as the standard error of estimates, or sigma. Assuming that the random variables $y(t_i)$ in (5-9) are independent normally distributed with the mean $a+bt_i$ and having the common variance σ^2, the following (1-α) 100% confidence limits for *a* and *b* can be made:

$$a: \quad \hat{a} \pm T_{\alpha/2} \cdot s_e \sqrt{\frac{1}{n} + \frac{\bar{t}^2}{S_{tt}}}, \qquad b: \quad \hat{b} \pm T_{\alpha/2} \cdot s_e \frac{1}{\sqrt{S_{tt}}}, \tag{5-13}$$

where $T_{\alpha/2}$ is the *t*-distribution with n-2 degrees of freedom. Using (5-13) one can, for instance, test the hypotheses about the slope of the regression line. Then, the null hypothesis would be that b=0, and the alternative hypothesis that $b \neq 0$. The confidence limit for $y(t_i)$ for a given value of t_i, is given by:

$$\hat{a} + \hat{b}t_i \pm T_{\alpha/2} \cdot s_e \sqrt{\frac{1}{n} + \frac{(t_i - \bar{t})^2}{S_{tt}}}. \tag{5-14}$$

In connection to (5-14) it is also possible to formulate an expression for the limits of prediction:

$$\hat{a} + \hat{b}t_i \pm T_{\alpha/2} \cdot s_e \sqrt{1 + \frac{1}{n} + \frac{(t_i - \bar{t})^2}{S_{tt}}}. \tag{5-15}$$

Here, t_i is a future observed value.

5.2.2 Correlation analysis

One important question in linear regression is how much of the variations in $y(t_i)$ can be explained by the linear relationship with t_i. The sample correlation coefficient defined as:

$$r = \frac{S_{ty}}{\sqrt{S_{tt} S_{yy}}} \tag{5-16}$$

is a measure that provides an answer to this matter. For instance, if we have the value r = 0.8, then 100 r^2 = 64% of the variations in $y(t_i)$ can be explained by corresponding differences in t_i.

It is also possible to calculate how well the estimated curve fits to a straight line. This is commonly performed by calculating the so-called R^2-value, which is the ratio between the regression sum of squares and the total sum of squares:

$$R^2 = 1 - \frac{\sum_{i=1}^{n} (y(t_i) - \hat{y}(t_i))^2}{\sum (y(t_i) - \bar{y})^2}. \quad (5\text{-}17)$$

The closer this value is to one, the better the estimated curve fits to the straight line. R^2-values were calculated by Gustafson and Ljungberg (2010). These values are presented also in Table 4-2 in this report. Nevertheless, note that one has to be careful when the actual slope of the curve is close to zero, and when the variations in $y(t_i)$ are relatively large (e.g. the random noise in the signal is high). Then the R^2-value can become very small even though the estimate of the slope is correct and consistent. Thus, the R^2-value is often not a suitable quality measure when small linear motions are estimated from signals showing large variations.

Using the sample correlation coefficient in (5-16), it is possible to formulate statistics for inference about the so-called population correlation coefficient, ρ. As for the sample correlation coefficient, also ρ tells us what amount of the variation in $y(t_i)$ can be explained by the linear relationship with t_i. Assuming that r in (5-16) is based on random samples from a bivariate normal population – this means that $y(t_i)$ and t_i are values of a pair of random variables from a joint (bivariate normal) density –, then the null hypothesis, $\rho = 0$, can be tested with the following statistics:

$$Z = \frac{\sqrt{n-3}}{2} \ln \frac{1+r}{1-r}. \quad (5\text{-}18)$$

This is based on Fisher Z transformation, and the statistic tests are performed by looking up proper values in statistical tables for normally distributed functions.

5.2.3 Coordinate transformation of a covariance matrix

The purpose of this sub-section is to explain how a covariance matrix in one coordinate system can be calculated from a covariance matrix in another coordinate system. The transformation is based on a first order Taylor expansion (or linearization). The motivation for this is that later on, in Section 6.1, the BLUE estimates will be performed on distances which can be considered as the range in a polar coordinate system calculated as the Euclidian distance in a Cartesian coordinate system. The available variances are given in a Cartesian coordinate system, and thus need to be converted to the polar-range coordinates. The Euclidian distance (i.e. the range) between two points, $P_0 = (x_0\, y_0,\, z_0)$ and $P = (x, y, z)$, in a Cartesian coordinate system is given by:

$$d = \sqrt{(x - x_0)^2 + (y - y_0)^2 + (z - z_0)^2}. \quad (5\text{-}19)$$

If the covariances for the point (x, y, z) are given by R, then the "linearized" covariance for the distance is given by:

$$R_d = FRF^T, \quad (5\text{-}20)$$

where F is the matrix of partial derivatives:

$$F = \frac{\partial d}{\partial P}. \quad (5\text{-}21)$$

5.3 Black-box modelling

This section describes the parametric models and the model parameter estimation methods used for determination of the nonlinear baseline motions. The model structure used in this investigation is an autoregressive moving average (ARMA) model, which is a standard so-called black-box model, frequently used in signal processing applications. The ARMA model is especially suitable for modelling sinusoidal signals and, thus, this model is commonly used in parametric spectral estimation methods. After estimating the sinusoidal portion of the baseline motion, the linear curve fitting method explained

in Section 5.3 may again be applied to the data. However, in this section a novel method, where the linear trend is simultaneously estimated with the nonlinear behavior, is also investigated.

In the following sub-sections (5.3.1–5.3.5) the model structure and the method to identify the model parameters are described. An explanation of how to investigate the frequency content in the data is also provided.

5.3.1 ARMA and AR model structure

The ARMA model can be described as a polynomial difference equation model where:

$A(q^{-1}) = 1 + a_1 q^{-1} \ldots + a_{na} q^{-na}$ and (5-22)

$C(q^{-1}) = 1 + c_1 q^{-1} \ldots + c_{nc} q^{-nc}$

are the involved polynomials. In (5-22) the argument q^{-1} denotes the backward shift operator, and the parameters to be estimated are:

$\theta = (a_1 \ldots a_{na} \ldots c_1 \ldots c_{nc})$. (5-23)

Let $y(t)$ denote the output signal and $e(t)$ denote a sequence of independent and identically distributed random variables with zero mean (often called white noise). Obviously, both signals are a function of time t. Moreover, the time index t is expressed in units of sampling interval, i.e. $y(t) = y_c(t \cdot T)$, where T is the sampling time interval and $y_c(\cdot)$ is the continuous signal from which the output signal is sampled. The ARMA model structure is now compactly given by:

$A(q^{-1})y(t) = C(q^{-1})e(t)$, (5-24)

which can be written explicitly as the difference equation:

$y(t) + a_1 y(t-1) + \ldots + a_{na} y(t-na) = e(t) + c_1 e(t-1) \ldots + c_{nc} e(t-nc)$. (5-25)

From (5-23) one can see that the number of parameters to be estimated is $na+nc$. If $nc = 0$, an autoregressive (AR) model is obtained, for this case:

$A(q^{-1})y(t) = e(t)$, (5-26)

and the model parameters are:

$\theta = (a_1 \ldots a_{na})$. (5-27)

5.3.2 Parameter estimation

The least square method described in Section 5.2 is in general not applicable to models of the form (5-24), at least if consistent estimates are required. The standard method of estimating the parameters of ARMA models (and many other linear polynomial models) is the so-called prediction error method (PEM). The prediction error is defined as:

$$\varepsilon(t,\theta) = y(t) - \hat{y}(t \mid t-1;\theta) \cdot \quad (5\text{-}28)$$

The idea in PEM is to minimize a criterion (also called loss function) where the prediction error is involved. This loss function can be chosen in many ways. A common choice is:

$$V_N(\theta) = tr \quad \frac{1}{N}\sum_{t=1}^{N} \varepsilon(t,\theta)\varepsilon^T(t,\theta) \ , \quad (5\text{-}29)$$

where N is the number of data points. In general the minimization of (5-29) must be performed numerically, for instance using the Gauss-Newton algorithm. Denoting $\Psi(t, \theta)$ as the gradient of $V_N(\theta)$ we can write the recursive Gauss-Newton algorithm as:

$$\theta_{k+1} = \theta_k + \alpha_k \left[\sum_{t=1}^{N} \Psi(t,\theta_k)\Psi^T(t,\theta_k)\right]^{-1} \left[\sum_{t=1}^{N} \Psi(t,\theta_k)\varepsilon(t,\theta_k)\right], \quad (5\text{-}30)$$

where α_k is a tuning variable step length parameter. For ARMA models the gradient can effectively be computed as:

$$\Psi(t,\theta) = -\left(\bar{y}(t-1) \quad \ldots \quad \bar{y}(t-na) \quad -\bar{\varepsilon}(t-1) \quad \ldots \quad -\bar{\varepsilon}(t-nc)\right)^T, \tag{5-31}$$

where the concerned signals are filtered as:

$$\bar{y}(t) = \frac{1}{C(q^{-1})} y(t) \text{ and } \bar{\varepsilon}(t) = \frac{1}{C(q^{-1})} \varepsilon(t). \tag{5-32}$$

In (5-29)–(5-32) the prediction errors have to be calculated from (5-28). The predictions, $\hat{y}(t \mid t-1;\theta)$ in (5-28), are preferably calculated from the optimal prediction which can be obtained as:

$$C(q^{-1})\hat{y}(t \mid t-1;\theta) = (C(q^{-1}) - A(q^{-1})\ y(t). \tag{5-33}$$

It is straightforward to generalize the calculations in (5-28)–(5-33) for the multivariable case. Then the polynomials in (5-22) are matrix polynomials, having the dimension *(ny|ny)*, where *ny* is the number of output signals. A more detailed description of ARMA-modelling and system identification in general can be found in Söderström and Stoica (1989).

As shown in (5-26) the AR model is obtained if *nc* = 0. This is a pure time series model, where the present output signal is fully described by previous outputs and a white noise term *e(t)*. In contrast to the ARMA model, consistent estimates can be obtained using standard LS methods applied to the AR model. For the scalar case we can write (5-26) as:

$$e(t) = y(t) + \sum_{i=1}^{na} a_i y(t-i) = y(t) + \varphi^T(t)\theta, \tag{5-34}$$

where $\theta = (a_1 \ldots a_{na})^T$. This is a model of the same structure as in (5-1), and standard LS methods can be used to estimate the parameters θ. In (5-34) it is assumed that the white noise term has a variance equal to σ^2. It is, in fact, possible to estimate this variance from (5-34) via the following equation:

$$R_1 (1\ \theta^T)^T = \sigma^2. \tag{5-35}$$

The vector $R_1 = (r(0)\ r(1) \ldots r(na))$ contains covariance elements of the signal obtained from:

$$r(k) = \frac{1}{N} \sum_{t=k+1}^{N} y(t) y(t-k). \tag{5-36}$$

It is also possible to include estimation of drifting disturbances in the model (5-34). Assume that the output signal can be described by the following model:

$$e(t) = y(t) + \varphi^T(t)\theta - b\ . \tag{5-37}$$

Then, the parameter vector and the regression vector can be augmented as $\theta = (\theta\ b)^T$ and $\varphi_b(t) = (-y(t-1) \ldots -y(t-na)\ t)^T$, respectively. For the multivariate case we can write the linear regression parameter model as follows:

$$E(t) = Y(t) + \Psi^T(t)\theta_b, \tag{5-38}$$

where *Y(t)* is an output vector and *E(t)* a vector of independent white noise sequences. Both vectors have the dimension *ny*. Moreover, $\theta_b = (\theta\ b_1 \ldots b_{ny})^T$ and

$$\Psi^T(t) = \begin{pmatrix} -y_1(t-1) & \cdots & -y_1(t-na) & t & 0 & 0 \\ \vdots & & \vdots & 0 & \ddots & 0 \\ -y_{ny}(t-1) & \cdots & -y_{ny}(t-na) & 0 & 0 & t \end{pmatrix}. \tag{5-39}$$

From (5-39), it is straightforward to estimate the parameters θ_b using the linear regression techniques in (5-4)–(5-5).

5.3.3 Spectrum of the output signal

The spectrum is often defined as the mean frequency content of a signal. Dependent on the characteristics of the signal, different methods can be used to estimate the spectrum of it. From signals where a number of, say N observations have been collected, a convenient way of estimating the spectrum is to formulate the so-called periodogram of the signal, defined as:

$$\hat{\Phi}_N(\omega) = \frac{1}{N} |\, Y_N(\omega) \,|^2 , \tag{5-40}$$

where,

$$Y_N(\omega) = \sum_{t=1}^{N} y(t) e^{-i\omega t} . \tag{5-41}$$

The sum in (5-41) is the truncated discrete-time Fourier transform for the signal $y(t)$. If one lets $N \to \infty$ and takes the expectation of (5-40), the definition is often called the power spectral density (PSD). If the PSD is rational, a rational spectral density can be formulated as:

$$\Phi(\omega) = \left| \frac{C(\omega)}{A(\omega)} \right|^2 \sigma^2 , \tag{5-42}$$

where σ is a scalar and $A(\omega)$ and $C(\omega)$ are polynomials of the same form as in (5-22), but where the operator q^{-k} is replaced by $E^{-ik\omega}$. It is known that a rational PSD can be associated with a signal obtained by filtering the signal through a transfer function described by the ARMA model in (5-24). This explains the exhaustive use of ARMA models in signal processing and spectral analysis applications.

5.3.4 Determination of model order

An important issue in black-box modelling is the determination of the model structure. For the AR- and ARMA-modelling used in this report this means that the orders of the polynomials in (5-22), in other words the numbers *na* and *nc*, have to be decided. The choice of model orders is a trade-off between getting a model order large enough to describe the most important dynamics of the system, versus to avoid overparameterization. One way of determining this is to compare models having different polynomial orders. In this report the so-called Akaike information criterion (AIC) is used for determination of the model structure. The AIC is defined as:

$$\min_{d,\theta} (1 + \frac{2d}{N}) \sum_{t=1}^{N} \varepsilon^2(t, \theta) , \tag{5-43}$$

where d is the size of θ and $\varepsilon(\cdot)$ is the prediction error defined in (5-28).

5.3.5 Pre-preparation of the signal

In practical system identification applications it is important to design the experiment properly. Aspects one have to consider include the choice of sampling interval (to avoid the aliasing effect, see Sub-section 6.3.4), pre-filtering the data (e.g. low-pass filtering), and treating non-zero means and drifts in disturbances.

In this report the possibility to pre-prepare the data is limited. The sampling interval is already defined. Moreover, the fact that the sampling interval is not equidistant further complicates the system identification problem. The way to overcome this chosen in the present report is to interpolate the data using linear interpolation. In this way an equidistant sampling interval is obtained and, hence, standard system identification methods can be used. However, one should be aware of the fact that this also introduces an approximation of the signal content in-between the "real" samples.

In black-box modelling it is important to handle non-zero means and drifts in disturbances. However, in this report these factors are important parts of the model parameters. Linear drifts will even be estimated as a part of the model parameters in the AR- modelling. Otherwise the non-zero means, and in the ARMA-modelling also drifts, are "eliminated" by first explicitly estimating those using the standard linear regression methods described above, and then subtracting the output signal with the estimated non-zero means and drifts. Thereafter, the identification method can by used on the new "de-trended" signal.

6 Analysis and evaluation of GPS data from the Forsmark site investigation area

The results from the linear curve fitting and the black-box modelling, along with the results from the various statistical analysis methods described in Section 5.2, are presented in this chapter. All results emerge from the data displayed in Appendix 2, Table A2-1. The data subjected to the new analyses are the output data from the Bernese processing, without network adjustment. The linear curve fitting based on LS is in Section 6.1 compared with the best linear unbiased estimate (BLUE), where prior information about the errors for each GPS position measurement is included in the calculation. Section 6.2 presents the results from the inferences and correlation analysis. Finally, in Section 6.3 the results from the black-box AR- and ARMA-modelling are shown and compared with the standard linear curve fitting.

All through this chapter the outcome of the analyses is compared with the results in Gustafson and Ljungberg (2010). Where possible, the same baseline curves and linear trends as in Gustafson and Ljungberg (2010) are reconstructed from the data in Appendix 2, Table A2-1. Data points in the linear curves that deviate from the figures in Gustafson and Ljungberg (2010) are pointed out and briefly discussed in Appendix 3.

6.1 Comparison of standard LS and BLUE

In this section the standard LS method for linear curve fitting described in Section 5.2, and used in Gustafson and Ljungberg (2010) as well, is compared to the BLUE estimation, also described in Section 5.2.

The covariances in (5-7) involved in the BLUE estimate (5-8) emanate from the formal errors calculated by the Bernese software for all coordinate points. These errors are calculated as the mean value of the Bernese formal errors for the 24 hours sessions in each campaign. It is sometimes argued that Berenese formal errors often underestimate the variance of the coordinate positions of the stations (Poutanen et al. 2010). One way to overcome this is to, instead of using the Bernese formal errors, calculate the standard deviation between the sessions in one campaign. However, since the maximum number of sessions for each station and campaign in the Forsmark GPS survey is not more than three, the statistical significance is very poor. Nevertheless, the BLUE of the linear trends, using the calculated standard deviation between the sessions, is also plotted and compared with the standard LS estimates. The standard deviation is normalized with the number of samples, N. Thus, this produces the square root of the second moment of the sample about its mean – often called the root mean square (RMS) errors. The reason for using this, instead of normalizing with N-1, is that the number of samples is very small. In those cases where N=1, the standard deviation was replaced with the Bernese formal errors.

One should note that since the station PFM006484 was kept fixed during the formal error calculations, the variances are zero for this station. This implies that the baseline variances between this fixed station and other stations are smaller than between non-fixed stations. As in Gustafson and Ljungberg (2010) the Euclidian distance in the geocentric coordinate system was calculated.

In order to obtain the variances for the baselines between all stations, a standard covariance transformation described in (5-19)–(5-21) was performed, but where variances from the two involved geocentric points are taken into account.

Figures A4-1–A4-42 in Appendix 4 show the baseline variations between the different stations. Figures A4-1–A4-21 display the squared variances of the baselines based on the Bernese formal errors, as described above, whereas Figures A4-22–A4-42 in the same appendix expose the variances based on the RMS. Figures A4-22–A4-42 correspond to the Figures 6-2a–6-2u in Gustafson and Ljungberg (2010), which are also shown in the present report as Figures A1-1–A1-21 in Appendix 1.

6.2 Inference and Correlation analysis

The slopes of the estimated linear trends for the LS and BLUE estimates in connection to the figures in Appendix 4 mentioned in the previous section are demonstrated in Table 6-1. Those are expressed as changes in millimetres per year. Also the slope parameter, *b*, is provided in the table. Moreover, for the standard LS estimates a more extensive analysis of the curves is performed where the R^2-value, as defined in (5-17), together with the standard error estimate expressed in mm given by expression (5-12), are also calculated and illustrated. For the standard LS estimates the 95% confidence limit for the linear trends, defined by (5-14), are shown in the table (column 5) as well.

The results of a correlation analysis, together with computation of the limits of prediction for each station pair, is shown in Table 6-2. This analysis is based on the statistics for the Fisher Z-transformation, given by (5-18). A null hypothesis for the correlation coefficient can be defined – meaning that there is no correlation at all between time and baselines – which can be tested against the alternative non-null hypothesis at the 0.05 level of significance. This gives that the null hypothesis should be rejected if the Z-value in the second column is less than –1.96 or larger than 1.96. It is worth mentioning that for $n \leq 20$ this test should be used with caution.

In the third column in Table 6-2 the amount of the variations in the baselines that can be explained by the relationship with time is presented. The value is based on the sample correlation coefficient in (5-16), and is expressed in percent of the variations that are explained. Hence, a small value indicates that differences in the baseline are not attributed to differences in time.

Finally, in the last column in Table 6-2 the limits of prediction, defined in (5-15), are illustrated. However, only the confidence limit is shown. The actual value is easily calculated as $\hat{a} + \hat{b}t_i$, where t_i is the future time. In the table the future time is chosen as one year (365 days) from the last measurement campaign. By studying (5-15) it is obvious that not only the size of the sigma values is affecting the limits of prediction but also the number of data, *n*. The larger the *n*, the smaller the limits of prediction. Thus, the reason for the large values in Table 6-2 is a combination of larges sigmas and few data points. Therefore, with the current data set it is very cumbersome to forecast the motion of the baselines one year ahead.

Table 6-1. Linear regression parameters for Standard LS and BLUE. The BLUE parameters are shown for both the Bernese and the RMS errors between the sessions.

Statistical analysis of LS					Resulting slopes of BLUE			
Baseline PFM00-	R^2 (LS)	Sigma [mm] (LS)	b (LS)	Change [mm/yr] (LS)	b (BLUE-Berne)	Change [mm/yr] (BLUE-Berne)	b (BLUE-RMS)	Change [mm/yr] (BLUE-RMS)
6483 to 6484	0.458	2.055	$-3.75E^{-6}$	–1.37±0.812	$-3.64E^{-6}$	–1.33	$-3.28E^{-6}$	–1.20
6483 to 6486	0.083	2.666	$-6.58E^{-6}$	–2.40±1.106	$-6.12E^{-6}$	–2.23	$-6.18E^{-6}$	–2.25
6483 to 6487	0.422	3.934	$-6.68E^{-6}$	–2.44±1.570	$-6.67E^{-6}$	–2.43	$-5.24E^{-6}$	–1.91
6483 to 6488	0.263	4.514	$-5.18E^{-6}$	–1.89±1.898	$-5.79E^{-6}$	–2.11	$-7.17E^{-6}$	–2.62
6483 to 6489	0.308	5.441	$-7.10E^{-6}$	–2.59±2.323	$-7.66E^{-6}$	–2.79	$-7.78E^{-6}$	–2.84
6483 to 5786	0.372	3.040	$-5.36E^{-6}$	–1.96±1.689	$-4.66E^{-6}$	–1.70	$-6.94E^{-6}$	–2.53
6484 to 6486	0.371	2.516	$-3.63E^{-6}$	–1.33±0.99	$-3.35E^{-6}$	–1.22	$-3.95E^{-6}$	–1.44
6484 to 6487	0.256	3.213	$-3.71E^{-6}$	–1.36±1.226	$-3.73E^{-6}$	–1.36	$-2.50E^{-6}$	–0.91
6484 to 6488	0.281	4.609	$-5.52E^{-6}$	–2.02±1.849	$-5.27E^{-6}$	–1.92	$-6.83E^{-6}$	–2.49
6484 to 6489	0.262	4.744	$-5.29E^{-6}$	–2.01±1.932	$-5.12E^{-6}$	–1.87	$-6.25E^{-6}$	–2.28
6484 to 5786	0.076	6.155	$-4.08E^{-6}$	–1.49±3.271	$-3.41E^{-6}$	–1.24	$-6.35E^{-6}$	–2.32
6486 to 6487	$2.0E^{-4}$	2.738	$-7.16E^{-8}$	–0.03±1.077	$-2.87E^{-7}$	–0.10	$1.26E^{-6}$	0.46
6486 to 6488	0.200	3.980	$-3.72E^{-6}$	–1.36±1.629	$-3.54E^{-6}$	–1.29	$-2.27E^{-6}$	–0.83
6486 to 6489	0.103	3.780	$-2.45E^{-6}$	–0.89±1.571	$-2.64E^{-6}$	–0.96	$-5.28E^{-6}$	–1.93
6486 to 5786	0.706	2.030	$-6.69E^{-6}$	–2.44±1.109	$-6.42E^{-6}$	–2.34	$-5.95E^{-6}$	–2.17
6487 to 6488	0.328	4.329	$-5.80E^{-6}$	–2.12±1.737	$-5.01E^{-6}$	–1.83	$-6.02E^{-6}$	–2.20
6487 to 6489	0.198	3.771	$-3.65E^{-6}$	–1.33±1.536	$-2.78E^{-6}$	–1.02	$-4.67E^{-6}$	–1.71
6487 to 5786	0.134	4.110	$-3.74E^{-6}$	–1.36±2.185	$-4.50E^{-6}$	–1.64	$-4.49E^{-6}$	–1.64
6488 to 6489	0.443	2.075	$-3.63E^{-6}$	–1.32±0.890	$-3.59E^{-6}$	–1.31	$-3.28E^{-6}$	–1.20
6488 to 5786	0.415	6.000	$-2.77E^{-6}$	–1.01±3.222	$-3.53E^{-6}$	–1.29	$-3.79E^{-6}$	–1.38
6489 to 5786	0.177	4.550	$-4.68E^{-6}$	–1.71±2.44	$-5.44E^{-6}$	–1.98	$-6.44E^{-6}$	–2.35

Table 6-2. Correlation analysis and limits of prediction for the standard LS estimates.

Baseline PFM00	Statistics for Fisher Z-transformation (Null hypothesis 95% Conf: ±1.96)	Explained variations [%]	Limits of prediction [mm]
6483 to 6484	–3.08	45.8	±5.2
6483 to 6486	–3.73	62.8	±7.0
6483 to 6487	–2.90	42.2	±10.0
6483 to 6488	–1.96	26.3	±11.8
6483 to 6489	–2.17	30.8	±14.2
6483 to 5786	–2.24	37.2	±8.4
6484 to 6484	–2.55	37.1	±6.4
6484 to 6487	–2.15	25.6	±8.0
6484 to 6488	–2.13	28.1	±11.7
6484 to 6489	–2.03	26.2	±12.1
6484 to 5786	–0.94	7.6	±16.4
6486 to 6487	–0.05	0.02	±7.0
6486 to 6488	–1.66	20.0	±10.3
6486 to 6489	–1.16	10.4	±9.8
6486 to 5786	–3.67	70.6	±5.6
6487 to 6488	–2.35	32.8	±11.0
6487 to 6489	–1.73	19.8	±9.6
6487 to 5786	–1.27	13.4	±11.0
6488 to 6489	–2.78	44.3	±5.3
6488 to 5786	–0.65	4.1	±16.2
6489 to 5786	–1.42	17.7	±12.3

6.2.1 Comments on comparison of LS and BLUE and statistical analysis of LS

Comparison of the BLUE estimation with the standard LS estimation in Table 6-1 reveals that the difference in baseline motion between the two methods is in most cases rather small. The results for the linear trends are overall in line with the results for the baseline changes shown in Figures (6-2a)–(6-2u) in Gustafson and Ljungberg (2010). All estimated linear trends have a negative slope – thus, there is an overall contractive deformation – except for the BLUE estimation based on RMS between the stations PFM006486 and PFM006487, which demonstrates a positive slope.

The conclusion is that adding variances to the LS estimates is not drastically changing the linear trends compared to the standard LS. However, there is a strong argument that the statistical significance of especially the standard deviations (or RMS-values) is very low, since the number of data, i.e. the duration of each measurement campaign is far too short in order to obtain consistent estimates. However, the formal errors calculated by the Bernese program might have a better statistical relevancy, because those errors are based on a larger number of data. On the other hand, it is known that the formal errors from the Bernese program sometimes underestimate the true errors, see e.g. Poutanen et al. (2010).

The statistical analysis of the linear trends, presented in Tables 6-1 and 6-2, shows that several long-term motions between stations have no significant linear trend at all. That is, statistically, within a 95% significance level, it cannot be stated whether the long-term motion is contracting or expanding. Hence, the baseline variations shown in these curves are either just random noise or due to some un-modelled non-linear motions. Thus, several of the estimated linear trends can be rejected based on *t*-distribution hypothesis tests, see further Equation (5-13). The rejected baseline curves are shown in Table 6-3. This can be compared with Table 6-1 where the rejected baselines also show that the 95% confidence limit for the linear trends exceeds the estimated change in mm/yr. Also the R^2-values and the sigma values are exposed in Table 6-3. The R^2-values are all very small (extremely small for the baseline motions between stations PFM006486 and PFM006487), whereas the sigma values are relatively large, especially for the baseline motions between the stations PFM006486 and PFM006487. However, the R^2-value might in this case not be a reliable quality measure of the linear motion estimates, since the estimated slopes of the curves are very small, and the variations in the baseline motions are relatively large.

The estimated Fisher Z-transformation values are illustrated in Table 6-3. The Fisher Z-transformation hypothesis test shows the same result as the *t*-distribution hypothesis test. This supports the proposition that the baselines in Table 6-3 should be rejected. It is worth noticing that almost all baseline displacements where station PFM005786 is involved are rejected. The Fisher Z-test and the fact that data for the first four measurement campaigns are missing for this station, indicates that the data from station PFM005786 should not be trusted. Also note that the baseline between stations PFM006486 and PFM006487 shows small values for the Fisher Z-transformation as well as for the R^2.

Table 6-3. Rejected baselines.

Rejected Baseline PFM00-	R^2	Sigma [mm]	Fisher Z-transformation
6483 to 6488	0.263	4.514	–1.96
6484 to 5786	0.076	6.155	–0.94
6486 to 6487	$2.0E^{-4}$	2.738	–0.05
6486 to 6488	0.200	3.980	–1.66
6486 to 6489	0.103	3.780	–1.16
6487 to 6489	0.198	3.771	–1.73
6487 to 5786	0.134	4.110	–1.27
6488 to 5786	0.415	6.000	–0.65
6489 to 5786	0.177	4.550	–1.42

6.3 AR- and ARMA-modelling

In order to obtain unbiased estimates using LS methods, the residuals should ideally be white noise. However, the baseline plots in figures A4-1–A4-42 in Appendix 4 indicate that there exist some non-linear motions in the baseline variations. This renders that these variations cannot be satisfactorily modelled as linear trends. Hence, the unexplained variations not captured by the linear regression should also be modelled. Comparison of the variations for the respective baselines also exposes some common features of the oscillatory pattern for each baseline. This becomes obvious by plotting all baselines in the same figure. Figure 6-1 displays the baselines for almost all stations. Station PFM005786 is however excluded due to missing data during the first four measurement campaigns, and, hence, likewise all baselines starting/ending at that station are discarded. Also the baseline between stations PFM006486–PFM006487 is left out from the plot, depending on poor statistical data quality, which indicates that there is no, or a very limited, evidence for a linear trend for this baseline.

Computing the periodogram, using the expression in (5-40), confirms that there exist some periodical baseline motions. As an example, Figure 6-2 shows the periodogram for the baseline variations between stations PFM006488 and PFM006489, whereas Figure 6-3 demonstrates the mean periodogram for all stations plotted in Figure 6-1. The curve in Figure 6-2 shows a major peak at approximately $7.0E^{-4}$ cycles/day, and two smaller peaks at approximately $2.1E^{-3}$ and $5E^{-3}$ cycles/day, respectively. In terms of number of cycles per year, this corresponds approximately to 0.3, 0.8 and 1.8 cycles/year. One interesting observation is that this is roughly in line with the main periods estimated in the periodograms in Ahola et al. (2008). However, the periodograms in Ahola et al. (2008) were based on a larger number of data points, whereas the periodogram in Figure 6-3 is founded on the mean baseline points from each measurement campaign. By studying Figure 6-3 it is obvious that there are some common oscillations, (mean periods), at the approximate frequencies $7.0E^{-4}$ and $2.9E^{-3}$ cycles/day, and perhaps also at $5.0E^{-3}$ and $6.4E^{-3}$cycles/day (0.3, 1.1, 1.8 and 2.3 cycles per year, respectively). It should however be pointed out that the combination of few data and the aliasing effect makes the frequency estimation rather uncertain and may even introduce false frequencies, cf. Sub-section 6.3.3.

The periodogram in Figure 6-3 indicates that the dynamics of the baseline variations could be imaged by a sinusoidal model. In this section the parametric models AR and ARMA will be used to capture the sinusoidal motions of the baselines; we further refer to Stoica and Moses (1997) for a comprehensive explanation of why AR and ARMA are suitable for modelling sinusoidal behaviour.

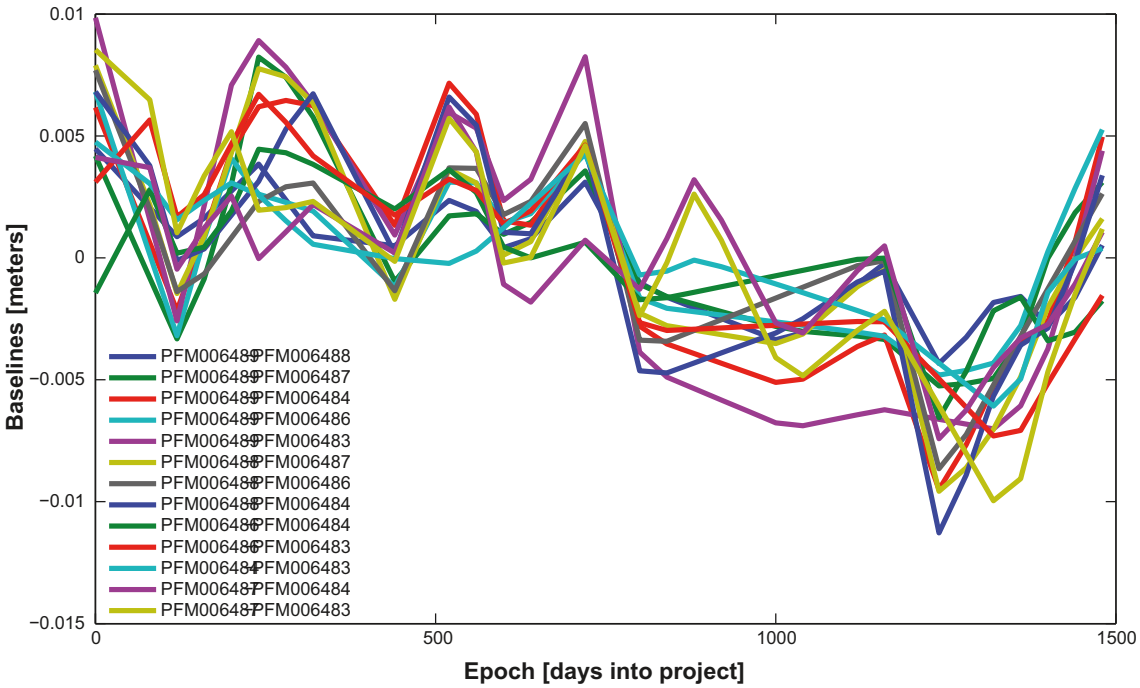

Figure 6-1. *Baseline variations between the different stations. Station PFM005786 and the baseline between the stations PFM006486 and PFM006487 are excluded.*

It should be emphasized that the LS methods explored in the previous section will in theory give a consistent estimate of the linear trend, even if it is assumed that the measurements are originating from an AR or ARMA process. However, a consistent estimate also requires that the amount of measurement data is large enough. A main hypothesis in this report is that the number of data points is in fact too small in order to provide reliable estimates of the linear trends. One heuristic approach to decrease the variance of the estimates when there is a shortage of measurements data is to model possible underlying signal processes. Then, the linear trends can be estimated simultaneously, or in a course of action where the signal process model is estimated first and then, in a second step, the linear trends are estimated using standard LS. Both approaches are explored in this section.

When estimating the model parameters in the AR and ARMA models, it is assumed that the time distances are the same between the different measurements. Thus, the baseline data need to be interpolated in order to obtain baseline measurements equidistant in time. This interpolation will also have some effect on the outcome in the model parameter estimation. In this report 40 days are used as equidistant interpolating points, where standard linear interpolation is utilized. Figure 6-4 shows one example of the interpolation, where the baseline between the stations PFM006488 and PFM006489 is illustrated.

In the parametric model estimation in this section some baselines have been excluded: the baselines for station PFM005786 as well as the baseline between stations PFM006486 and PFM006487. As mentioned above, the reason for excluding station PFM005786 is missing data for the four first measurement campaigns. Hence, the first 244 days of the time series cannot be appropriately interpolated. The baseline between stations PFM006486 and PFM006487 is expelled due to poor statistical quality.

6.3.1 AR-modelling

The Akaike Information Criterion (AIC), defined in (5-43), is used for determination of the model order for the $A(q^{-1})$ polynomial in (5-22). Observe that the order for the b-parameters in (5-38) is 14. The result, which can be seen in Figure 6-5, indicates that a suitable choice for n_a in (5-39) is 4. In Figure 6-6 the optimal one-step prediction in (5-33) for the baseline variations between stations PFM006488 and PFM006489 is plotted for a third-, fourth- and sixth-order $A(q^{-1})$ polynomial (it is worth mentioning that the estimated linear trend is also included in the calculation of the prediction). This is compared to the true data in the same figure. It can be noticed that there is no significant difference in the prediction for the three compared models.

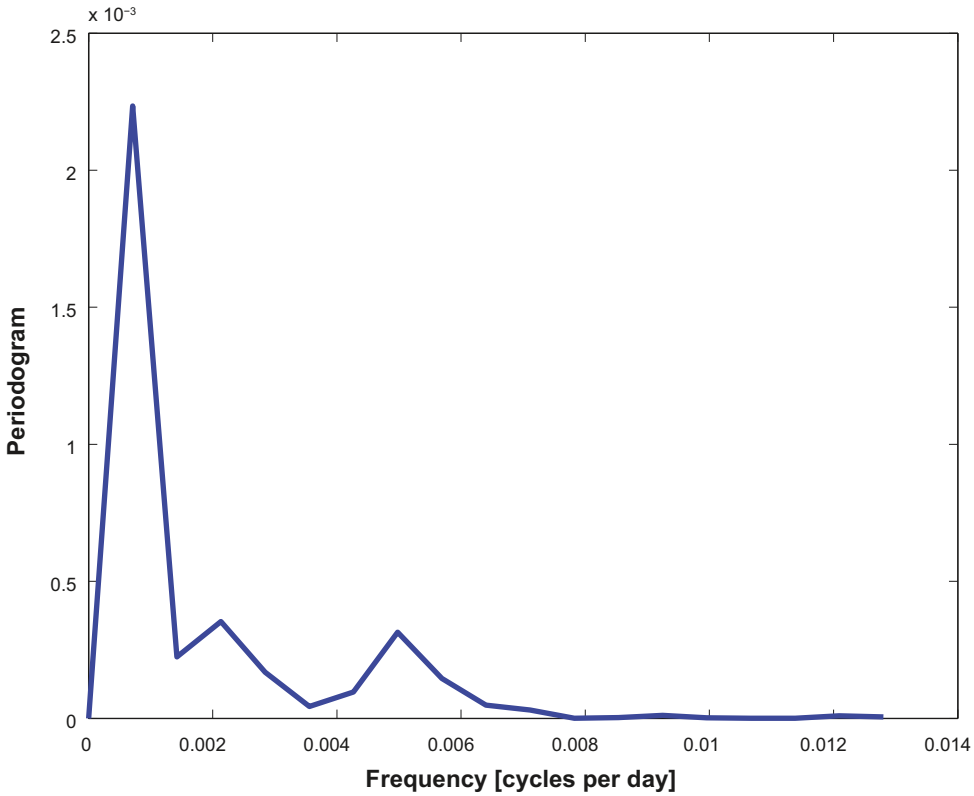

Figure 6-2. *Periodogram for the baseline variations between the stations PFM006488 and PFM006489.*

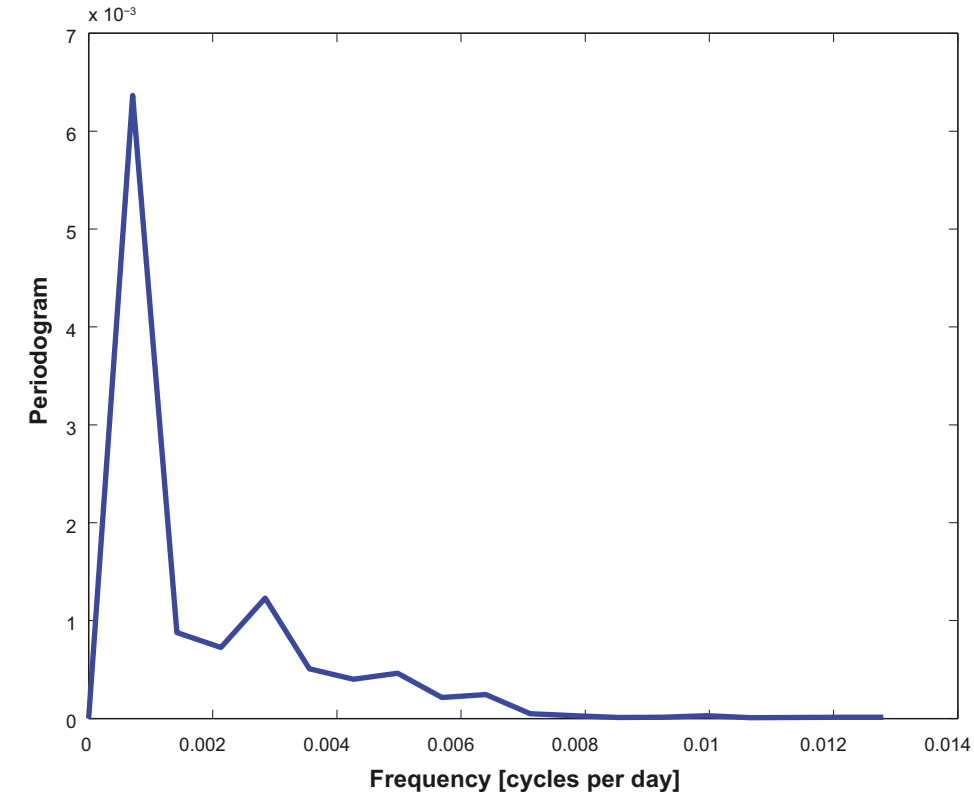

Figure 6-3. *Mean periodogram for all baselines shown in Figure 6-1.*

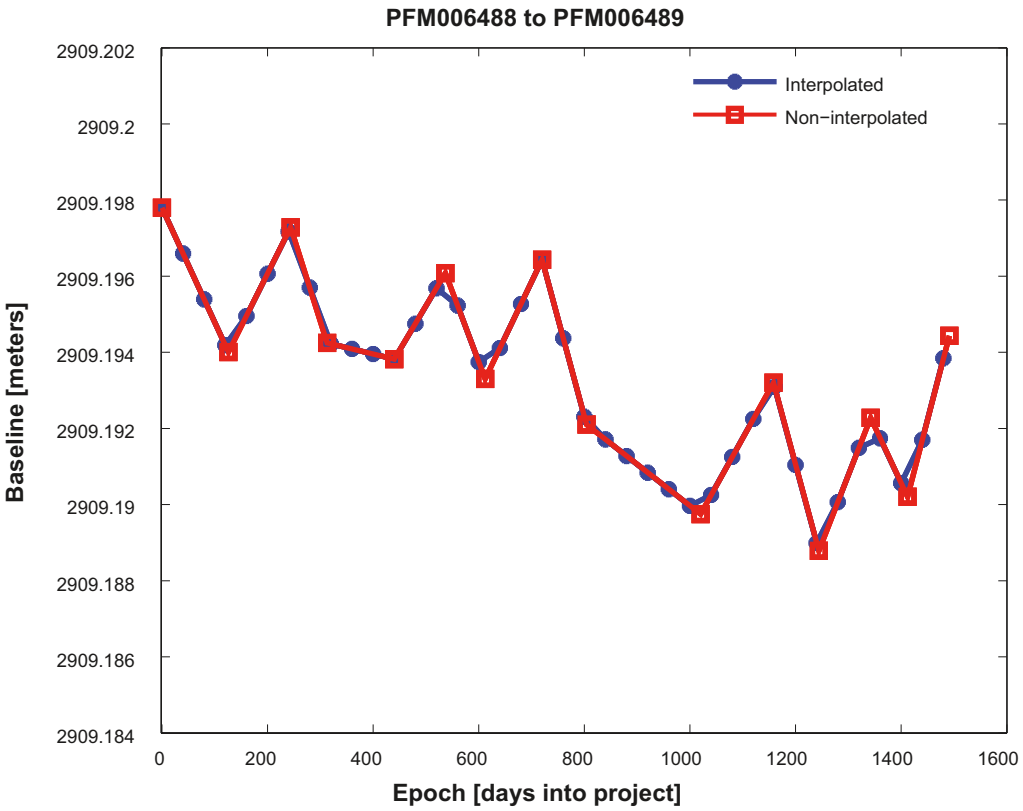

Figure 6-4. *Example of interpolated baseline variations compared with the original baseline variations for the stations PFM006488 and PFM006489.*

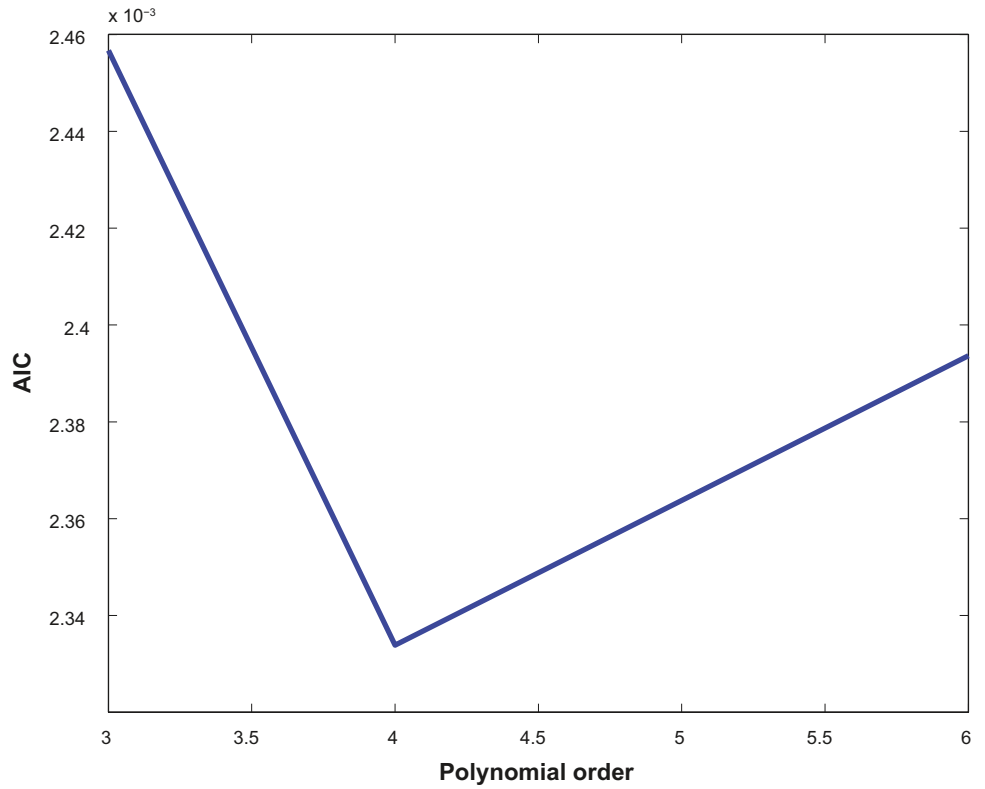

Figure 6-5. *AIC for the AR model.*

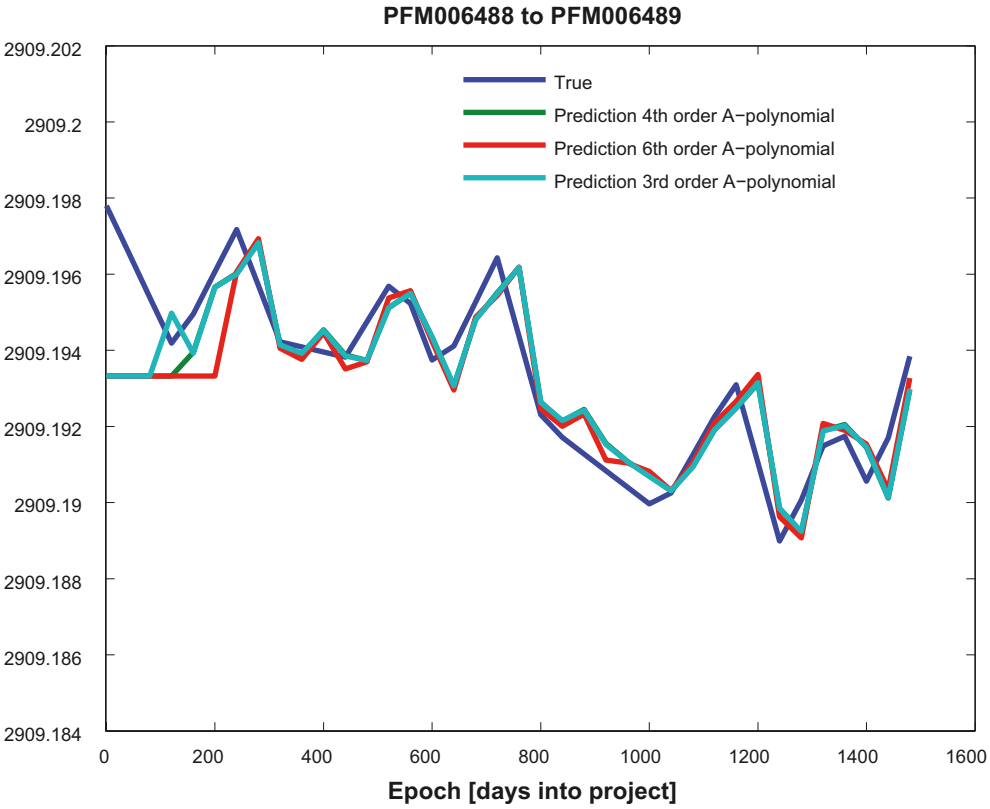

Figure 6-6. *Example of AR predictions for the baseline variations using different A(q-1) polynomial orders. This is compared with the origin baseline variations for the stations PFM006488–PFM006489.*

The forth-order $A(q^{-1})$ polynomial is used in this report for modelling the common oscillatory motions. The $A(q^{-1})$ polynomial together with the long-term linear trends are estimated around the mean of each baseline, see further equations (5-34)–(5-39). Figures A5-1–A5-14 in Appendix 5 illustrate the results from the AR-modelling using a fourth-order $A(q^{-1})$ polynomial. The model parameters are shown in Table 6-4. The performance of the one-step prediction is compared with the true data. The results in the figures indicate that the model is able to capture most of the dynamics in the data. Note that the same polynomial parameters are used in all figures. It is only the linear trends that are estimated uniquely for each baseline. The results of the long-term linear trends for the baselines are presented in Table 6-5.

Figure 6-7 shows the power spectral density (PSD) for the fourth-order AR-model. The PSD is defined in Equation (5-42). Comparing this figure with the mean periodogram illustrated in Figure 6-3 reveals that the main frequency pattern is captured by the fourth-order AR-model. In the figure the spectral density is ad-hoc scaled with a sigma value of $3.0E^{-3}$.

Table 6-4. Values of the AR model.

$A(q^{-1})$	Value
a_1	–1.4093
a_2	0.9730
a_3	–0.3877
a_4	–0.0182

Table 6-5. Linear trend parameters for the AR-modelling.

Baseline PFM00-	Sigma Residuals [mm]	b	Change [mm/yr]
6483 to 6484	0.7	$-1.48E^{-7}$	–0.05
6483 to 6486	1.2	$-3.17E^{-7}$	–0.12
6483 to 6487	1.5	$-2.36E^{-7}$	–0.09
6483 to 6488	1.9	$-1.22E^{-7}$	–0.04
6483 to 6489	4.5	$-1.35E^{-7}$	–0.05
6484 to 6486	1.0	$-1.84E^{-7}$	–0.07
6484 to 6487	1.4	$-1.00E^{-7}$	–0.04
6484 to 6488	1.7	$-9.63E^{-8}$	–0.03
6484 to 6489	1.7	$-4.01E^{-8}$	–0.01
6486 to 6488	1.4	$-5.13E^{-8}$	–0.02
6486 to 6489	1.3	$-7.84E^{-8}$	–0.03
6487 to 6488	1.7	$-1.64E^{-7}$	–0.06
6487 to 6489	1.5	$-2.35E^{-8}$	–0.01
6488 to 6489	0.8	$-1.12E^{-7}$	–0.04

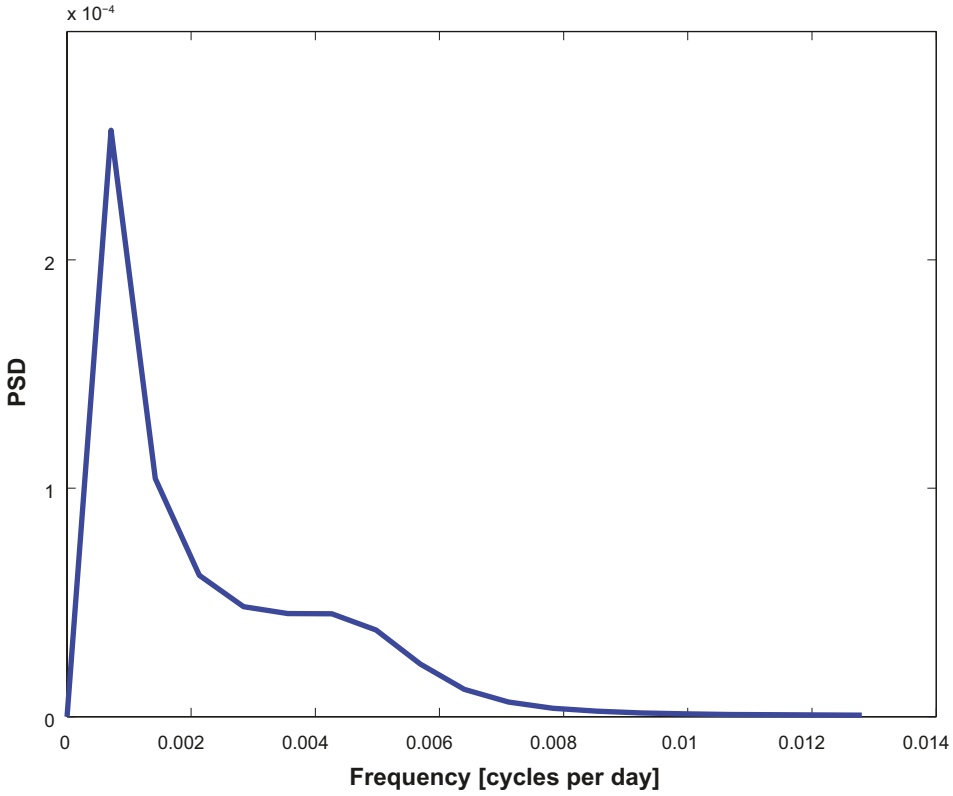

Figure 6-7. *The spectral density for the fourth-order AR model.*

6.3.2 ARMA-modelling

The ARMA model used in this section is a fourth-order $A(q^{-1})$ polynomial and a second-order $C(q^{-1})$ polynomial. The model parameters are shown in Table 6-6. The spectral density is illustrated in Figure 6-8. This figure should be compared with Figures 6-3 and 6-7. The figures indicate that the ARMA model estimates the frequency content of the mean signal slightly better than the AR model.

Table 6-6. Values of the ARMA model.

$A(q^{-1})$ and $C(q^{-1})$	Value
a_1	–1.7144
a_2	1.4182
a_3	–0.8220
a_4	0.1569
c_1	–0.0373
c_2	0.0962

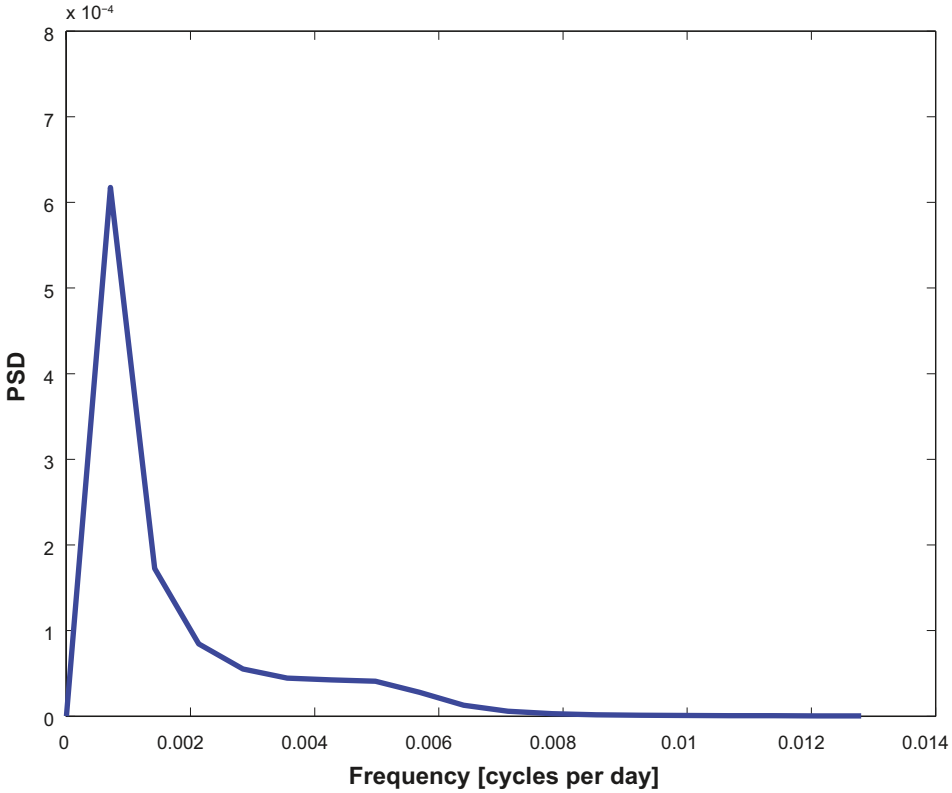

Figure 6-8. *The spectral density for the fourth-order ARMA model.*

The ARMA-modelling is performed on "de-trended" measurements. Hence, in a first step the mean values and linear trends are subtracted from the measurements for each baseline. Here, the standard LS method described in Section 5.2 is used. The ARMA-modelling is performed on the de-trended measurements and the optimal predictor is, thereafter, used to obtain the residuals between the true signal and the optimal prediction. The final estimation of the linear trend is then performed on the residuals, again using standard LS methods. In Figure 6-9 one example of the "residuals" is shown, viz. the signal where the optimal prediction around zero mean is subtracted from the true measurement for the baseline between the stations PFM006488 and PFM006489. One might consider this as the signal left after the ARMA process has been subtracted. Ideally, this should be as close as possible to white noise, and in that case the ARMA model has been able to capture the underlying process causing the non-linear motions.

In the last step, LS estimation is performed on this signal and the corresponding signals for the other baselines. In figures A6-1–A6-14 in Appendix 6 the one-step optimal predictions, including estimated linear trends and offsets, compared with the true baseline measurements, are shown. Table 6-7 illustrates the linear trend parameters together with the standard deviation for the residual between the true signal and the one-step optimal predictor. Comparing this result with the result for the AR- modelling in Table 6-5 reveals that the linear baseline motions are slightly larger for the ARMA models, but still much smaller than the results from the LS methods in Table 6-1. One interesting observation is also

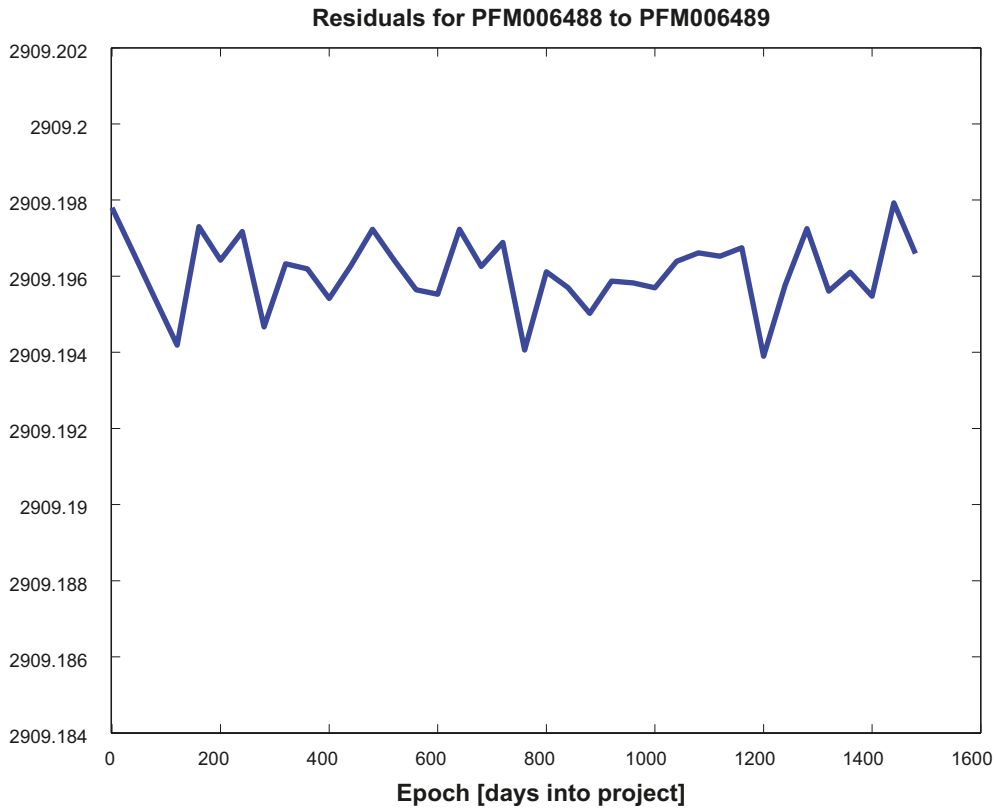

Figure 6-9. *The residuals between true measurements and the ARMA one-step predictions for the baseline variations between the stations PFM006488 and PFM006489.*

Table 6-7. Linear trend parameters for the ARMA-modelling.

Baseline PFM00-	Sigma Residuals [mm]	b	Change [mm/yr]
6483 to 6484	0.9	$-1.57E^{-7}$	–0.06
6483 to 6486	1.4	$1.40E^{-7}$	0.05
6483 to 6487	2.2	$-4.36E^{-7}$	–0.16
6483 to 6488	2.3	$-3.40E^{-7}$	–0.12
6483 to 6489	2.5	$6.04E^{-7}$	0.22
6484 to 6486	1.4	$4.18E^{-7}$	0.15
6484 to 6487	1.8	$-1.6E^{-7}$	–0.06
6484 to 6488	2.0	$1.31E^{-7}$	0.05
6484 to 6489	2.1	$8.19E^{-7}$	0.30
6486 to 6488	1.8	$-1.92E^{-7}$	–0.07
6486 to 6489	1.8	$1.78E^{-7}$	0.07
6487 to 6488	2.1	$1.41E^{-7}$	0.05
6487 to 6489	1.8	$6.63E^{-7}$	0.24
6488 to 6489	1.0	$-4.76E^{-8}$	–0.02

that approximately half of the baseline linear trends are of the opposite sign compared with the AR and LS linear trends. All previous linear trends except one (BLUE-RMS, see Table 6-1) had a negative slope of the curve, indicating that the overall motion was then a contraction of the studied area. The sigmas for the residuals for ARMA are relatively similar to the sigmas obtained from the AR-modelling, although slightly larger. Note that the estimated linear trends are also included in the calculation of the sigma values for both the AR and ARMA models. Compared to the sigmas of the standard LS estimates shown in Table 6-1, the sigma values from the AR- and ARMA-modelling are considerably reduced. In spite of that, also after the modelling exercises the sigma values are relatively large. This indicates that the estimates of the AR and ARMA model parameters, as well as the estimates of the linear trends, are still not sufficiently reliable.

6.3.3 Conclusions from the ARMA- and AR-modelling

One of the main hypotheses in this report is that the number of measurements is too small in order to obtain reliable estimates of the linear trends. One heuristic way of decreasing the variance of the estimates is to model possible underlying signal processes. This gives rise to another hypothesis, namely that there is some dynamics in the baseline motions that cannot be represented by a linear trend model. In other words, there exist possible nonlinear motions or measurement processes that have to be modelled by a nonlinear or a signal process model. The purpose of this report was not to examine the physical reasons for the nonlinear motions, although some possible causes are mentioned in Chapter 3. Instead, the focus was bent on to first establish if the assumption that there are nonlinear motions in the baseline trends is reasonable, and secondly to try to model this using other techniques than linear regression. Thus, one purpose of the nonlinear modelling was to show that the baseline variations can be represented by more sophisticated models than the linear trend model. Even though the nonlinear modelling exercises and validations are interesting in themselves, another aim was to investigate if the model can also improve the linear trend estimates. With this goal in mind, the linear trends were again estimated, either simultaneously with the nonlinear modelling (AR), or in an additional, final modelling step (ARMA).

The nature of the nonlinear baseline variations was examined both in the time domain and in the frequency domain. The result from this investigation reveals that there are some common sinusoidal motions between most of the baseline stations. The periodical behaviour of the baseline trends is the main reason why so-called AR and ARMA models (they belong to the polynomial difference equations model class) have been applied for the nonlinear modelling. Those models are frequently used in signal processing applications to model sinusoidal processes. The model order for the AR model was determined by the Akaike information criterion, and for the ARMA model the same size was chosen for the AR part of the model, whereas the model order for the MA part was chosen in a more ad hoc-like manner. In the AR- and ARMA-modelling it was decided that the station PFM005786 should be excluded, and also the baseline between stations PFM006486 and PFM006487 was disqualified. This decision was based on the statistical results presented in Section 6-1.

The result from the signal processing modelling confirmed that there are some sinusoidal motions that can be satisfactorily captured by the AR and ARMA models. This is verified by studying the model fit in both the time domain and in the frequency domain. The linear trends are estimated simultaneously in the AR-modelling, whereas they are estimated in an additional step in the ARMA-modelling. The linear trend estimates demonstrate at least one order of magnitude (10 times) smaller long-term linear motions for a majority of the baselines compared to the results from the LS estimations. Furthermore, the linear motions from the AR-modelling are significantly different from the corresponding estimated linear trends from the ARMA-modelling. In the AR-modelling the slopes of the baseline curves are all negative (this is in line with the results from the LS estimations), whereas in the ARMA-modelling some of the slopes were positive.

In this context it is important to emphasize that the LS methods explored in this report will in theory give a consistent estimate of the linear trend, even if the variances of the baseline motions are very large, as long as the variances are driven by white noise processes. Moreover, the LS estimates will be consistent also if it is assumed that the measurements are originating from an AR or ARMA process. Hence, they can be driven by sinusoidal processes. However, in both cases a consistent estimate requires that the number of measurements is sufficiently large. Thus, one could expect that the linear regression estimates and the linear trend estimates from the AR- or ARMA-modelling would give the same result if the number of measurements is significantly large, of course under the assumption that the actual sinusoidal process is correctly modelled by the AR or ARMA process. However, even if the AR or ARMA model is not able to exactly image the “true” underlying physical process, one would expect that the linear trend estimates should not differ much, presupposed that the AR or ARMA models are at least reasonably approximating the sinusoidal motions. Thus, the large differences between the different estimation approaches of the baseline motions established in this report support the hypothesis that the number of measurements is too small in order to enable reliably consistent estimates of the long-term linear motions.

In the next sub-section examples are given which illustrate possible consequences for data evaluation of a too short measurement period, as well as of a too slow sampling rate.

6.3.4 Examples of possible consequences for data evaluation of too short measurement period and too slow sampling rate

Example 1: Effect of shortage of data

The following example will illustrate that linear regression on sinusoidal signals can be hazardous if the number of data is too low. In Figure 6-10, a linear trend is estimated for a fictive sinusoidal curve with the frequency 1 period per year, and with amplitude 2.5 mm. The x-scale is in days (the number of days is the same, five years, as the period during which intermittent GPS campaigns proceeded at Forsmark), whereas the y-scale is motion, expressed as distance in mm. The result shows that, despite the fact that the actual long-term trend is zero, a value different from zero for the slope is estimated by applying linear regression methodology. The size and sign of this value depend on the amplitude and phase of the sinusoidal, but also on the length of the measurement period. In this case the number of data is high, imitating continuous GPS measurements with the sample rate of one sample per day. This illustrates that a high sampling rate per se does not help in this case. The estimated slope in Figure 6-10 is indeed misleading and suggests that the long term drift is –23 mm/year. However, if the measurement period is increased, the value of the estimated slope will converge to zero.

Example 2: Aliasing effect

The next example illustrates the so-called aliasing effect, which is the term for when the sampling rate of a sinusoidal signal is not high enough. If the sampling interval is too large, the data will contain little information about the high frequency. Frequencies larger than half the sampling frequency (the so-called Nyquist frequency) will be miss-interpreted as lower frequencies. One way to overcome this is to reduce frequency components higher than the Nyquist frequency by using an anti-aliasing filter. However, if the higher frequencies are an important part of the dynamics, it is better to choose a shorter sampling interval. Figure 6-11 shows a sinusoidal curve with the frequency 12 periods per year. This signal is sampled with a sampling rate similar to that of the GPS measurement campaigns at Forsmark. It is obvious that with this sampling rate the monthly variations of the signal are not correctly reproduced.

Example 3: Consequences of shortage of data in combination with aliasing effect

Figure 6-12 shows a sampled curve of the same almost continuous signal as in Figure 6-10. However, a sequence of random noise with the standard deviation 1 mm is also added to the fast-sampled signal. In the same figure an estimated linear trend, based on the sampled signal, is illustrated as well.

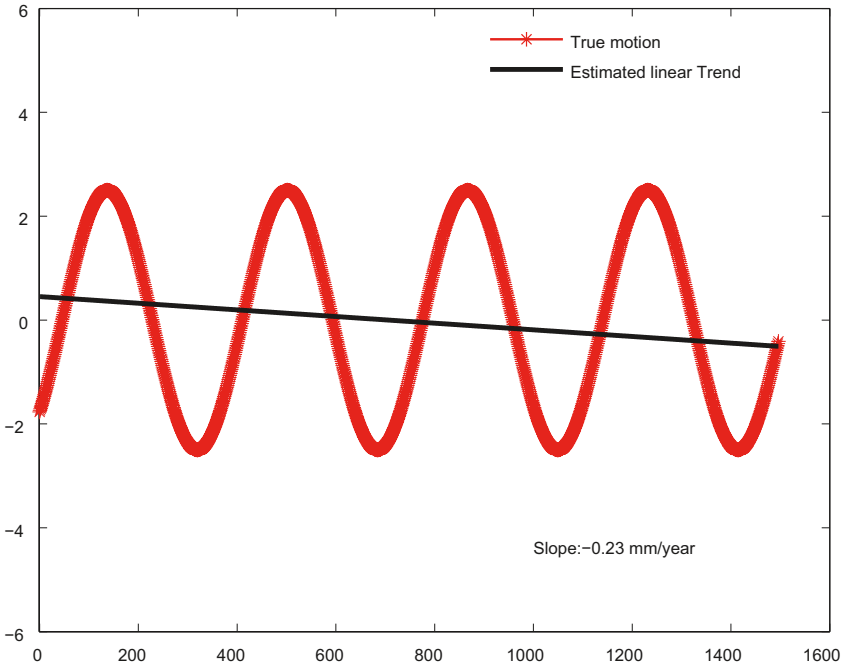

Figure 6-10. *Example illustrating effects for linear regression applied to data with sinusoidal behavior caused by too short timeline for measurements.*

The sampling rate is the same as in Figure 6-11. Although the linear trend is zero, the estimated slope is in this case –0,54 mm/year, in spite of the fact that linear regression methodology has been applied mathematically correct.

In the next chapter the results of crustal deformation calculated with different methods in Gustafson and Ljungberg (2010) and in the present report are briefly summarized. Furthermore, the most important conclusions of the analyses performed are provided. Based on that, some recommendations aiming at improving results in future GPS campaigns are given.

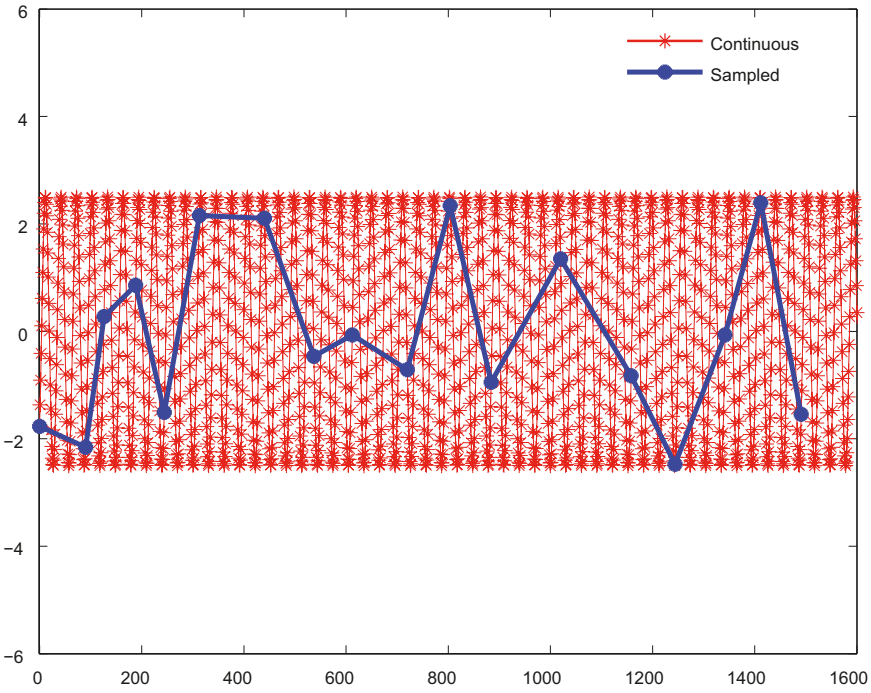

Figure 6-11. *Illustration of consequences of too slow sampling rate.*

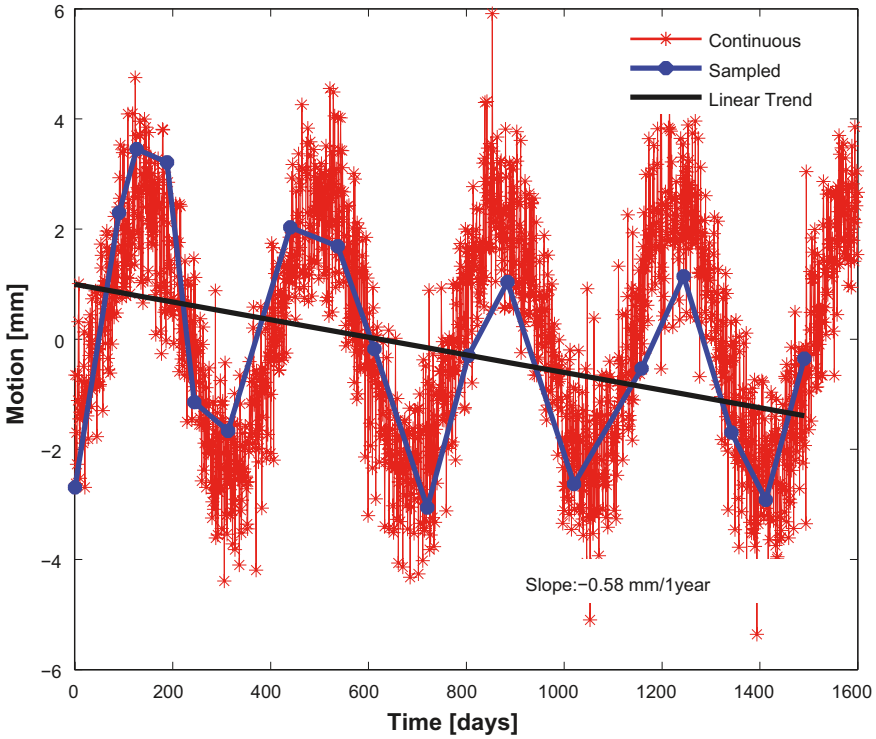

Figure 6-12. *Illustration of consequences of the aliasing effect in combination with too short timeline for measurements.*

7 Summary of results, conclusions and recommendations

7.1 Summary of results – Comparison of baseline length changes calculated with different methods

The preliminarily calculated yearly changes of the Forsmark baseline lengths in Gustafson and Ljungberg (2010), representing the bedrock motion between the GPS-stations, are in Table 7-1 compared to the corresponding results with linear regression according to LS, BLUE-Berne and BLUE-RMS together with results from AR- and ARMA-modelling performed in the present report.

The different methods for linear regression without subsequent non-linear modelling indicate changes of a magnitude of millimetres per year for most baselines, with the six maximum values –2.84 mm/year (BLUE RMS, this report), –2.79 mm/year (BLUE Berne, this report), –2.62 mm/year (BLUE RMS, this report), –2.59 mm/year (LS, this report), –2.53 mm/year (BLUE RMS, this report), and –2.5 mm/year (Gustafson and Ljungberg 2010), respectively. The first, second and fourth values all refer to the baseline between stations PFM006483 and PFM006489, where also Gustafson and Ljungberg (2010) indicate a large value, –2.1 mm/year. However, the largest value in Gustafson and Ljungberg (2010) refers to the baseline between stations PFM006483 and PFM006487. Observe that a negative sign is representing a decrease of the baseline length, i.e. contraction of a baseline, whereas a positive value represents expansion.

Table 7-1. Comparison of baseline length changes.

From	To	Baseline change [mm/yr]					
		(Gustafson and Ljungberg 2010)	LS	BLUE-Berne	BLUE-RMS	AR-modelling	ARMA-modelling
PFM006483	PFM006484	–1.1	–1.37	–1.33	–1.20	–0.05	–0.06
PFM006483	PFM006486	–2.3	–2.40	–2.23	–2.25	–0.12	0.05
PFM006483	PFM006487	–2.5	–2.44	–2.43	–1.91	–0.09	–0.16
PFM006483	PFM006488	–2.0	–1.89	–2.11	–2.62	–0.04	–0.12
PFM006483	PFM006489	–2.1	–2.59	–2.79	–2.84	–0.05	0.22
PFM006483	PFM005786	–1.7	–1.96	–1.70	–2.53	–	–
PFM006484	PFM006486	–1.2	–1.33	–1.22	–1.44	–0.07	0.15
PFM006484	PFM006487	–1.4	–1.36	–1.36	–0.91	–0.04	–0.06
PFM006484	PFM006488	–1.7	–2.02	–1.92	–2.49	–0.03	0.05
PFM006484	PFM006489	–1.3	–2.01	–1.87	–2.28	–0.01	0.30
PFM006484	PFM005786	–1.9	–1.49	–1.24	–2.32	–	–
PFM006486	PFM006487	–0.3	–0.03	–0.10	0.46	–	–
PFM006486	PFM006488	–1.1	–1.36	–1.29	–0.83	–0.02	–0.07
PFM006486	PFM006489	–0.3	–0.89	–0.96	–1.93	–0.03	0.07
PFM006486	PFM005786	–2.3	–2.44	–2.34	–2.17	–	–
PFM006487	PFM006488	–1.9	–2.12	–1.83	–2.20	–0.06	0.05
PFM006487	PFM006489	–0.6	–1.33	–1.02	–1.71	–0.01	0.24
PFM006487	PFM005786	–1.8	–1.36	–1.64	–1.64	–	–
PFM006488	PFM006489	–1.1	–1.32	–1.31	–1.20	–0.04	–0.02
PFM006488	PFM005786	–0.3	–1.01	–1.29	–1.38	–	–
PFM006489	PFM005786	–0.6	–1.71	–1.98	–2.35	–	–

Regarding minimum values, all four linear regression methods applied provide at least one baseline change value of considerably lower magnitude than one millimetre per year. In Gustafson and Ljungberg (2010) three baselines show motion rates amounting to –0.3 mm/year. The LS calculation made in this report displays the small value –0.03 mm/year between stations PFM006486 and PFM006487, where the minimum value is observed also for BLUE Berne and BLUE RMS, –0.10 mm/year and 0.46 mm/year, respectively. The last value is the only positive result obtained by the methods of linear regression applied. Moreover, also Gustafson and Ljungberg (2010) obtained a minimum value, –0.3 mm/year, between these stations.

The overall conclusion regarding linear regression is that all methods applied correspond well, which is also to be expected since the methodological differences between the calculations are small (cf. Section 6.2). Most baselines, 76%, 90%, 90% and 86%, respectively, of the values in columns 3, 4, 5 and 6 in Table 7-1, display motion rates larger than –1 mm/year, and 24%, 33%, 24% and 48%, respectively, point toward motions even exceeding or equal to –2 mm/year. All values except one (BLUE RMS between stations PFM006486 and PFM006487) are negative, indicating contraction of the investigated area.

Columns 7 and 8 in Table 7-1 present the linear trend results of baseline length changes after AR- and ARMA-modelling, including new linear trend estimates. In these columns one third (seven) of the baselines included in columns 3–6 are discarded for reasons explained previously. The AR and ARMA results are radically different from the linear regression results just described. For the AR-modelling the resulting data range between –0.01 and –0.12 mm/year, implying that the maximum motion rate for any baseline, –0.12 mm/year, is c. 24 times smaller than the maximum value in columns 3–6, which is –2.84 mm/year, and the minimum value for AR, –0.01 mm/year, is three times smaller than the smallest value, –0.03 mm/year, in columns 3–6. About 93% of the AR values fall below –0.1 mm/year. Besides these considerable differences in motion magnitudes, it is difficult to identify any similarity in mutual motion pattern between corresponding baselines, which means that baselines with the largest/smallest observed motions in AR results do not correspond undisputedly with the baselines with the largest/smallest motions in the linear regression results in Gustafson and Ljungberg (2010) and obtained by standard LS and BLUE in this report. The only obvious similarity between AR and linear regression is that the resulting motions with one exception are negative, indicating contraction.

The ARMA-modelling has provided motion rates in the range –0.02 to +0.30 mm/year, i.e. slightly larger, but still in the same order of magnitude as the AR-modelling. 57% of the motions are smaller than 0.1 mm/year (irrespective of sign). About 43% of the results have a negative sign, leaving 57% with a positive sign. The ARMA-modelling is (with one exception mentioned above) exclusive among the methods explored in this report in providing positive motions, indicating expansion in some parts of the investigated area and contraction in other parts.

The results of the GPS-measurements at Forsmark obtained from linear regression of existing data performed in this report as well as the results presented in Gustafson and Ljungberg (2010), also based on linear regression, indicate bedrock motions at Forsmark of, on the whole, the same order of magnitude as in the Äspö/Laxemar area as presented in Sjöberg et al. (2004). However, the AR- and ARMA-modellings have provided results indicating crustal motion rates at Forsmark of the same order of magnitude as at Olkiluoto, Kivetty, Romuvaara and Satakunta, Finland, presented in Ahola et al. (2008) and Poutanen et al. (2010), in other words motion rates at least one order of magnitude smaller than those presented in Gustafson and Ljungberg (2010) and in Sjöberg et al. (2004).

Figure 7-1 represents the same type of graphical presentation as exposed in Figure 4-1 of the estimated annual changes of the baseline lengths according to the AR-modelling results. A corresponding presentation for the ARMA-modelling is provided in Figure 7-2.

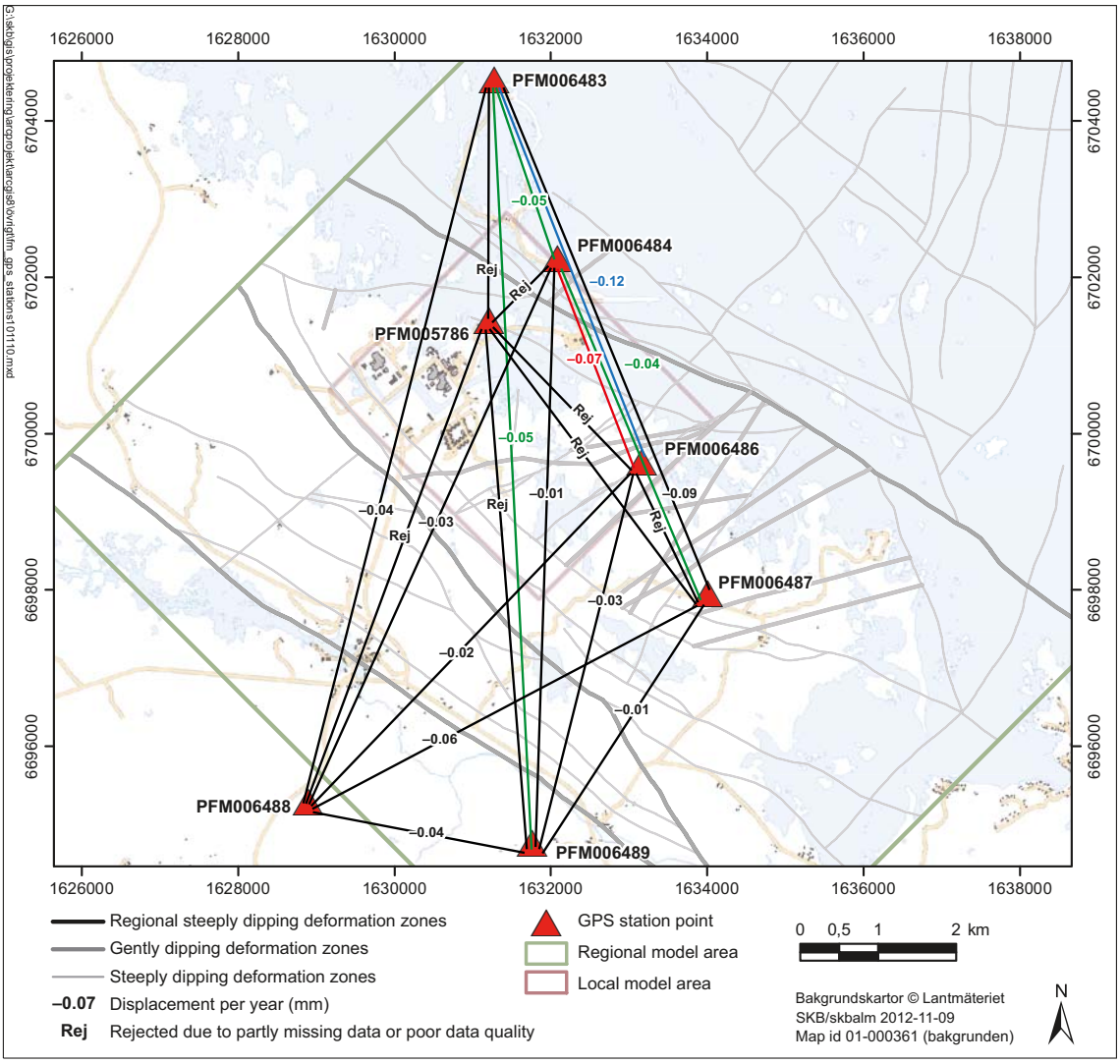

Figure 7-1. *Graphical presentation of the estimated annual changes of the baseline lengths according to Table 7-1, column 7, AR-modelling. Green, blue and red colours are used for some baselines in order to help the reader to visualize these lines and separate them from closely situated black baselines.*

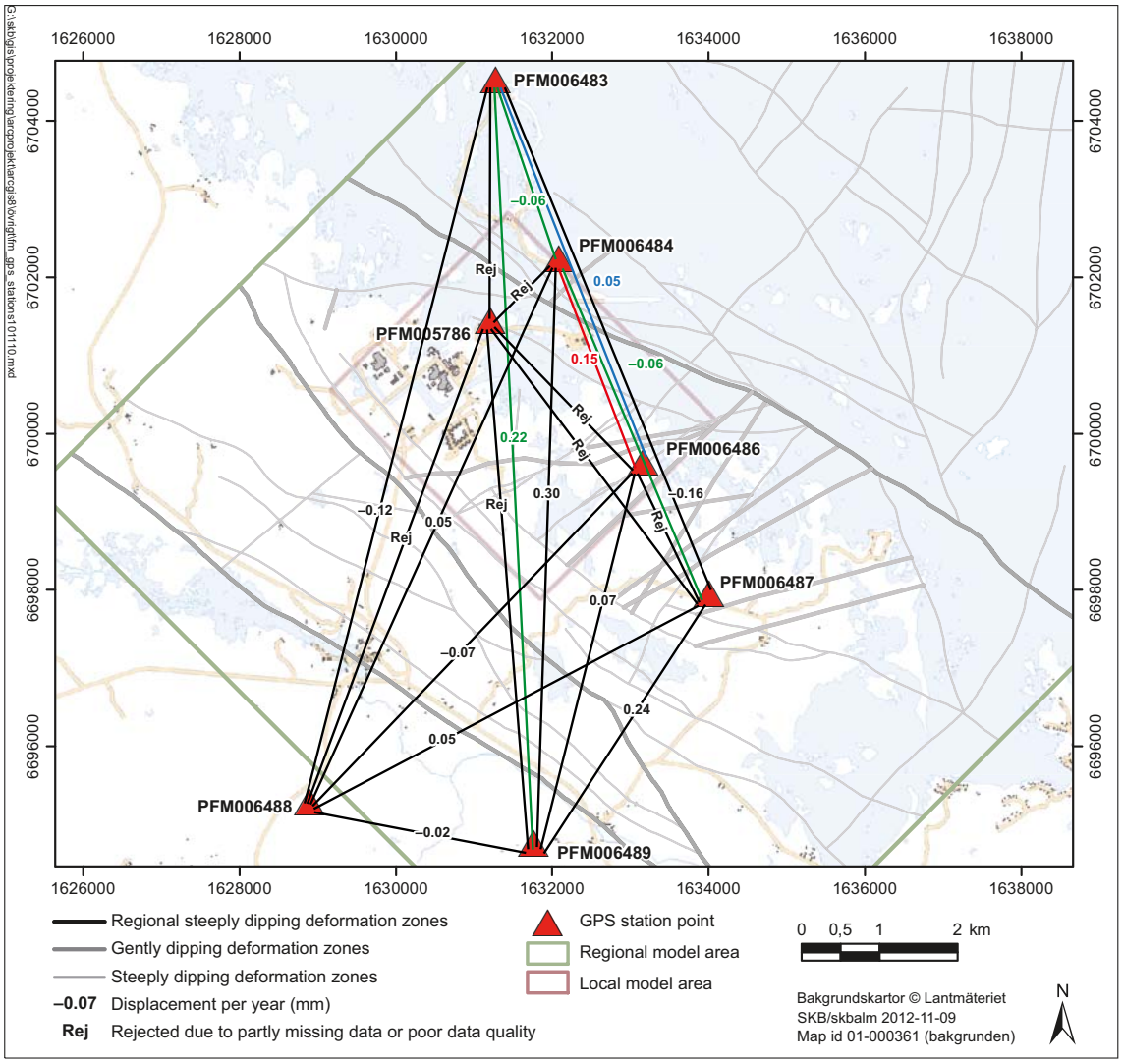

Figure 7-2. *Graphical presentation of the estimated annual changes of the baseline lengths according to Table 7-1, column 8, ARMA-modelling. Green, blue and red colours are used for some baselines in order to help the reader to visualize these lines and separate them from closely situated black baselines.*

7.2 Conclusions

The main conclusion in this report is that the GPS baseline time series so far available from Forsmark is too short to enable undisputedly reliable and consistent estimates of the long-term linear baseline motions between the different stations. This conclusion is based on the statistical analysis of the GPS data performed, and on the outcome of the linear regression. Besides this, also the discrepancies between the different modelling methods applied on GPS data in this report indicate that the number of data is insufficient.

Furthermore, it is also concluded that the sinusoidal motions shown in the baseline time series can be well modelled using standard signal processing time series models. These models, which in opposite to the standard linear regression are common to all baselines, are also used in the report to achieve better estimates of the long-term linear baseline motions compared to those obtained from standard linear regression. The resulting estimates show a decrease of the baseline motions by a factor of more than 10 (in average 14 times for ARMA and 35 times for AR compared to LS), which is in line with the results from the GPS-measurements by Posiva at Olkiluoto, Kivetty, Romuvaara and Satakunta in Finland.

However, the modelling exercises demonstrated in this report cannot fully compensate for the deficiencies in the available data set, as indicated by the values of sigma residuals obtained by the modelling. It is therefore concluded that the only possible way to further increase reliability concerning long-term bedrock motions at Forsmark is to increase the time series of GPS data. The same conclusion is drawn by Ollikainen at al. (2004) and Poutanen et al. (2010) regarding GPS data from Olkiluoto, Kivetty, Romuvaara and Satakunta, Finland.

7.3 Recommendations

It is, as previously emphasized, necessary to increase the GPS data set in order to improve the consistency and reliability of the long-term linear estimates. This may be accomplished in two manners: either by continuing intermittent GPS campaigns at Forsmark for a number of years, or by introducing continuous measurements, which likewise ought to proceed for a period of some years. The second alternative enables identification of, besides slow, also rapid periodicities, a task which is much more difficult with intermittent campaigns separated by long non-active periods. Besides, continuous measurements counteract the aliasing effect, as demonstrated in Sub-section 6.3.4, and are therefore strongly recommended. The approach of continuous measurement has been suggested also by other authors, e.g. Bergstrand (2006).

If GPS measurements will be continued at Forsmark, it is also recommended that L1 and L2 data are analysed separately in order to possibly expose an atmospheric systematic error source.

Futhermore, future GPS measurements should include collection of GLONASS (*Globalnaya Navigationnaya Sputnikovaya Sistema* or *Global Navigation Satellite System*) data. The advantage with using that GNSS system is that it is similar to GPS, but independent of it. The accuracy at present is almost, but not quite as good as that for GPS. However, relevant errors are ephemerid errors that probably will be very small after the post-processing. Another error is due to frequency shifts, but also this error can most likely be handled and is generally removed, depending on how the post-processing is done. Including GLONASS would, however, demand some technical updates of the receivers at Forsmark, primarily by installing the Mk3 Chamelon modem, which is available with GPS L1 and L2 and GLONASS L1 and L2.

Since the modelling methods demonstrated in the present report were tested on this type of data for the first time (as far is known to the authors), another recommendation is, although the outcome of this test was satisfactory, to further develop the method by applying it to other, preferably longer time series of GPS data.

Finally, because sinusoidal variances in GPS data are observed at Forsmark, as well as at the sites with which Forsmark GPS measurements were compared, and since these oscillations have not been convincingly explained, a third recommendation is to further explore this field. It ought to be revealed if the observed oscillations are due to imperfections in the measurement/modelling performance or to genuine, cyclic bedrock motions, or to a combination of both. In the latter case at least the approximate proportions of the influence of the respective factors ought to be elucidated. A first step to do this could be to apply the methods demonstrated for Forsmark data in this report to data from other sites and, secondly, to analyse and compare the results regarding oscillatory patterns.

Acknowledgements

The authors of this report are much grateful to professor Bo Gustafson, University of Florida and Datagrid International Inc., and Lars Gustafson, Caliterra AB, for guidance and help during the quality control of the Forsmark GPS data, as well as for many supportive comments on this paper. Dr Raymond Munier, SKB, is acknowledged for his careful review of and valuable contributions to the manuscript. Much appreciation is also expressed to dr Hans-Georg Scherneck, Chalmers University of Technology, for his constructive expert comments on the report.

References

SKB's (Svensk Kärnbränslehantering AB) publications can be found at www.skb.se/publications.

Ahola J, Koivula H, Jokela J, 2008. GPS operations at Olkiluoto, Kivetty and Romuvaara in 2007. Posiva Working Report 2008-35, Posiva Oy, Finland.

AIUB, 2012. Bernese GNSS Software, Version 5.0. Bern: Astronomical Institute of the University of Bern.

Anderson J G, 1986. Seismic strain rates in the central and eastern United States. Bulletin of the Seismological Society of America 76, 273–290.

Bergstrand S E G, 2006. GPS for geophysics: glacial isostatic adjustment and tests of ionospheric models. PhD thesis. Dept. of Radio- and Space Science, Space Geodetics and Geodynamics, Chalmers University of Technology, Sweden.

Gokall-Norman K, Ludvigson J-E, 2007. Forsmark site investigation. Large-scale interference test with borehole HFM14 used as pumping borehole, 2007. SKB P-07-228, Svensk Kärnbränslehantering AB.

Gustafson L, Ljungberg A, 2007. Forsmark site investigation. GPS deformation measurements in Forsmark. Annual report 2006. SKB P-07-89, Svensk Kärnbränslehantering AB.

Gustafson L, Ljungberg A, 2008. Forsmark site investigation. GPS deformation measurements in Forsmark. Annual report 2007. SKB P-08-49, Svensk Kärnbränslehantering AB.

Gustafson L, Ljungberg A, 2009. Forsmark site investigation. GPS deformation measurements in Forsmark. Annual report 2008. SKB P-09-27, Svensk Kärnbränslehantering AB.

Gustafson L, Ljungberg A, 2010. Forsmark site investigation. A deformation analysis of the Forsmark GPS monitoring network from 2005 to 2009. SKB P-10-29, Svensk Kärnbränslehantering AB.

Harte L, Levitan B, 2009. Global Positioning System (GPS): systems, technology and operation. 2nd ed. Cary, NC: Althos.

Muir-Wood R, 1995. Reconstructing the tectonic history of Fennoscandia from its margins: the past 100 million years. SKB TR 95-36, Svensk Kärnbränslehantering AB.

Ollikainen M, Ahola J, Koivula H, 2004. GPS operations at Olkiluoto, Kievetty and Romuvaara in 2002–2003. Posiva Working Report 2004-12, Posiva Oy, Finland.

Poutanen M, Nyberg S, Ahola J, 2010. GPS measurements in Satakunta area. Posiva Working Report 2010-61, Posiva Oy, Finland.

Sandiford M, Wallace M, Coblentz D, 2004. Origin of the *in situ* stress field in south-eastern Australia. Basin Research 16, 325–338.

Scherneck H-G, Lidberg M, Haas R, Johansson J M, Milne G A, 2010. Fennoscandian strain rates from BIFROST GPS: a gravitating, thick-plate approach. Journal of Geodynamics 50, 19–26.

Sjöberg L E, Pan M, Asenjo E, 2004. Oskarshamn site investigation. A deformation analysis of the Äspö GPS monitoring network from 2000 to 2004. SKB P-04-196, Svensk Kärnbränslehantering AB.

SKB, 2007. Forsmark site investigation. Programme for long-term observations of geosphere and biosphere after completed site investigations. SKB R-07-34, Svensk Kärnbränslehantering AB.

Slunga R S, 1991. The Baltic Shield earthquakes. Tectonophysics 189, 323–331.

Stoica P, Moses R L, 1997. Introduction to spectral analysis. Upper Saddle River, NJ: Prentice Hall.

Söderström T, Stoica P, 1989. System identification. Hemel Hempstead, UK: Prentice Hall International.

Appendix 1

Baseline length variations based on the RMS (from Gustafson and Ljungberg 2010)

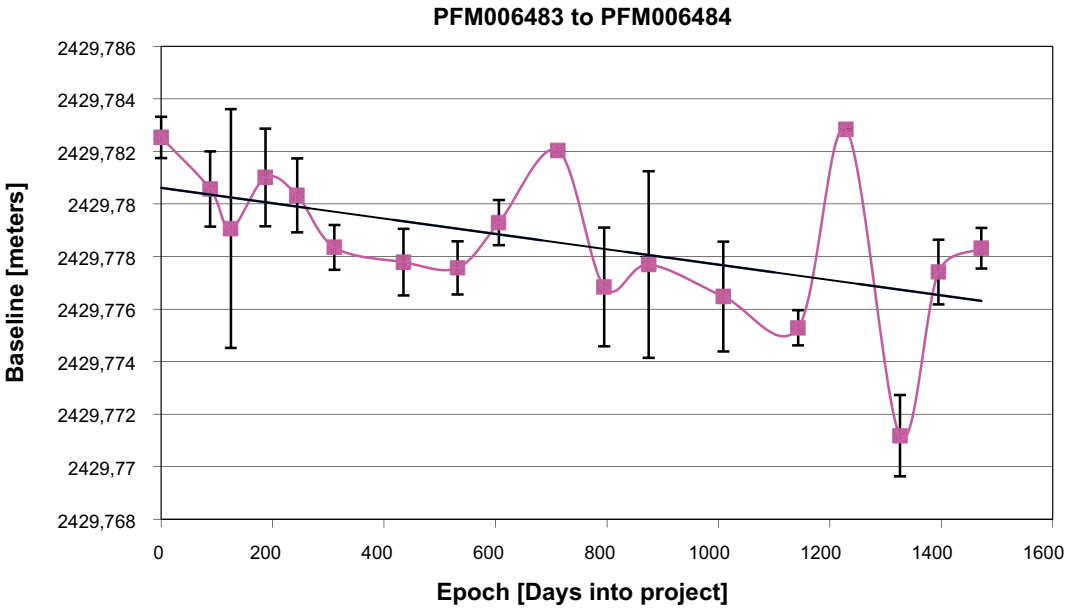

Figure A1-1. *Variation in baseline length between stations PFM006483 and PFM006484 as a function of days into the project.*

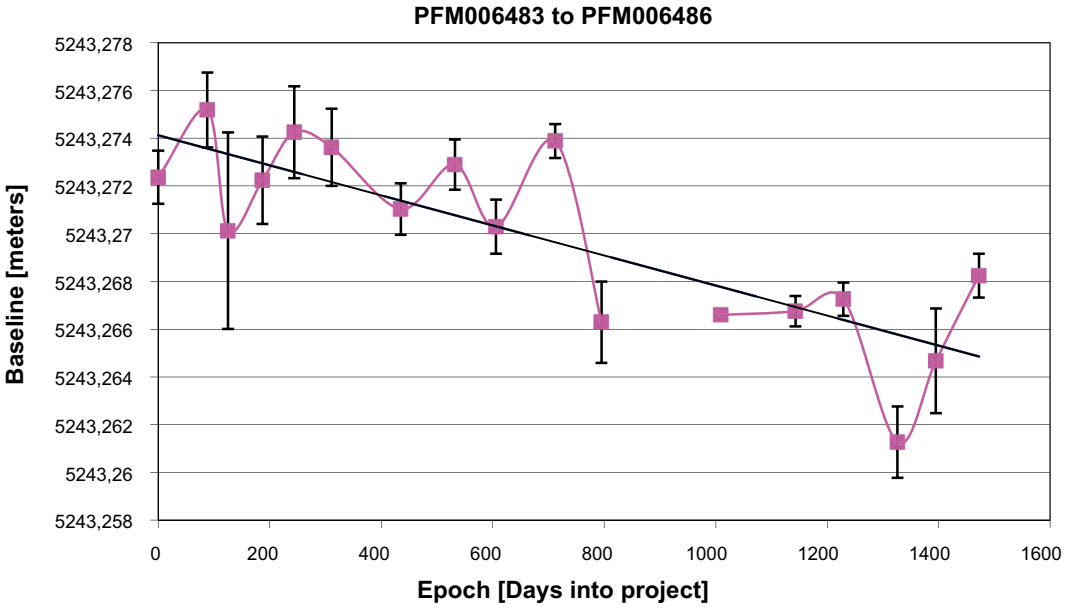

Figure A1-2. *Variation in baseline length between stations PFM006483 and PFM006486 as a function of days into the project.*

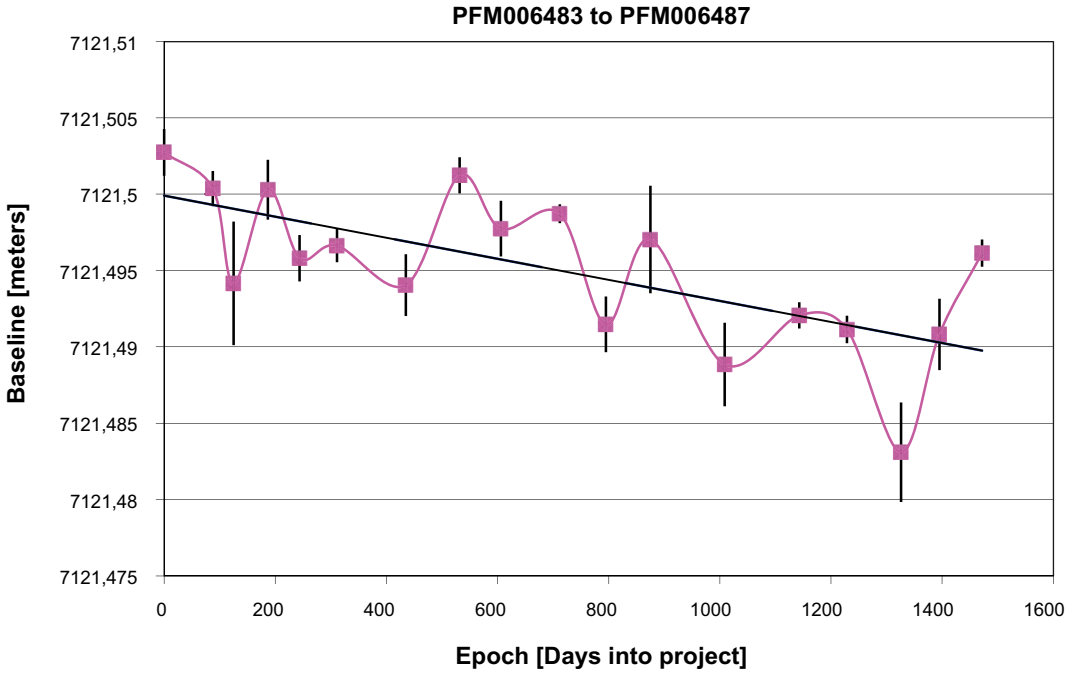

Figure A1-3. *Variation in baseline length between stations PFM006483 and PFM006487 as a function of days into the project.*

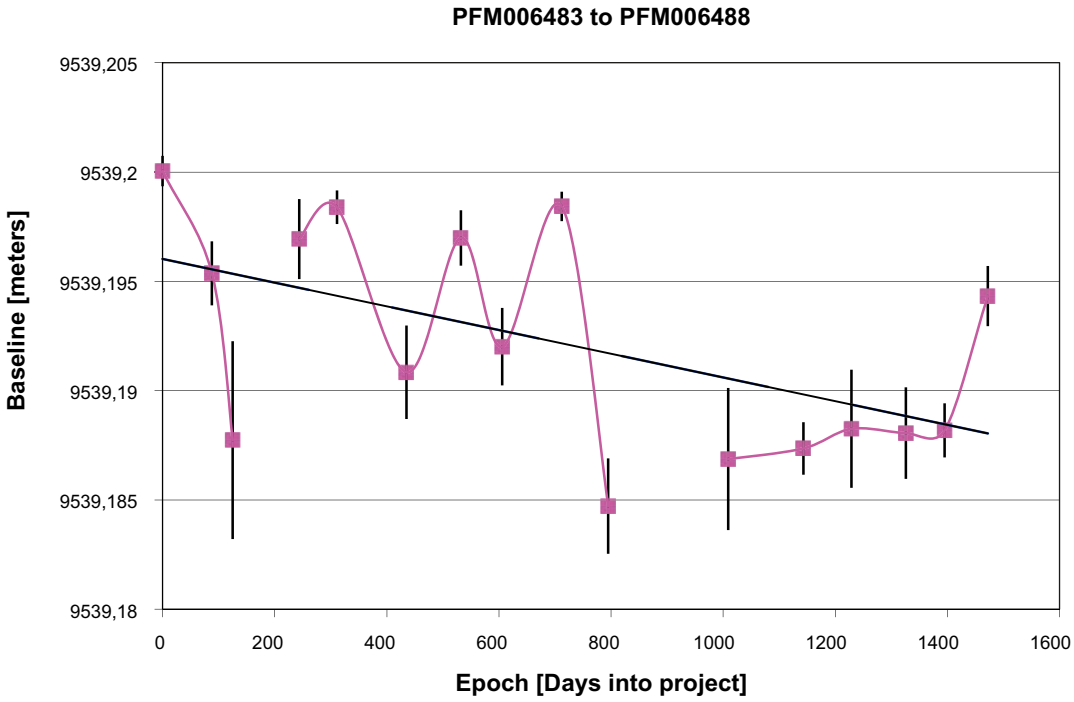

Figure A1-4. *Variation in baseline length between stations PFM006483 and PFM006488 as a function of days into the project.*

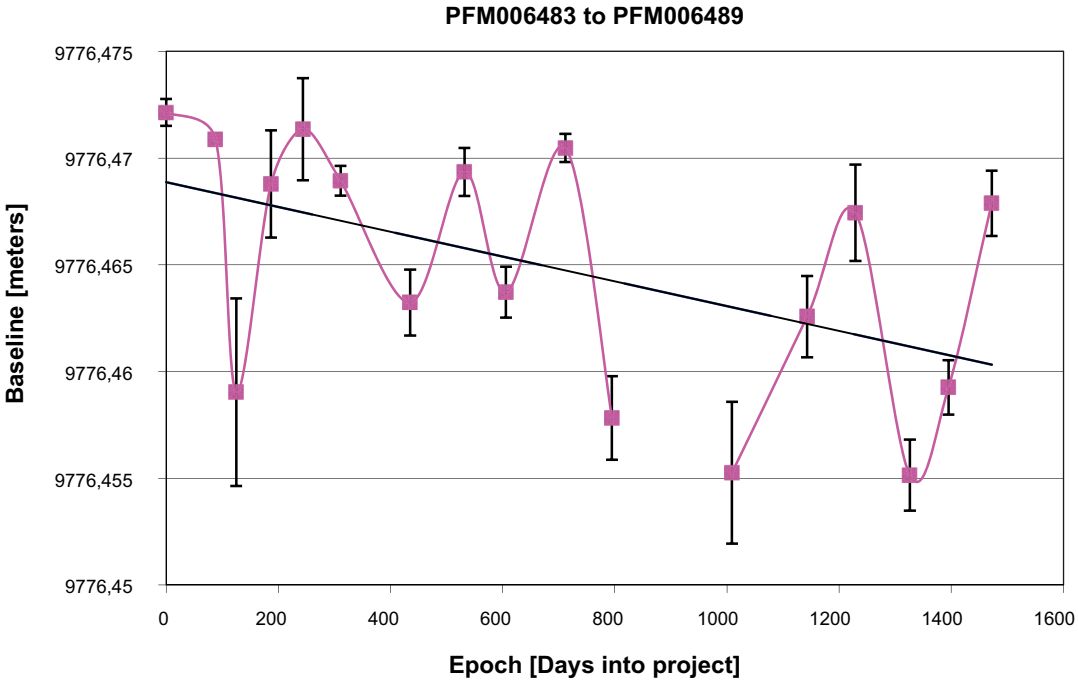

Figure A1-5. *Variation in baseline length between stations PFM006483 and PFM006489 as a function of days into the project.*

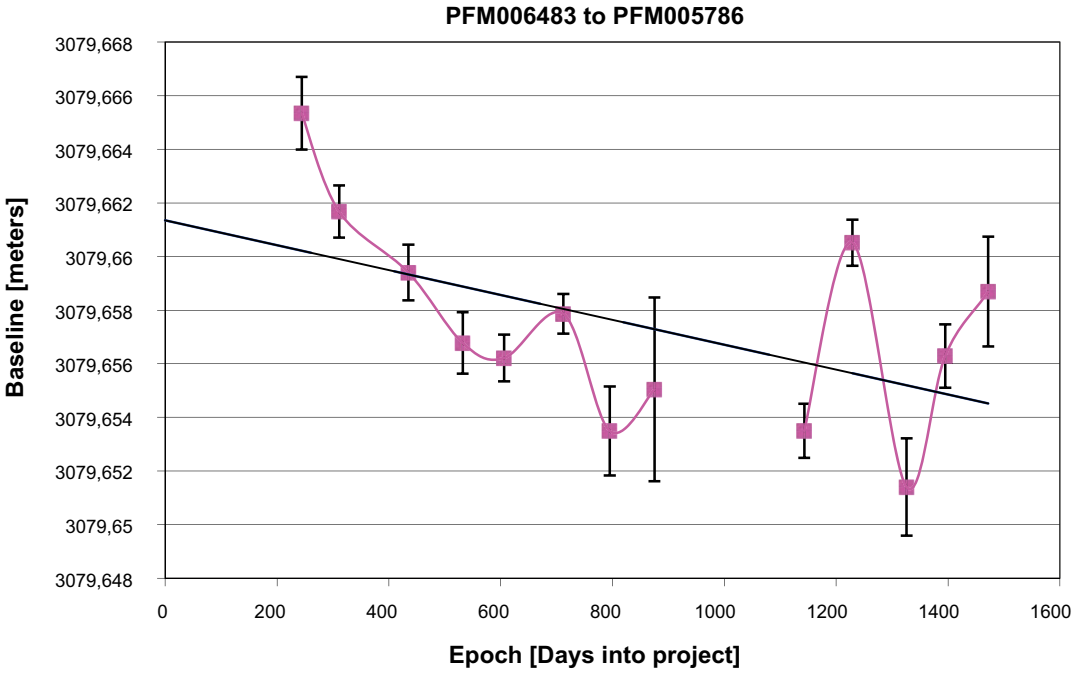

Figure A1-6. *Variation in baseline length between stations PFM006483 and PFM005786 as a function of days into the project.*

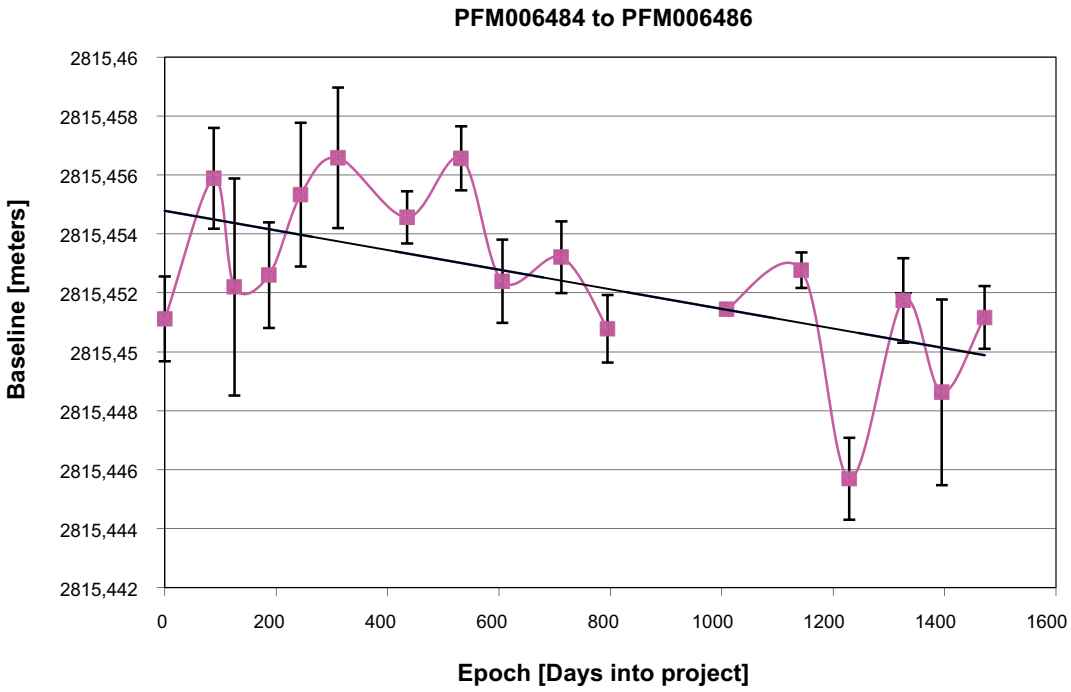

Figure A1-7. *Variation in baseline length between stations PFM006484 and PFM006486 as a function of days into the project.*

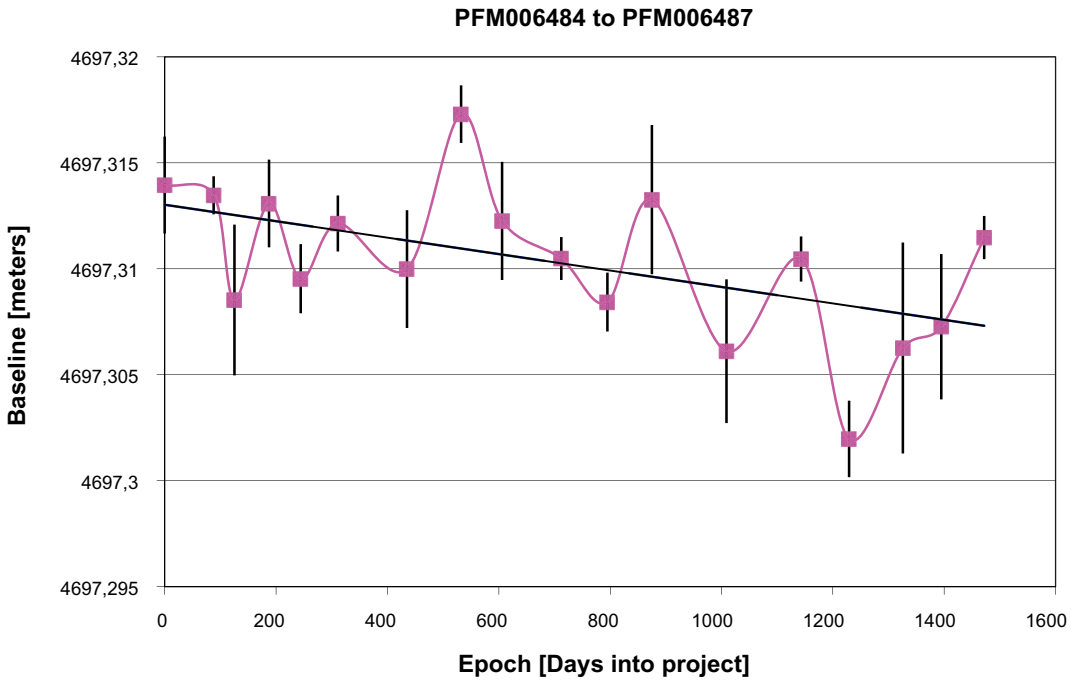

Figure A1-8. *Variation in baseline length between stations PFM006484 and PFM006487 as a function of days into the project.*

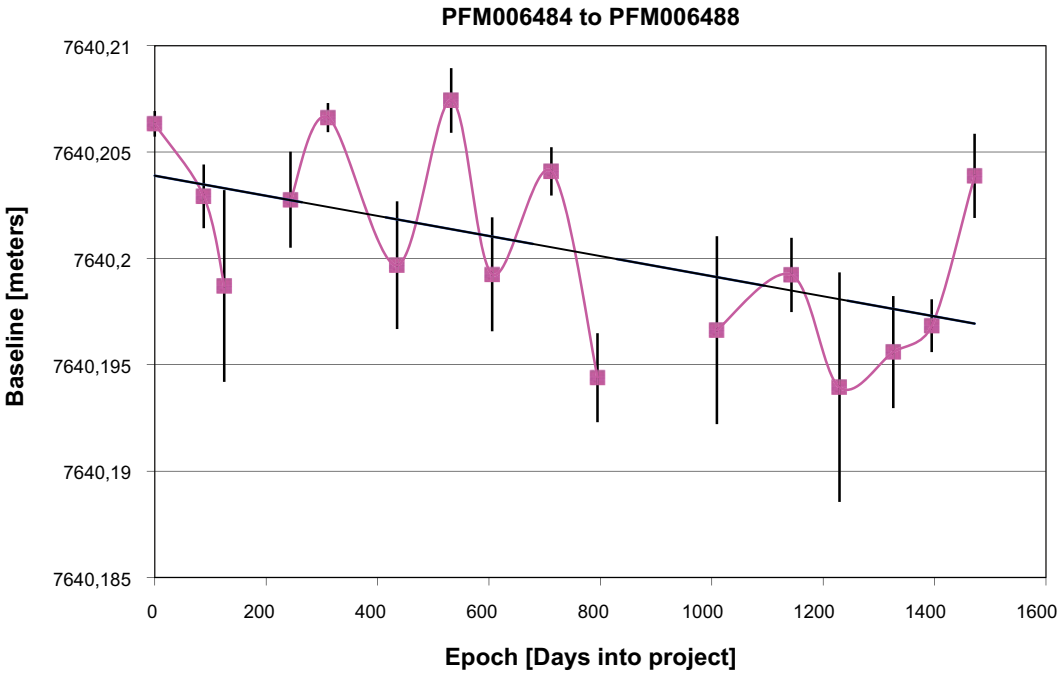

Figure A1-9. *Variation in baseline length between stations PFM006484 and PFM006488 as a function of days into the project.*

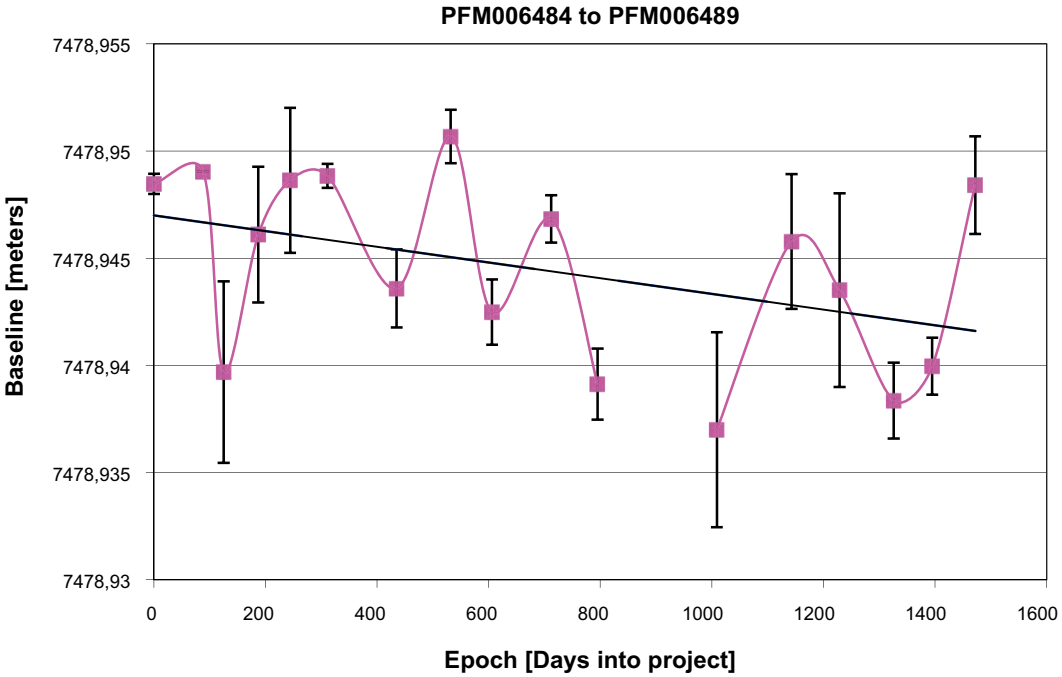

Figure A1-10. *Variation in baseline length between stations PFM006484 and PFM006489 as a function of days into the project.*

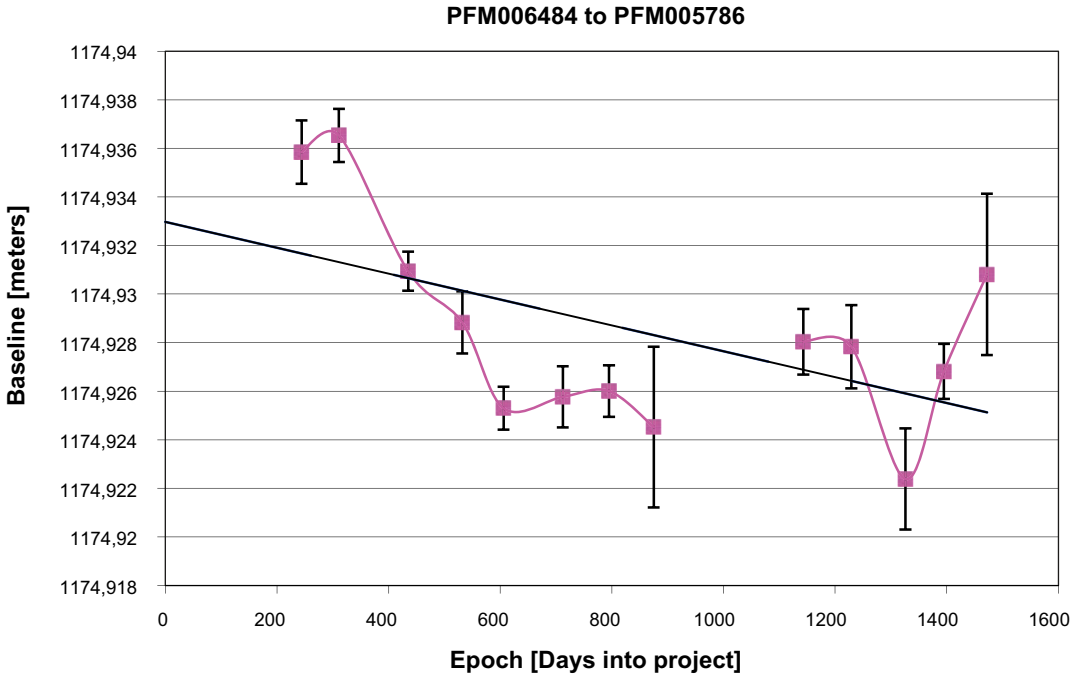

Figure A1-11. *Variation in baseline length between stations PFM006484 and PFM005786 as a function of days into the project.*

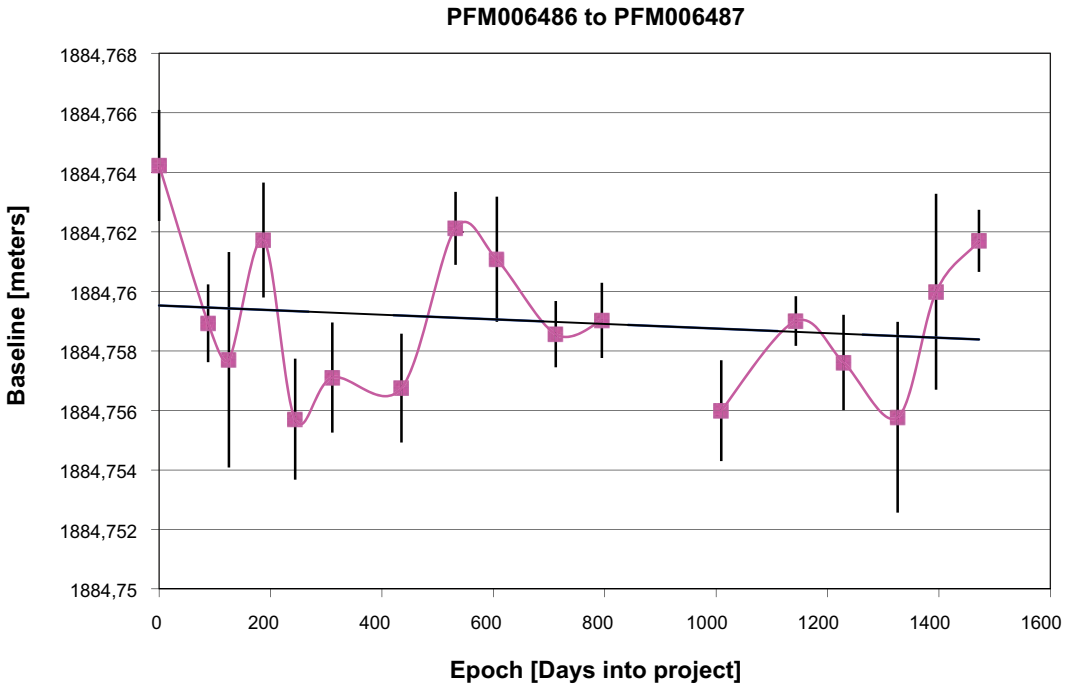

Figure A1-12. *Variation in baseline length between stations PFM006486 and PFM006487 as a function of days into the project.*

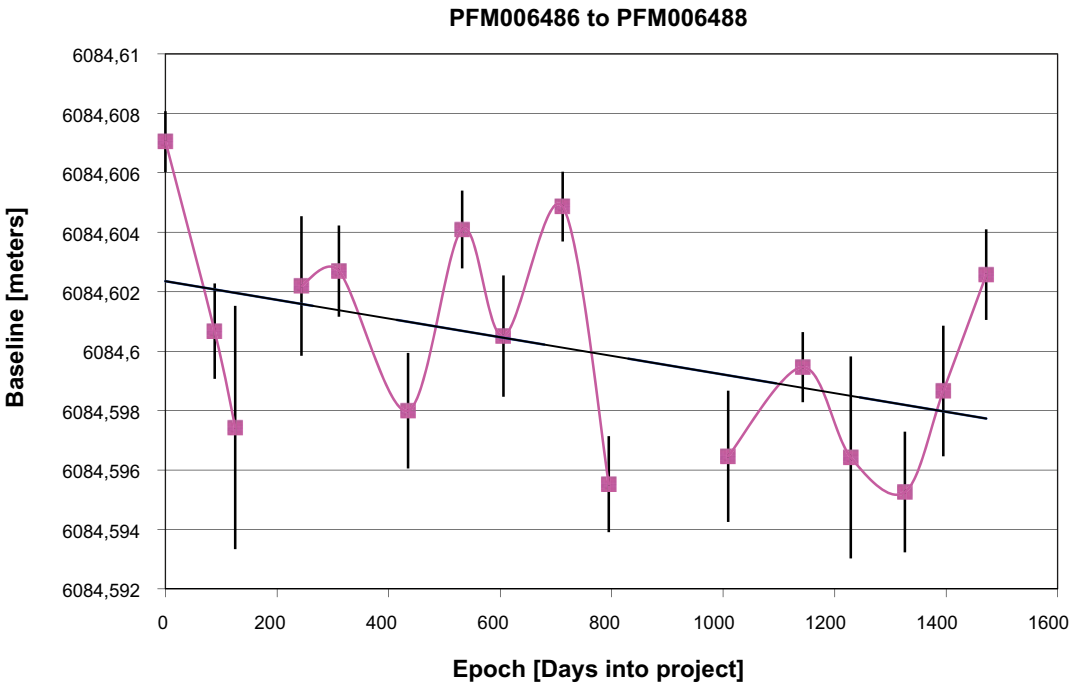

Figure A1-13. *Variation in baseline length between stations PFM006486 and PFM006488 as a function of days into the project.*

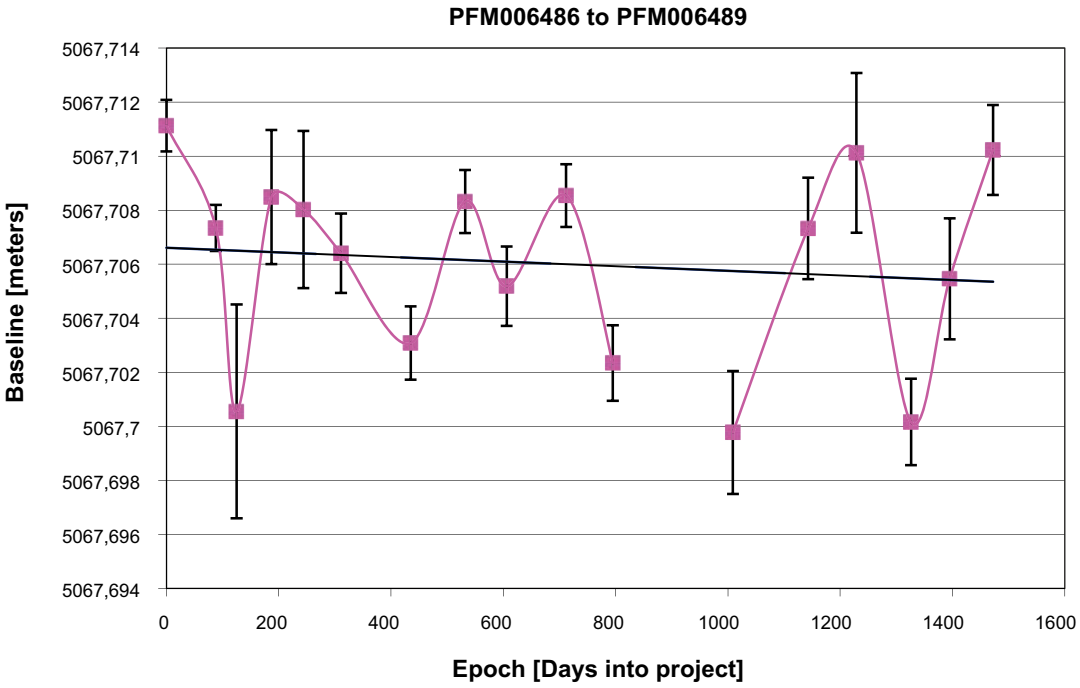

Figure A1-14. *Variation in baseline length between stations PFM006486 and PFM006489 as a function of days into the project.*

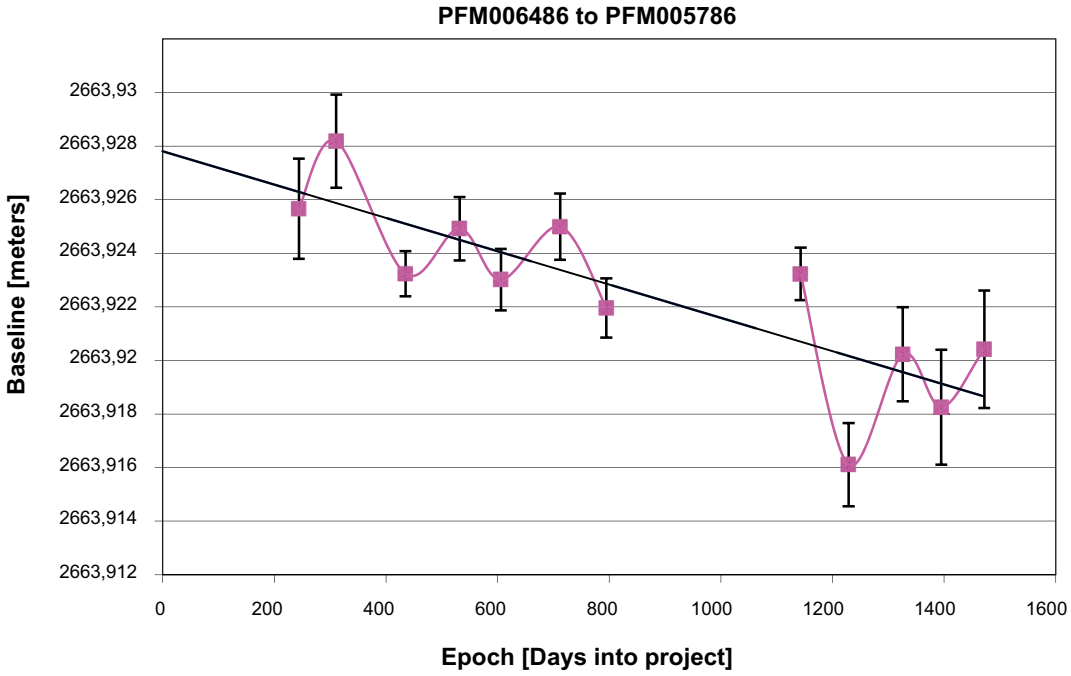

Figure A1-15. *Variation in baseline length between stations PFM006486 and PFM005786 as a function of days into the project.*

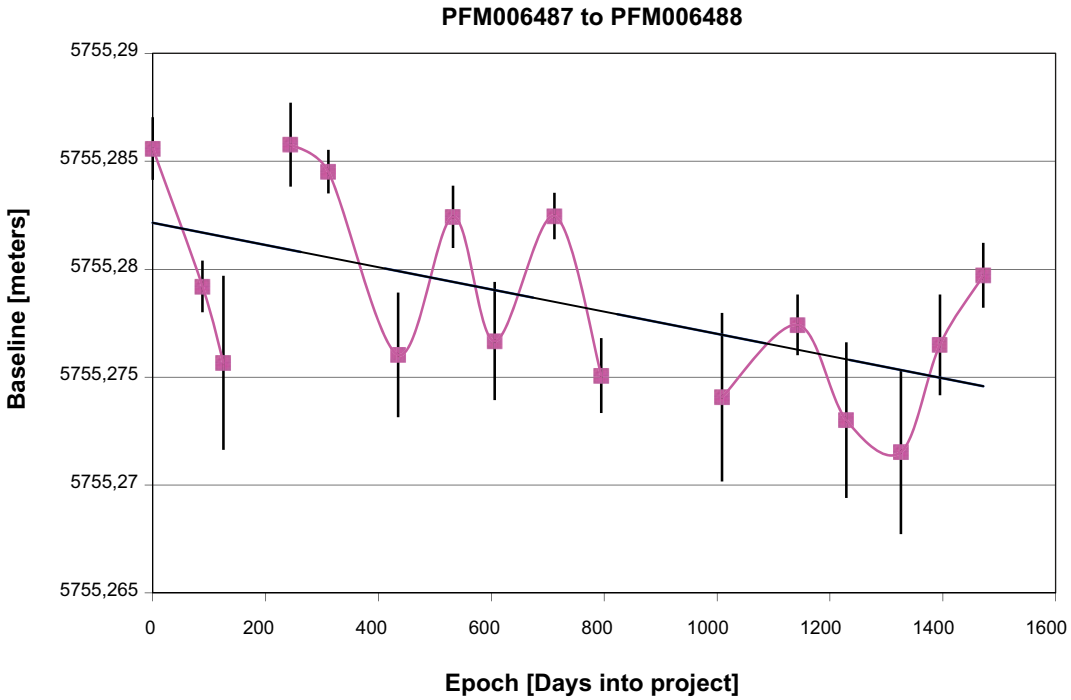

Figure A1-16. *Variation in baseline length between stations PFM006487 and PFM006488 as a function of days into the project.*

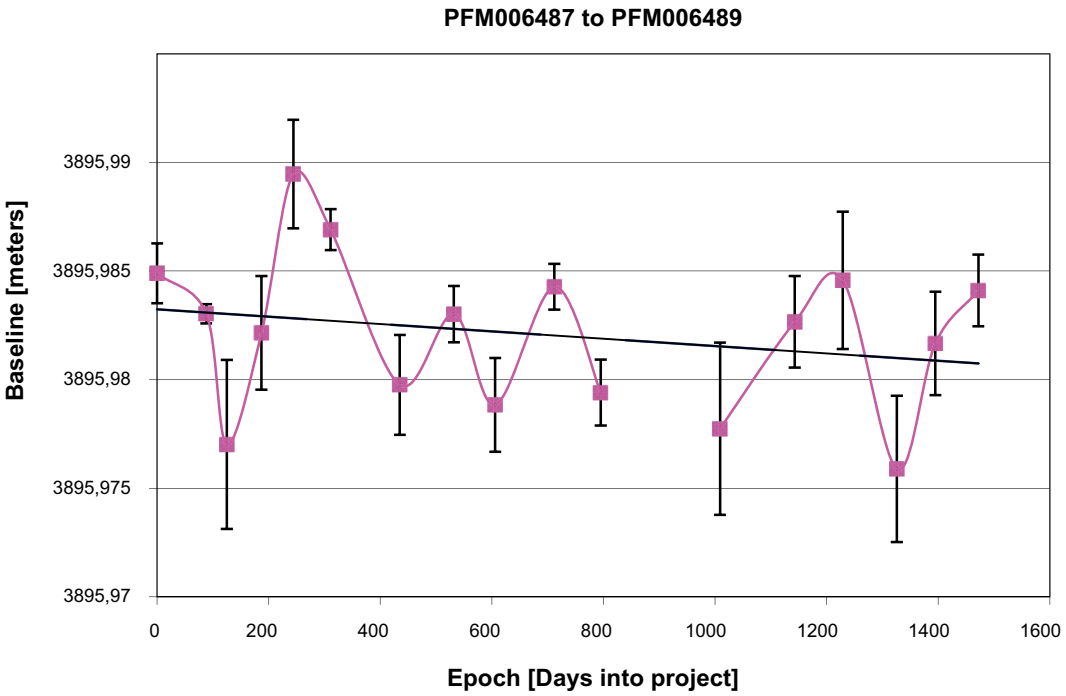

Figure A1-17. *Variation in baseline length between stations PFM006487 and PFM006489 as a function of days into the project.*

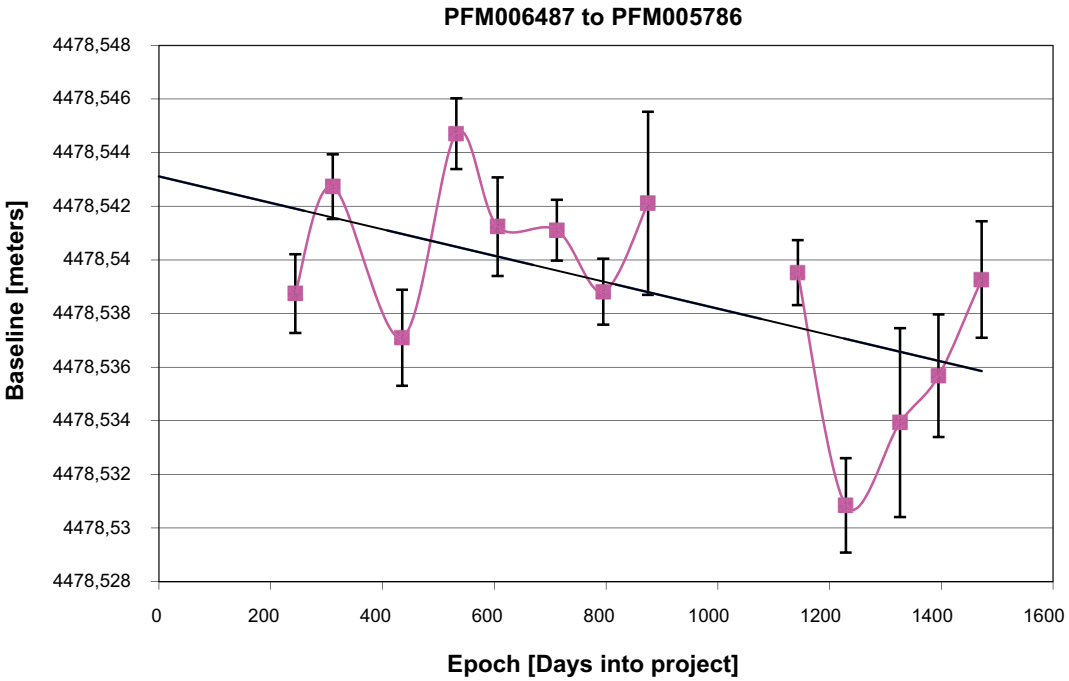

Figure A1-18. *Variation in baseline length between stations PFM006487 and PFM005786 as a function of days into the project.*

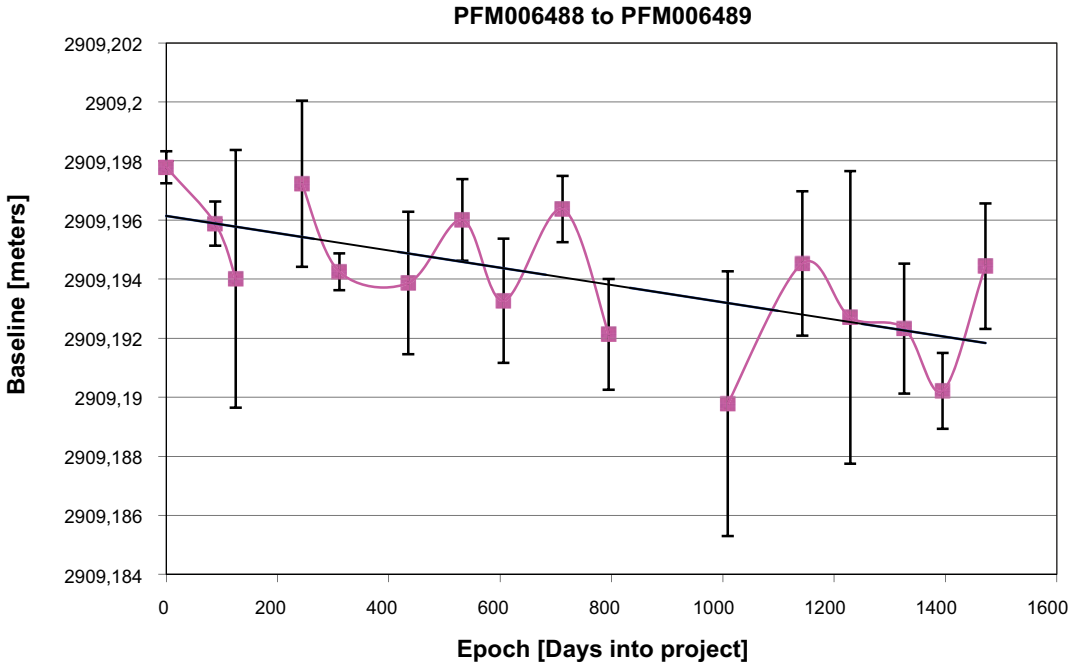

Figure A1-19. *Variation in baseline length between stations PFM006488 and PFM006489 as a function of days into the project.*

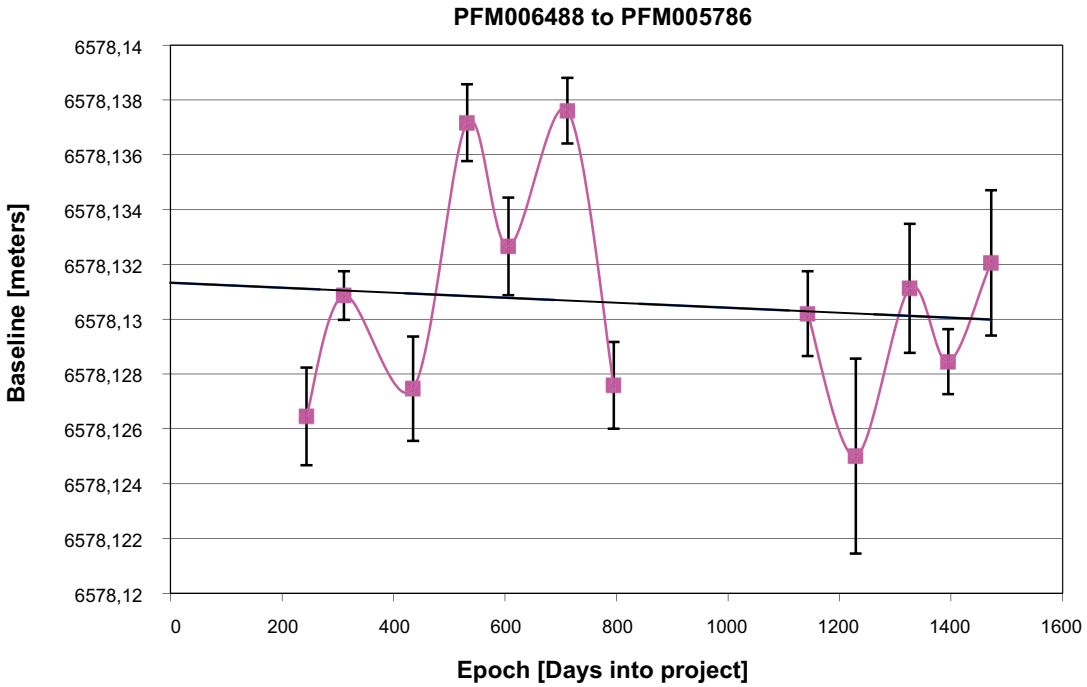

Figure A1-20. *Variation in baseline length between stations PFM006488 and PFM005786 as a function of days into the project.*

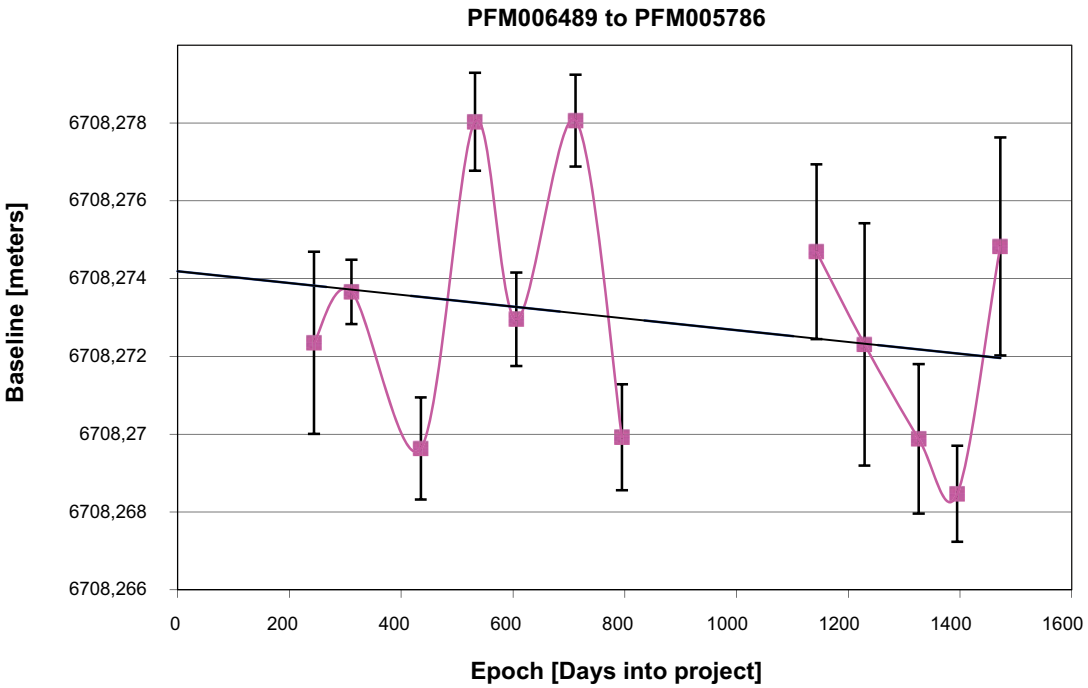

Figure A1-21. *Variation in baseline length between stations PFM006489 and PFM005786 as a function of days into the project.*

Appendix 2

Mean values of the Geocentric coordinates and the Bernese formal errors

Table A2-1. Mean values of the Geocentric coordinates and the Bernese formal errors for each station and Campaign. In the table the RMS between the 24 hours sessions and the number of sessions are also displayed.

Campaign	Stations	Geocentric coordinates	Mean values	Bernese formal errors	RMS for the 24 hours sessions	Number of sessions for each station
1	83FA	X	2,997,251.0597	0.00110	0.0010	3
	83FA	Y	984,787.4318	0.00063	0.0003	3
	83FA	Z	5,524,666.1257	0.00200	0.0013	3
	84FA	X	2,998,942.1212	0.00000	–	3
	84FA	Y	986,102.9668	0.00000	–	3
	84FA	Z	5,523,520.0359	0.00000	–	3
	85FN	X				0
	85FN	Y				0
	85FN	Z				0
	86FA	X	3,000,815.6422	0.00140	0.0016	3
	86FA	Y	987,752.8466	0.00080	0.0002	3
	86FA	Z	5,522,218.2752	0.00247	0.0026	3
	87FA	X	3,001,988.5360	0.00143	0.0016	3
	87FA	Y	988,962.0201	0.00093	0.0026	3
	87FA	Z	5,521,372.9613	0.00250	0.0038	3
	88FA	X	3,005,657.6307	0.00207	0.0008	3
	88FA	Y	984,697.4712	0.00070	–	3
	88FA	Z	5,520,158.5977	0.00247	0.0010	3
	89FA	X	3,005,287.1997	0.00187	0.0006	3
	89FA	Y	987,565.4500	0.00070	0.0006	3
	89FA	Z	5,519,840.9339	0.00237	0.0005	3
	85FA	X	3,000,189.9640	0.00397	0.0062	3
	85FA	Y	985,244.6405	0.00120	0.0019	3
	85FA	Z	5,523,005.3498	0.00613	0.0062	3
2	83FA	X	2,997,251.0621	0.00113	0.0025	3
	83FA	Y	984,787.4334	0.00063	0.0014	3
	83FA	Z	5,524,666.1270	0.00200	0.0010	3
	84FA	X	2,998,942.1212	0.00000	–	3
	84FA	Y	986,102.9668	0.00000	–	3
	84FA	Z	5,523,520.0359	0.00000	–	3
	85FN	X				0
	85FN	Y				0
	85FN	Z				0
	86FA	X	3,000,815.6449	0.00133	0.0010	3
	86FA	Y	987,752.8482	0.00077	0.0008	3
	86FA	Z	5,522,218.2708	0.00237	0.0034	3
	87FA	X	3,001,988.5325	0.00140	0.0005	3
	87FA	Y	988,962.0157	0.00097	0.0015	3
	87FA	Z	5,521,372.9515	0.00237	0.0010	3
	88FA	X	3,005,657.6277	0.00223	0.0014	3
	88FA	Y	984,697.4728	0.00080	0.0007	3
	88FA	Z	5,520,158.5988	0.00270	0.0028	3
	89FA	X				0
	89FA	Y				0
	89FA	Z				0
	85FA	X	3,000,189.9744	0.00377	0.0013	3
	85FA	Y	985,244.6448	0.00130	0.0013	3
	85FA	Z	5,523,005.3567	0.00583	0.0017	3

Campaign	Stations	Geocentric coordinates	Mean values	Bernese formal errors	RMS for the 24 hours sessions	Number of sessions for each station
3	83FA	X	2,997,251.0662	0.00170	0.0075	3
	83FA	Y	984,787.4326	0.00087	0.0034	3
	83FA	Z	5,524,666.1289	0.00260	0.0051	3
	84FA	X	2,998,942.1212	0.00000	–	3
	84FA	Y	986,102.9668	0.00000	–	3
	84FA	Z	5,523,520.0359	0.00000	–	3
	85FN	X				0
	85FN	Y				0
	85FN	Z				0
	86FA	X	3,000,815.6486	0.00187	0.0074	3
	86FA	Y	987,752.8457	0.00093	0.0022	3
	86FA	Z	5,522,218.2811	0.00277	0.0009	3
	87FA	X	3,001,988.5358	0.00190	0.0068	3
	87FA	Y	988,962.0118	0.00110	0.0026	3
	87FA	Z	5,521,372.9618	0.00287	0.0018	3
	88FA	X	3,005,657.6220	0.00250	0.0074	3
	88FA	Y	984,697.4689	0.00093	0.0040	3
	88FA	Z	5,520,158.5986	0.00300	0.0046	3
	89FA	X	3,005,287.1952	0.00240	0.0083	3
	89FA	Y	987,565.4452	0.00090	0.0027	3
	89FA	Z	5,519,840.9420	0.00297	0.0020	3
	85FA	X	3,000,189.9680	0.00237	0.0077	3
	85FA	Y	985,244.6373	0.00093	0.0042	3
	85FA	Z	5,523,005.3465	0.00363	0.0047	3
4	83FA	X	2,997,251.0610	0.00125	–	2
	83FA	Y	984,787.4340	0.00120	0.0015	2
	83FA	Z	5,524,666.1269	0.00195	0.0043	2
	84FA	X	2,998,942.1212	0.00000	–	2
	84FA	Y	986,102.9668	0.00000	–	2
	84FA	Z	5,523,520.0359	0.00000	–	2
	85FN	X				0
	85FN	Y				0
	85FN	Z				0
	86FA	X	3,000,815.6394	0.00140	–	1
	86FA	Y	987,752.8502	0.00130	–	1
	86FA	Z	5,522,218.2701	0.00220	–	1
	87FA	X	3,001,988.5338	0.00155	0.0043	2
	87FA	Y	988,962.0184	0.00145	0.0026	2
	87FA	Z	5,521,372.9577	0.00225	0.0004	2
omitted	88FA	X				0
	88FA	Y				0
	88FA	Z				0
	89FA	X	3,005,287.1925	0.00215	0.0053	2
	89FA	Y	987,565.4490	0.00125	0.0016	2
	89FA	Z	5,519,840.9258	0.00235	0.0054	2
	85FA	X				0
	85FA	Y				0
	85FA	Z				0
5	83FA	X	2,997,251.0577	0.00157	0.0012	3
	83FA	Y	984,787.4355	0.00090	0.0007	3
	83FA	Z	5,524,666.1223	0.00277	0.0027	3
	84FA	X	2,998,942.1212	0.00000	–	3
	84FA	Y	986,102.9668	0.00000	–	3
	84FA	Z	5,523,520.0359	0.00000	–	3
	85FN	X	2,999,846.5405	0.00160	0.0009	3
	85FN	Y	985,452.0172	0.00090	0.0005	3

Campaign	Stations	Geocentric coordinates	Mean values	Bernese formal errors	RMS for the 24 hours sessions	Number of sessions for each station
	85FN	Z	5,523,147.5247	0.00280	0.0026	3
	86FA	X	3,000,815.6423	0.00195	0.0011	2
	86FA	Y	987,752.8498	0.00115	0.0004	2
	86FA	Z	5,522,218.2661	0.00335	0.0003	2
	87FA	X	3,001,988.5183	0.00207	0.0025	3
	87FA	Y	988,962.0158	0.00140	0.0008	3
	87FA	Z	5,521,372.9401	0.00340	0.0022	3
	88FA	X	3,005,657.6224	0.00313	0.0039	3
	88FA	Y	984,697.4711	0.00107	0.0006	3
	88FA	Z	5,520,158.5892	0.00357	0.0027	3
	89FA	X	3,005,287.1943	0.00437	0.0056	3
	89FA	Y	987,565.4496	0.00317	0.0010	3
	89FA	Z	5,519,840.9240	0.00620	0.0044	3
	85FA	X				0
	85FA	Y				0
	85FA	Z				0
6	83FA	X	2,997,251.0622	0.00140	0.0002	3
	83FA	Y	984,787.4354	0.00080	0.0001	3
	83FA	Z	5,524,666.1247	0.00247	0.0018	3
	84FA	X	2,998,942.1212	0.00000	–	3
	84FA	Y	986,102.9668	0.00000	–	3
	84FA	Z	5,523,520.0359	0.00000	–	3
	85FN	X	2,999,846.5420	0.00150	0.0013	3
	85FN	Y	985,452.0157	0.00080	0.0002	3
	85FN	Z	5,523,147.5287	0.00253	0.0019	3
	86FA	X	3,000,815.6465	0.00170	0.0018	3
	86FA	Y	987,752.8487	0.00100	0.0012	3
	86FA	Z	5,522,218.2724	0.00290	0.0046	3
	87FA	X	3,001,988.5289	0.00180	0.0011	3
	87FA	Y	988,962.0180	0.00120	0.0004	3
	87FA	Z	5,521,372.9524	0.00297	0.0026	3
	88FA	X	3,005,657.6302	0.00260	0.0009	3
	88FA	Y	984,697.4746	0.00087	0.0004	3
	88FA	Z	5,520,158.5946	0.00300	0.0011	3
	89FA	X	3,005,287.1984	0.00250	0.0012	3
	89FA	Y	987,565.4497	0.00087	0.0001	3
	89FA	Z	5,519,840.9308	0.00300	0.0002	3
	85FA	X	3,000,189.9988	0.00477	0.0069	3
	85FA	Y	985,244.6417	0.00170	0.0011	3
	85FA	Z	5,523,005.3854	0.00707	0.0091	3
7	83FA	X	2,997,251.0591	0.00120	0.0009	2
	83FA	Y	984,787.4347	0.00070	0.0013	2
	83FA	Z	5,524,666.1180	0.00210	0.0027	2
	84FA	X	2,998,942.1212	0.00000	–	2
	84FA	Y	986,102.9668	0.00000	–	2
	84FA	Z	5,523,520.0359	0.00000	–	2
	85FN	X	2,999,846.5422	0.00165	0.0005	2
	85FN	Y	985,452.0222	0.00100	0.0010	2
	85FN	Z	5,523,147.5355	0.00310	0.0016	2
	86FA	X	3,000,815.6400	0.00150	0.0016	2
	86FA	Y	987,752.8463	0.00090	0.0005	2
	86FA	Z	5,522,218.2642	0.00265	0.0013	2
	87FA	X	3,001,988.5264	0.00150	0.0052	2
	87FA	Y	988,962.0121	0.00105	0.0017	2
	87FA	Z	5,521,372.9456	0.00255	0.0041	2
	88FA	X	3,005,657.6181	0.00225	0.0069	2

Campaign	Stations	Geocentric coordinates	Mean values	Bernese formal errors	RMS for the 24 hours sessions	Number of sessions for each station
	88FA	Y	984,697.4721	0.00080	0.0005	2
	88FA	Z	5,520,158.5872	0.00260	0.0026	2
	89FA	X	3,005,287.1908	0.00215	0.0045	2
	89FA	Y	987,565.4478	0.00075	0.0003	2
	89FA	Z	5,519,840.9275	0.00255	0.0001	2
	85FA	X				0
	85FA	Y				0
	85FA	Z				0
8	83FA	X	2,997,251.0655	0.00110	0.0014	3
	83FA	Y	984,787.4344	0.00063	0.0006	3
	83FA	Z	5,524,666.1266	0.00203	0.0015	3
	84FA	X	2,998,942.1212	0.00000	–	3
	84FA	Y	986,102.9668	0.00000	–	3
	84FA	Z	5,523,520.0359	0.00000	–	3
	85FN	X	2,999,846.5412	0.00100	0.0018	3
	85FN	Y	985,452.0235	0.00060	0.0012	3
	85FN	Z	5,523,147.5375	0.00187	0.0017	3
	86FA	X	3,000,815.6459	0.00130	0.0010	3
	86FA	Y	987,752.8487	0.00073	0.0008	3
	86FA	Z	5,522,218.2715	0.00223	0.0019	3
	87FA	X	3,001,988.5339	0.00137	0.0010	3
	87FA	Y	988,962.0185	0.00087	0.0002	3
	87FA	Z	5,521,372.9489	0.00240	0.0027	3
	88FA	X	3,005,657.6308	0.00187	0.0013	3
	88FA	Y	984,697.4731	0.00063	0.0007	3
	88FA	Z	5,520,158.5945	0.00227	0.0029	3
	89FA	X	3,005,287.2015	0.00177	0.0014	3
	89FA	Y	987,565.4506	0.00070	0.0004	3
	89FA	Z	5,519,840.9327	0.00227	0.0022	3
	85FA	X				0
	85FA	Y				0
	85FA	Z				0
9	83FA	X	2,997,251.0607	0.00110	0.0010	3
	83FA	Y	984,787.4351	0.00067	0.0006	3
	83FA	Z	5,524,666.1241	0.00207	0.0014	3
	84FA	X	2,998,942.1212	0.00000	–	3
	84FA	Y	986,102.9668	0.00000	–	3
	84FA	Z	5,523,520.0359	0.00000	–	3
	85FN	X	2,999,846.5351	0.00107	0.0003	3
	85FN	Y	985,452.0237	0.00067	0.0005	3
	85FN	Z	5,523,147.5336	0.00207	0.0018	3
	86FA	X	3,000,815.6396	0.00143	0.0004	3
	86FA	Y	987,752.8480	0.00083	0.0004	3
	86FA	Z	5,522,218.2706	0.00250	0.0030	3
	87FA	X	3,001,988.5352	0.00320	–	1
	87FA	Y	988,962.0156	0.00170	–	1
	87FA	Z	5,521,372.9691	0.00640	–	1
	88FA	X	3,005,657.6226	0.00210	0.0030	3
	88FA	Y	984,697.4748	0.00070	0.0012	3
	88FA	Z	5,520,158.5961	0.00250	0.0047	3
	89FA	X	3005,287.1926	0.00197	0.0013	3
	89FA	Y	987,565.4493	0.00070	0.0004	3
	89FA	Z	5519,840.9335	0.00237	0.0029	3
	85FA	X				0
	85FA	Y				0
	85FA	Z				0

Campaign	Stations	Geocentric coordinates	Mean values	Bernese formal errors	RMS for the 24 hours sessions	Number of sessions for each station
10	83FA	X	2,997,251.0576	0.00100	0.0003	3
	83FA	Y	984,787.4328	0.00060	0.0003	3
	83FA	Z	5,524,666.1227	0.00190	0.0001	3
	84FA	X	2,998,942.1212	0.00000	–	3
	84FA	Y	986,102.9668	0.00000	–	3
	84FA	Z	5,523,520.0359	0.00000	–	3
	85FN	X	2,999,846.5322	0.00100	0.0011	3
	85FN	Y	985,452.0213	0.00060	0.0007	3
	85FN	Z	5,523,147.5291	0.00190	0.0023	3
	86FA	X	3,000,815.6373	0.00130	0.0004	3
	86FA	Y	987,752.8468	0.00073	0.0007	3
	86FA	Z	5,522,218.2639	0.00220	0.0025	3
	87FA	X	3,001,988.5282	0.00130	0.0004	3
	87FA	Y	988,962.0151	0.00090	0.0004	3
	87FA	Z	5,521,372.9510	0.00220	0.0021	3
	88FA	X	3,005,657.6248	0.00183	0.0006	3
	88FA	Y	984,697.4710	0.00063	0.0004	3
	88FA	Z	5,520,158.5911	0.00227	0.0023	3
	89FA	X	3,005,287.1935	0.00177	0.0003	3
	89FA	Y	987,565.4482	0.00070	0.0006	3
	89FA	Z	5,519,840.9257	0.00217	0.0022	3
	85FA	X				0
	85FA	Y				0
	85FA	Z				0
11	83FA	X	2,997,251.0579	0.00120	0.0035	3
	83FA	Y	984,787.4348	0.00070	0.0008	3
	83FA	Z	5,524,666.1144	0.00223	0.0032	3
	84FA	X	2,998,942.1212	0.00000	–	3
	84FA	Y	986,102.9668	0.00000	–	3
	84FA	Z	5,523,520.0359	0.00000	–	3
	85FN	X	2,999,846.5304	0.00107	0.0015	3
	85FN	Y	985,452.0207	0.00063	0.0004	3
	85FN	Z	5,523,147.5250	0.00207	0.0017	3
	86FA	X	3,000,815.6349	0.00143	0.0008	3
	86FA	Y	987,752.8438	0.00083	0.0010	3
	86FA	Z	5,522,218.2620	0.00243	0.0021	3
	87FA	X	3,001,988.5252	0.00147	0.0022	3
	87FA	Y	988,962.0134	0.00097	0.0005	3
	87FA	Z	5,521,372.9491	0.00250	0.0019	3
	88FA	X	3,005,657.6157	0.00210	0.0017	3
	88FA	Y	984,697.4726	0.00073	0.0014	3
	88FA	Z	5,520,158.5942	0.00253	0.0039	3
	89FA	X	3,005,287.1864	0.00197	0.0021	3
	89FA	Y	987,565.4456	0.00077	0.0005	3
	89FA	Z	5,519,840.9282	0.00250	0.0028	3
	85FA	X				0
	85FA	Y				0
	85FA	Z				0
12	83FA	X	2,997,251.0615	0.00170	0.0052	3
	83FA	Y	984,787.4380	0.00163	0.0021	3
	83FA	Z	5,524,666.1253	0.00260	0.0051	3
	84FA	X	2,998,942.1212	0.00000	–	3
	84FA	Y	986,102.9668	0.00000	–	3
	84FA	Z	5,523,520.0359	0.00000	–	3
	85FN	X	2,999,846.5368	0.00157	0.0044	3
	85FN	Y	985,452.0249	0.00147	0.0021	3

Campaign	Stations	Geocentric coordinates	Mean values	Bernese formal errors	RMS for the 24 hours sessions	Number of sessions for each station
	85FN	Z	5,523,147.5380	0.00243	0.0050	3
	86FA	X				0
	86FA	Y				0
	86FA	Z				0
	87FA	X	3,001,988.5344	0.00210	0.0017	3
	87FA	Y	988,962.0177	0.00213	0.0041	3
	87FA	Z	5,521,372.9573	0.00280	0.006	3
	88FA	X				0
	88FA	Y				0
	88FA	Z				0
	89FA	X				0
	89FA	Y				0
	89FA	Z				0
	85FA	X				0
	85FA	Y				0
	85FA	Z				0
13	83FA	X	2,997,251.0611	0.00140	0.0014	3
	83FA	Y	984,787.4355	0.00083	0.0005	3
	83FA	Z	5,524,666.1193	0.00250	0.0042	3
	84FA	X	2,998,942.1212	0.00000	–	3
	84FA	Y	986,102.9668	0.00000	–	3
	84FA	Z	5,523,520.0359	0.00000	–	3
	85FN	X	2,999,846.5196	0.00603	0.0332	3
	85FN	Y	985,451.9934	0.00363	0.0520	3
	85FN	Z	5,523,147.4841	0.00620	0.0904	3
	86FA	X				0
?	86FA	Y				0
	86FA	Z				0
	87FA	X	3,001,988.5333	0.00157	0.0040	3
	87FA	Y	988,962.0140	0.00110	0.0037	3
	87FA	Z	5,521,372.9665	0.00253	0.0047	3
	88FA	X	3,005,657.6201	0.00247	0.0081	3
	88FA	Y	984,697.4756	0.00100	0.0006	3
	88FA	Z	5,520,158.5967	0.00287	0.0046	3
	89FA	X	3,005,287.1895	0.00223	0.0068	3
	89FA	Y	987,565.4469	0.00083	0.0014	3
	89FA	Z	5,519,840.9384	0.00273	0.0067	3
	85FA	X				0
	85FA	Y				0
	85FA	Z				0
14	83FA	X	2,997,251.0639	0.00103	0.0008	3
	83FA	Y	984,787.4358	0.00067	0.0008	3
	83FA	Z	5,524,666.1211	0.00187	0.0008	3
	84FA	X	2,998,942.1212	0.00000	–	3
	84FA	Y	986,102.9668	0.00000	–	3
	84FA	Z	5,523,520.0359	0.00000	–	3
	85FN	X	2,999,846.5393	0.00100	0.0016	3
	85FN	Y	985,452.0226	0.00060	0.0004	3
	85FN	Z	5,523,147.5370	0.00180	0.0023	3
	86FA	X	3,000,815.6424	0.00123	0.0006	3
	86FA	Y	987,752.8472	0.00073	0.0003	3
	86FA	Z	5,522,218.2728	0.00203	0.0011	3
	87FA	X	3,001,988.5339	0.00137	0.0002	3
	87FA	Y	988,962.0158	0.00093	0.0005	3
	87FA	Z	5,521,372.9601	0.00223	0.0022	3
	88FA	X	3,005,657.6229	0.00203	0.0023	3

Campaign	Stations	Geocentric coordinates	Mean values	Bernese formal errors	RMS for the 24 hours sessions	Number of sessions for each station
	88FA	Y	984,697.4727	0.00070	0.0016	3
	88FA	Z	5,520,158.5976	0.00227	0.0024	3
	89FA	X	3,005,287.1892	0.00220	–	1
	89FA	Y	987,565.4464	0.00110	–	1
	89FA	Z	5,519,840.9330	0.00330	–	1
	85FA	X				0
	85FA	Y				0
	85FA	Z				0
15	83FA	X				0
	83FA	Y				0
	83FA	Z				0
	84FA	X	2,998,942.1212	0.00000	–	3
	84FA	Y	986,102.9668	0.00000	–	3
	84FA	Z	5,523,520.0359	0.00000	–	3
	85FN	X	2,999,846.5361	0.00140	0.0024	3
	85FN	Y	985,452.0219	0.00077	0.0006	3
	85FN	Z	5,523,147.5310	0.00243	0.0027	3
	86FA	X	3,000,815.6348	0.00177	0.0024	3
	86FA	Y	987,752.8413	0.00110	0.0015	3
	86FA	Z	5,522,218.2696	0.00267	0.0009	3
	87FA	X	3,001,988.5303	0.00200	0.0024	3
	87FA	Y	988,962.0107	0.00157	0.0017	3
	87FA	Z	5,521,372.9668	0.00273	0.0025	3
	88FA	X	3,005,657.6127	0.00280	0.0030	2
	88FA	Y	984,697.4757	0.00085	0.0004	2
	88FA	Z	5,520,158.6022	0.00285	0.0018	2
	89FA	X	3,005,287.1865	0.00250	–	1
	89FA	Y	987,565.4464	0.00090	–	1
	89FA	Z	5,519,840.9422	0.00300	–	1
	85FA	X				0
	85FA	Y				0
	85FA	Z				0
16	83FA	X	2,997,251.0623	0.00170	0.0003	3
	83FA	Y	984,787.4457	0.00160	0.0024	3
	83FA	Z	5,524,666.1215	0.00273	0.0023	3
	84FA	X	2,998,942.1212	0.00000	–	3
	84FA	Y	986,102.9668	0.00000	–	3
	84FA	Z	5,523,520.0359	0.00000	–	3
	85FN	X	2,999,846.5369	0.00187	0.0007	3
	85FN	Y	985,452.0286	0.00180	0.0023	3
	85FN	Z	5,523,147.5386	0.00297	0.0037	3
	86FA	X	3,000,815.6345	0.00230	0.0025	3
	86FA	Y	987,752.8483	0.00183	0.0016	3
	86FA	Z	5,522,218.2649	0.00337	0.0007	3
	87FA	X	3,001,988.5149	0.00220	0.0074	3
	87FA	Y	988,962.0134	0.00187	0.0015	3
	87FA	Z	5,521,372.9392	0.00313	0.0074	3
	88FA	X	3,005,657.6233	0.00303	0.0043	3
	88FA	Y	984,697.4883	0.00180	0.0017	3
	88FA	Z	5,520,158.6001	0.00337	0.0031	3
	89FA	X	3,005,287.1790	0.00270	0.0022	3
	89FA	Y	987,565.4582	0.00163	0.0023	3
	89FA	Z	5,519,840.9220	0.00307	0.0021	3
	85FA	X				0
	85FA	Y				0
	85FA	Z				0

Campaign	Stations	Geocentric coordinates	Mean values	Bernese formal errors	RMS for the 24 hours sessions	Number of sessions for each station
17	83FA	X	2,997,251.0643	0.00137	0.0019	3
	83FA	Y	984,787.4368	0.00080	0.0007	3
	83FA	Z	5,524,666.1274	0.00243	0.0016	3
	84FA	X	2,998,942.1212	0.00000	–	3
	84FA	Y	986,102.9668	0.00000	–	3
	84FA	Z	5,523,520.0359	0.00000	–	3
	85FN	X	2,999,846.5378	0.00127	0.000 6	3
	85FN	Y	985,452.0241	0.00073	0.0008	3
	85FN	Z	5,523,147.5346	0.00237	0.0022	3
	86FA	X	3,000,815.6350	0.00170	0.0038	3
	86FA	Y	987,752.8442	0.00100	0.0007	3
	86FA	Z	5,522,218.2672	0.00280	0.0055	3
	87FA	X	3,001,988.5327	0.00157	0.0034	3
	87FA	Y	988,962.0167	0.00107	0.0012	3
	87FA	Z	5,521,372.9667	0.00253	0.0063	3
	88FA	X	3,005,657.6300	0.00230	0.0010	3
	88FA	Y	984,697.4790	0.00083	0.0009	3
	88FA	Z	5,520,158.6146	0.00293	0.0023	3
	89FA	X	3,005,287.1933	0.00220	0.0003	3
	89FA	Y	987,565.4481	0.00080	0.0006	3
	89FA	Z	5,519,840.9394	0.00267	0.0028	3
	85FA	X				0
	85FA	Y				0
	85FA	Z				0
18	83FA	X	2,997,251.0613	0.00127	0.0005	3
	83FA	Y	984,787.4334	0.00077	0.00017	3
	83FA	Z	5,524,666.1209	0.00240	0.0016	3
	84FA	X	2,998,942.1212	0.00000	–	3
	84FA	Y	986,102.9668	0.00000	–	3
	84FA	Z	5,523,520.0359	0.00000	–	3
	85FN	X	2,999,846.5379	0.00133	0.0041	3
	85FN	Y	985,452.0205	0.00077	0.0011	3
	85FN	Z	5,523,147.5286	0.00243	0.0057	3
	86FA	X	3,000,815.6392	0.00163	0.0009	3
	86FA	Y	987,752.8439	0.00093	0.0007	3
	86FA	Z	5,522,218.2674	0.00277	0.0020	3
	87FA	X	3,001,988.5350	0.00157	0.0014	3
	87FA	Y	988,962.0159	0.00103	0.0011	3
	87FA	Z	5,521,372.9597	0.00257	0.0012	3
	88FA	X	3,005,657.6248	0.00230	0.0005	3
	88FA	Y	984,697.4721	0.00080	0.0007	3
	88FA	Z	5,520,158.5911	0.00283	0.0041	3
	89FA	X	3,005,287.1942	0.00217	0.0043	3
	89FA	Y	987,565.4471	0.00077	0.0009	3
	89FA	Z	5,519,840.9233	0.00263	0.0019	3
	85FA	X				0
	85FA	Y				0
	85FA	Z				0

Appendix 3

Discrepancies between data set in this report and plots in Gustafson and Ljungberg (2010)

Below some minor discrepancies between the data set available for the analyses made in this report and the diagrams shown in Gustafson and Ljungberg (2010) are listed. The reasons for these discrepancies are not fully known, but are probably mainly the consequence of that not all assessments of data quality during the data post-processing after completed measurements, with subsequent rejection or minor adjustments of data points, have been fully documented. Moreover, a few data points have also been added to some of the figures in Gustafson and Ljungberg (2010) and also to the LS calculations of the corresponding linear trends, whereas they cannot be found in the output files from the Bernese programs. Those additional baselines are originating from pieces of data (i.e. data have not been successfully measured continuously during a whole measurement campaign day) in the original GPS log files, but are not used in the final Bernese program computations. Those "extra" data are excluded in the current report, since they are not fed into the Bernese program in the final baseline computations, and there is no description of how these additional points have been calculated in Gustafson and Ljungberg (2010). However, these discrepancies are not judged to exert any major influence on the results of the analyses.

- Baseline PFM006483 to PFM006486, see Appendix 4, Figures A2-2 and A2-23: Data points 4 and 5 differ 1 and 2 mm respectively in the data set used in the analyses presented in this report compared to in the plot in Gustafson and Ljungberg (2010). Moreover, data points 12 or 13 for PFM006486 and 15 for PFM006483 are missing in the data set, but are present in old plot (cf. Appendix 1, Figure A1-2).
- Baseline PFM006483 to PFM006487, see Appendix 4, Figures A2-3 and A2-24: Data point 9 (campaign 9) differs 5 mm from the old plot, and campaign 15 for PFM006483 is completely missing in the data set, but shown in old plot (cf. Appendix 1, Figure A1-3).
- Baseline PFM006483 to PFM006488, see Appendix 4, Figures A2-4 and A2-25: Campaign 15 for PFM006483 is missing in the data set but shown in old plot (cf. Appendix 1, Figure A1-4).
- Baseline PFM006483 to PFM006489, see Appendix 4, Figures A2-5 and A2-26: Campaign 14 differs 5 mm. Campaign 15 for PFM006483 is missing in the data set but shown in old plot. Also data point 2 is missing for PFM006489, but is shown in the old plot (cf. Appendix 1, Figure A1-5).
- Baseline PFM006483 to PFM005786, see Appendix 4, Figures A2-6 and A2-27: Data point 13 is missing in the old plot. Campaign 15 for PFM006483 is missing in the data set but shown in the old plot (cf. Appendix 1, Figure A1-6).
- Baseline PFM006483 to PFM006484, see Appendix 4, Figures A2-1 and A2-22. Data point 15 for PFM006483 is missing in the data set but shown in the old plot (cf. Appendix 1, Figure A1-1).
- Baseline PFM006484 to PFM006486, see Appendix 4, Figures A2-7 and A2-28: Data points 4 and 5 are slightly different than corresponding points in the old plot. Point 12 or 13 is shown in the old plot (without variance), but is missing in the data set (cf. Appendix 1, Figure A1-7).
- Baseline PFM005786 to PFM006484, see Appendix 4, Figures A2-11 and A2-32: Data point 9 (campaign 13) is excluded from old plot, possibly treated as outlier (cf. Appendix 1, Figure A1-11).
- Baseline PFM006484 to PFM006487, see Appendix 4, Figures A2-8 and A2-29: Data point 9 (campaign 9) differs considerably (cf. Appendix 1, Figure A1-8).
- Baseline PFM006484 to PFM006489, see Appendix 4, Figures A2-10 and A2-31: Campaigns 14 and 15 differ considerably from the old plots. Moreover, data point 2 (i.e. campaign 2) is missing in the data set, but is displayed in the old plot (cf. Appendix 1, Figure A1-10).
- Baseline PFM005786 to PFM006487, see Appendix 4, Figures A2-18 and A2-39: Data point 5 (campaign 9) differs considerably. Moreover, campaign 13 is excluded from the old plot, possibly treated as an outlier (cf. Appendix 1, Figure A1-18).

- Baseline PFM005786 to PFM006488, see Appendix 4, Figures A2-20 and A2-41: Campaign 15 differs considerably. Moreover, campaign 13 is excluded from the old plot, possibly treated as outlier (cf. Appendix 1, Figure A1-20).
- Baseline PFM005786 to PFM006489, see Appendix 4, Figures A2-21 and A2-42: Campaigns 14 and 15 differ considerably. Moreover, campaign 13 is excluded from the old plot, possibly treated as an outlier (cf. Appendix 1, Figure A1-21).
- Baseline PFM006486 to PFM006487, see Appendix 4, Figures A2-12 and A2-33: Campaigns 4, 5 and 9 differ considerably. Moreover, campaign 13 is missing in the data set, but shown in the old plot (cf. Appendix 1, Figure A1-12).
- Baseline PFM006486 to PFM006488, see Appendix 4, Figures A2-13 and A2-34: Only slightly difference for campaign 4, whereas campaign 15 differs considerably. Moreover, campaign 13 is missing in the data set but included in the old plot (cf. Appendix 1, Figure A1-13).
- Baseline PFM006486 to PFM006489, see Appendix 4, Figures A2-14 and A2-35: Only slightly difference for campaign 5. However, campaigns 14 and 15 differ considerably. Moreover, campaigns 2 and 13 are missing in the data set but shown in the old plot (cf. Appendix 1, Figure A1-14.
- Baseline PFM006487 to PFM006488, see Appendix 4, Figures A2-16 and A2-37: Campaign 15 differs considerably (cf. Appendix 1, Figure A1-16).
- Baseline PFM006487 to PFM006489, see Appendix 4, Figures A2-17 and A2-38: Campaigns 14 and 15 differ considerably. Moreover, campaign 2 is missing in the data set but displayed in the old plot (cf. Appendix 1, Figure A1-17).
- Baseline PFM006488 to PFM006489, see Appendix 4, Figures A2-19 and A2-40: Campaigns 14 and 15 differ considerably. Moreover, campaign 2 is missing in the data set, but shown in the old plot (cf. Appendix 1, Figure A1-19).

Other remarks:

- For PFM006487 only 1 day of measuring in the data set for campaign 9.
- For PFM006486 only 1 day of measuring in the data set for campaign 4.
- For PFM006486 only 2 days of measuring in the data set for campaign 5.
- For PFM006489 only 1 day of measuring in the data set for campaign 14.
- For PFM006489 only 1 day of measuring in the data set for campaign 15.
- For PFM006488 only 2 days of measuring in the data set for campaign 15.

Appendix 4

Baseline length variations based on the Bernese formal errors (A4-1–A4-21) and on the RMS (A4-22–A4-42), respectively

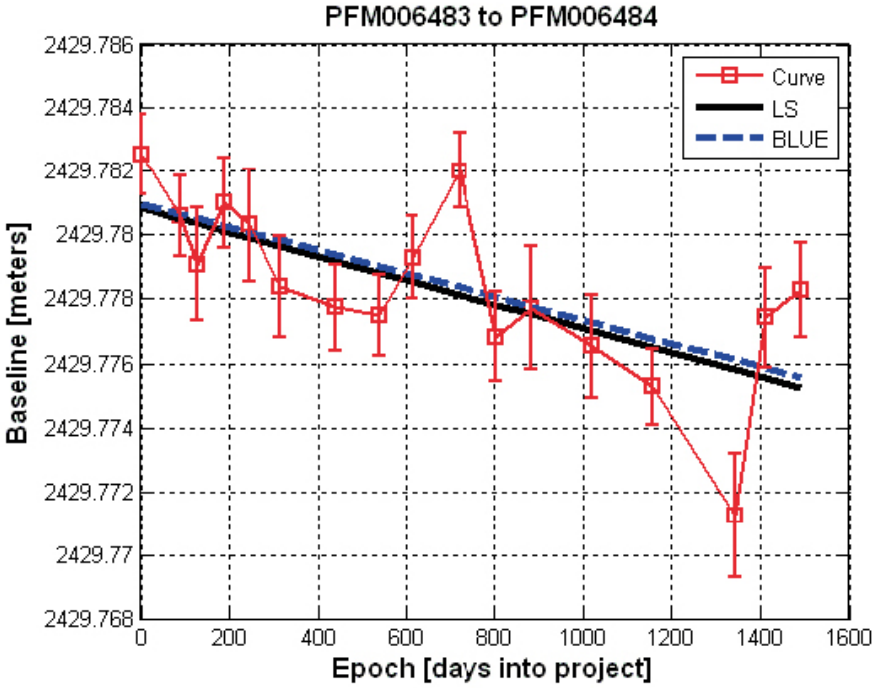

Figure A4-1. *Baseline variations between the stations PFM006483 and PFM006484. For the linear trends the black solid line is the LS estimate and the dashed-blue is the BLUE using Bernese formal errors.*

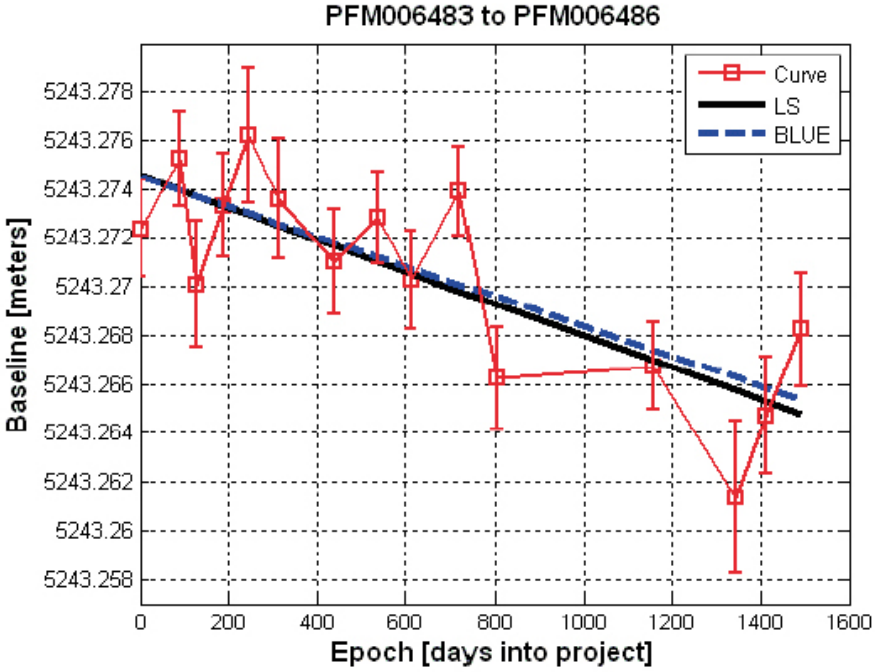

Figure A4-2. *Baseline variations between the stations PFM006483 and PFM006486. For the linear trends the black solid line is the LS estimate and the dashed-blue is the BLUE using Bernese formal errors.*

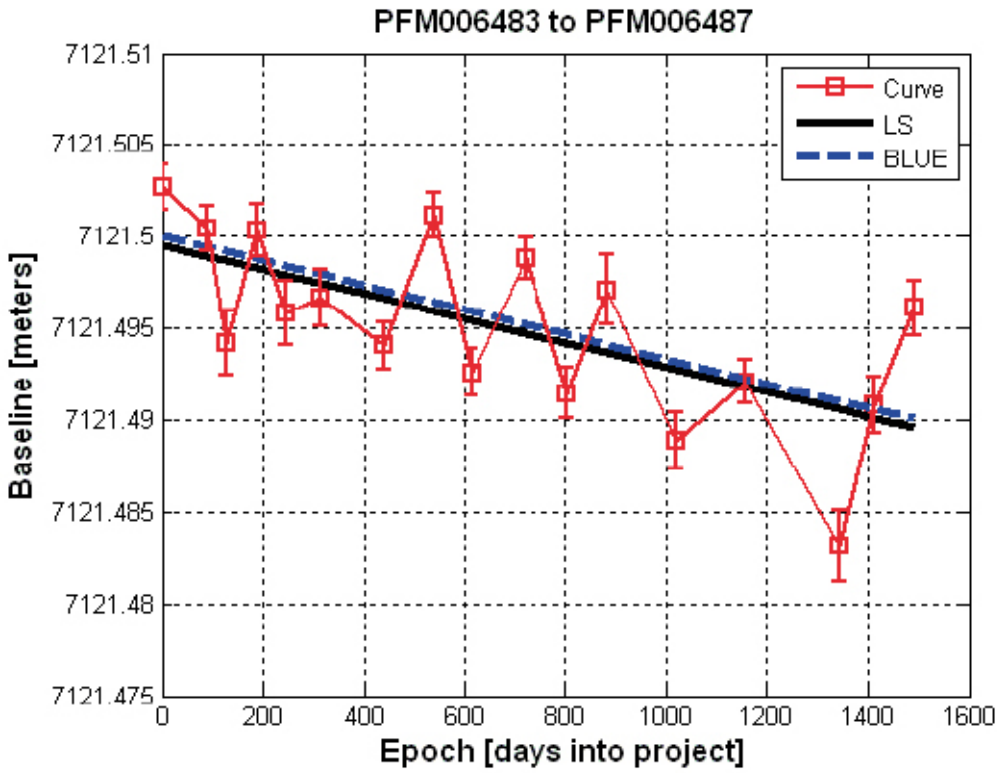

Figure A4-3. *Baseline variations between the stations PFM006483 and PFM006487. For the linear trends the black solid line is the LS estimate and the dashed-blue is the BLUE using Bernese formal errors.*

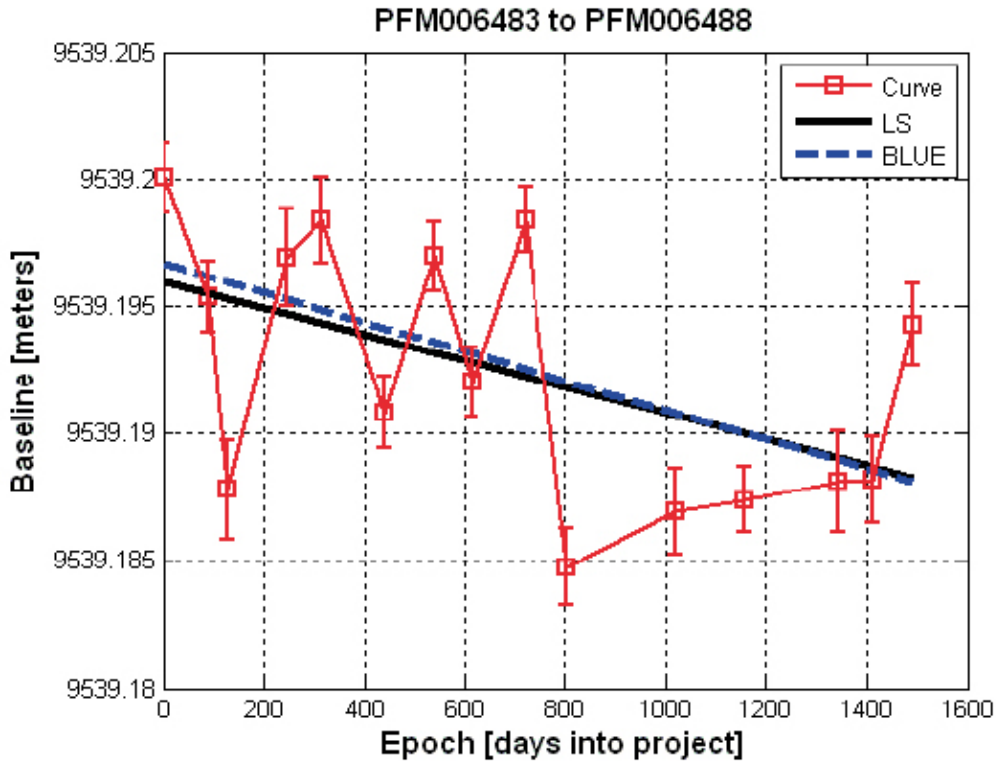

Figure A4-4. *Baseline variations between the stations PFM006483 and PFM006488. For the linear trends the black solid line is the LS estimate and the dashed-blue is the BLUE using Bernese formal errors.*

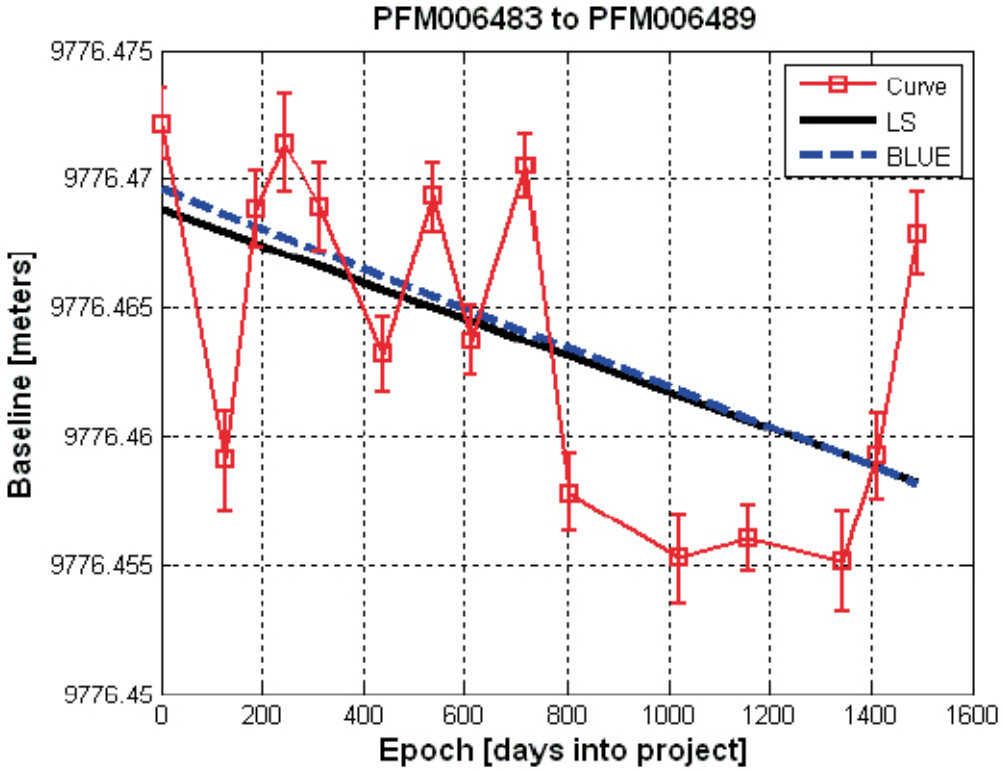

Figure A4-5. *Baseline variations between the stations PFM006483 and PFM006489. For the linear trends the black solid line is the LS estimate and the dashed-blue is the BLUE using Bernese formal errors.*

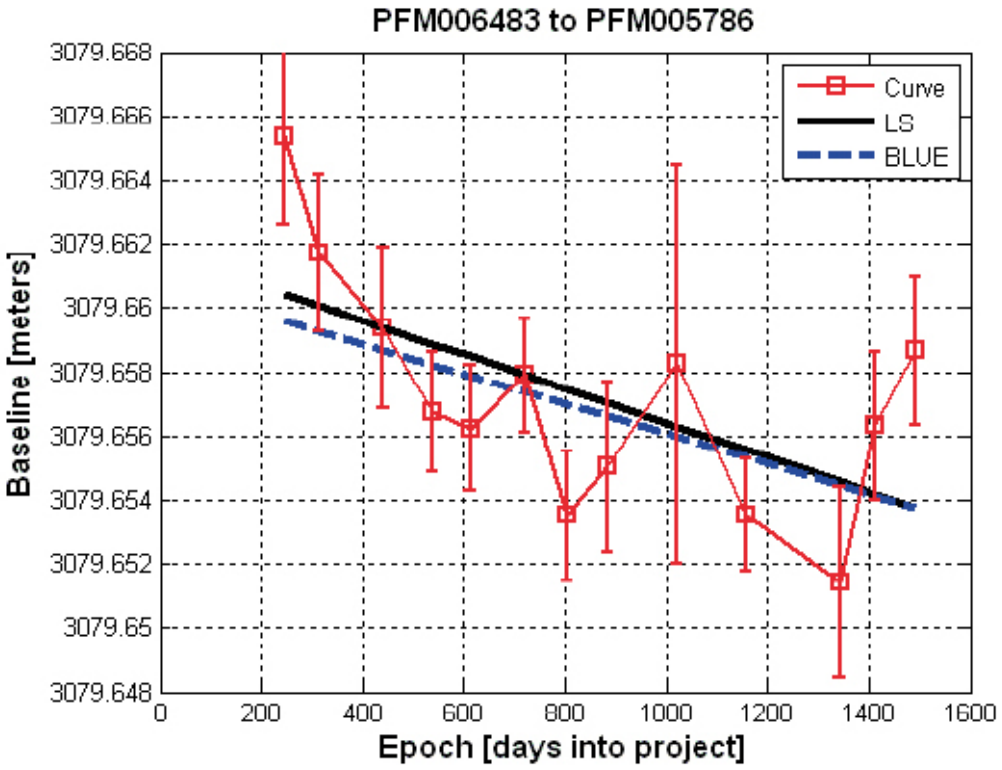

Figure A4-6. *Baseline variations between the stations PFM006483 and PFM005786. For the linear trends the black solid line is the LS estimate and the dashed-blue is the BLUE using Bernese formal errors.*

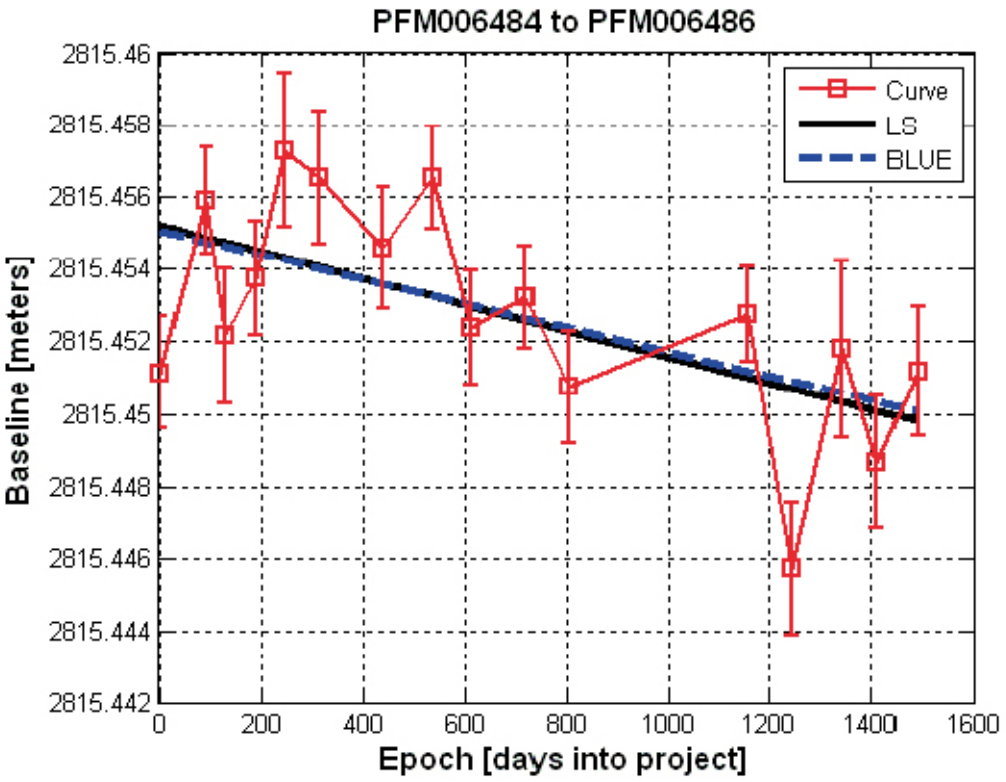

Figure A4-7. *Baseline variations between the stations PFM006484 and PFM006486. For the linear trends the black solid line is the LS estimate and the dashed-blue is the BLUE using Bernese formal errors.*

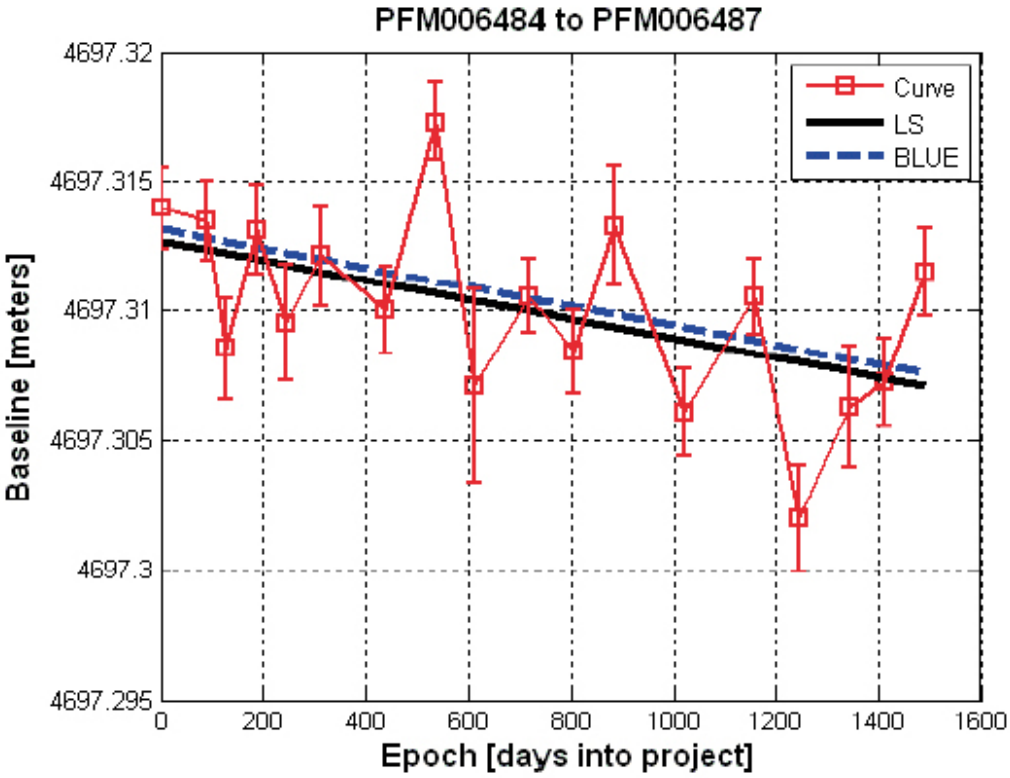

Figure A4-8. *Baseline variations between the stations PFM006484 and PFM006487. For the linear trends the black solid line is the LS estimate and the dashed-blue is the BLUE using Bernese formal errors.*

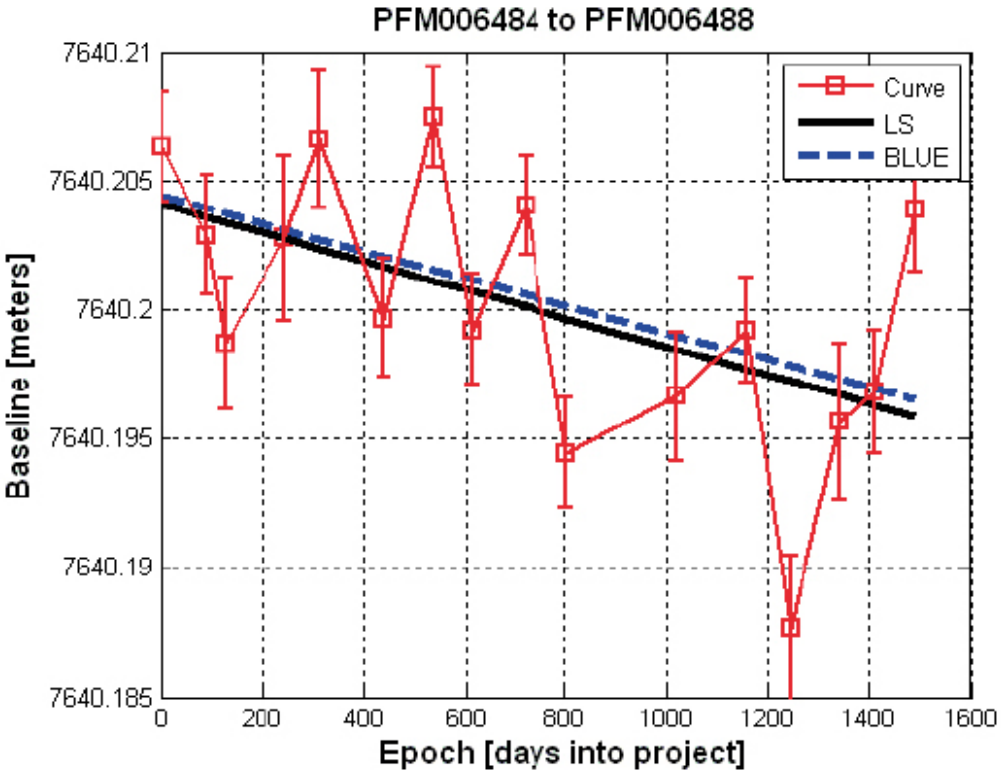

Figure A4-9. *Baseline variations between the stations PFM006484 and PFM006488. For the linear trends the black solid line is the LS estimate and the dashed-blue is the BLUE using Bernese formal errors.*

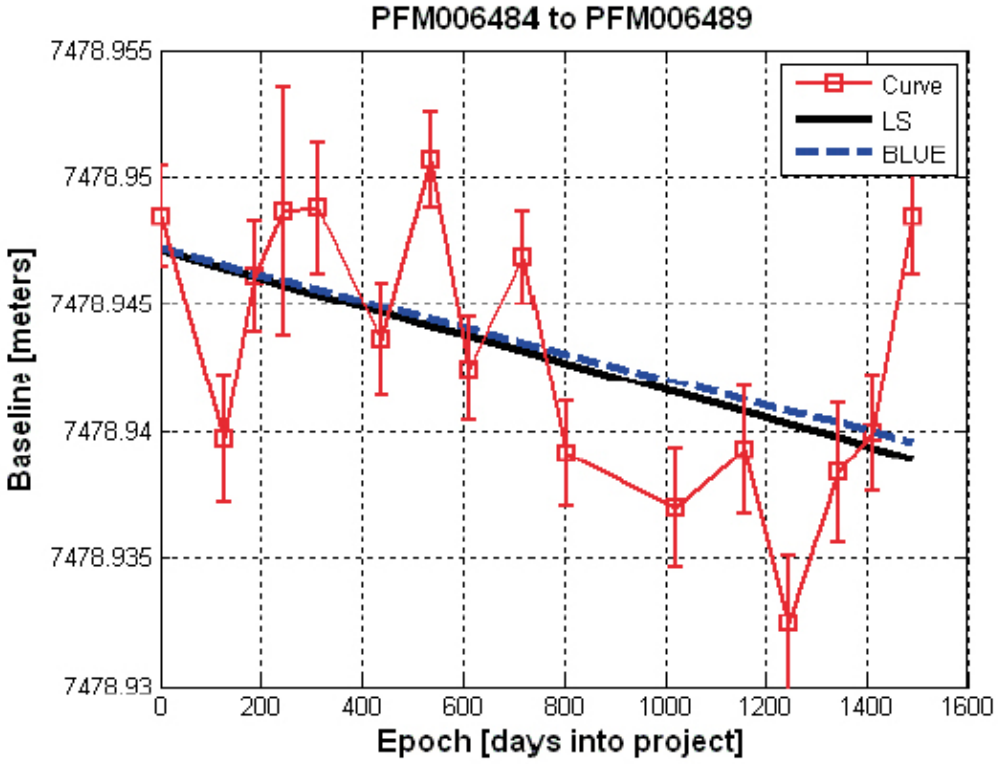

Figure A4-10. *Baseline variations between the stations PFM006484 and PFM006489. For the linear trends the black solid line is the LS estimate and the dashed-blue is the BLUE using Bernese formal errors.*

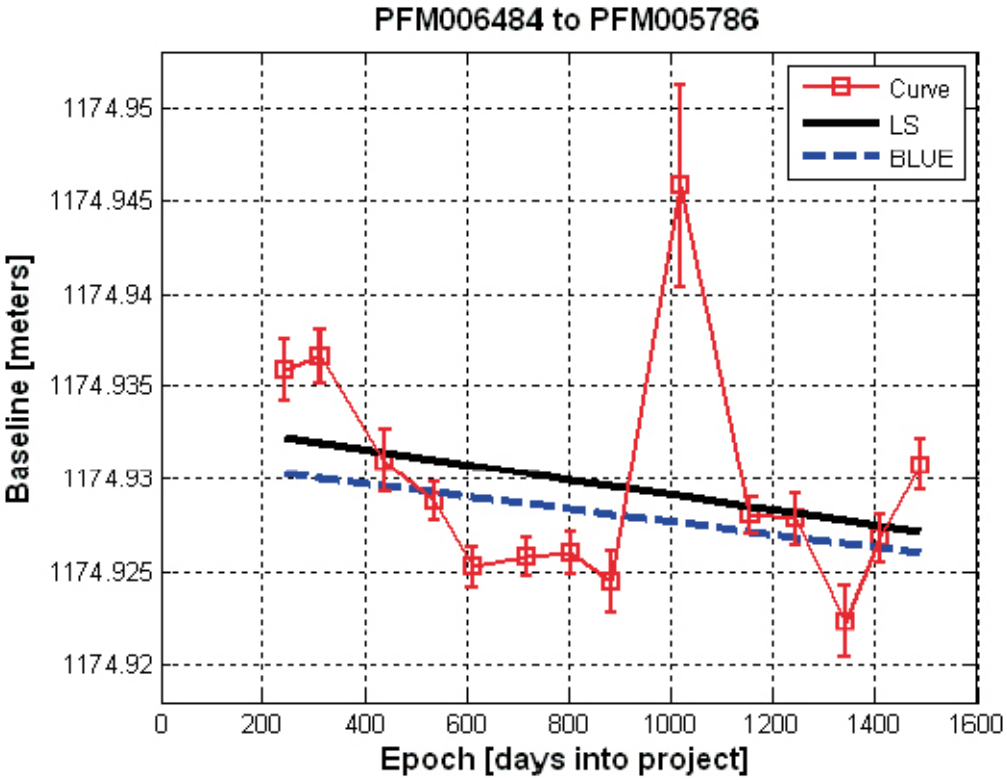

Figure A4-11. *Baseline variations between the stations PFM006484 and PFM005786. For the linear trends the black solid line is the LS estimate and the dashed-blue is the BLUE using Bernese formal errors.*

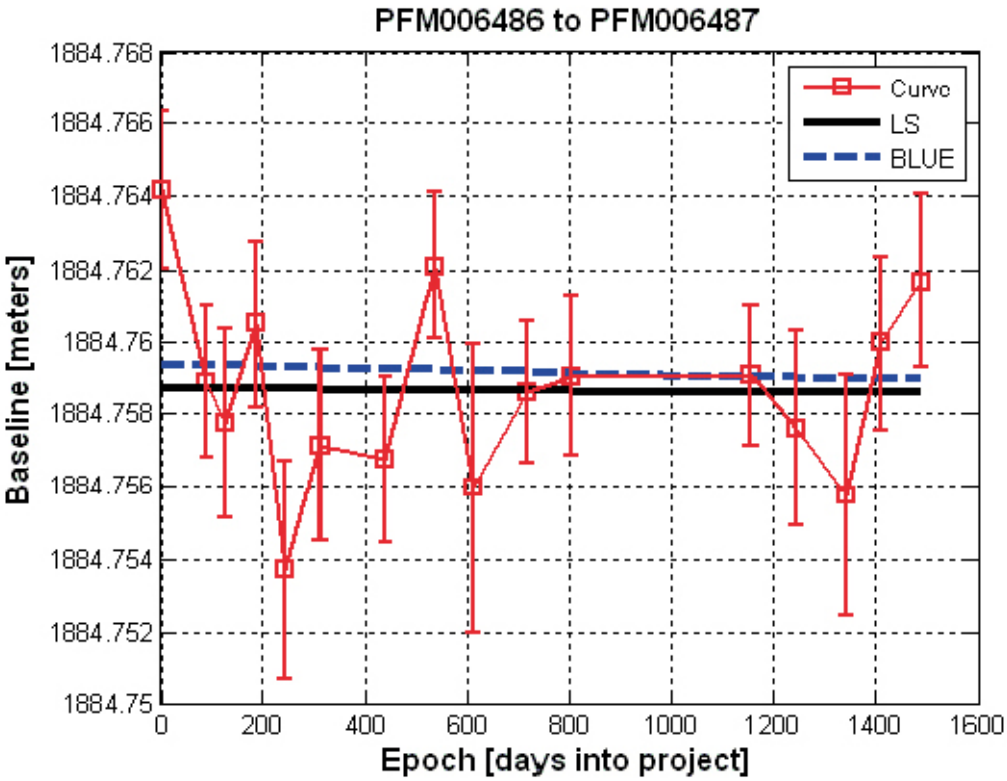

Figure A4-12. *Baseline variations between the stations PFM006486 and PFM006487. For the linear trends the black solid line is the LS estimate and the dashed-blue is the BLUE using Bernese formal errors.*

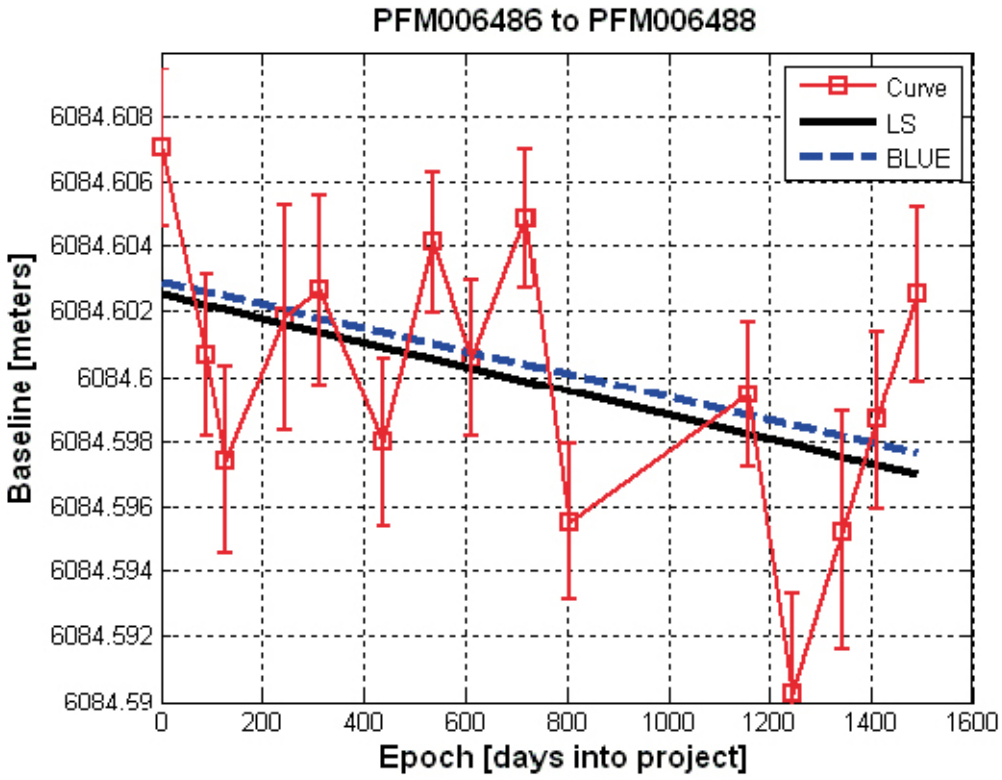

Figure A4-13. *Baseline variations between the stations PFM006486 and PFM006488. For the linear trends the black solid line is the LS estimate and the dashed-blue is the BLUE using Bernese formal errors.*

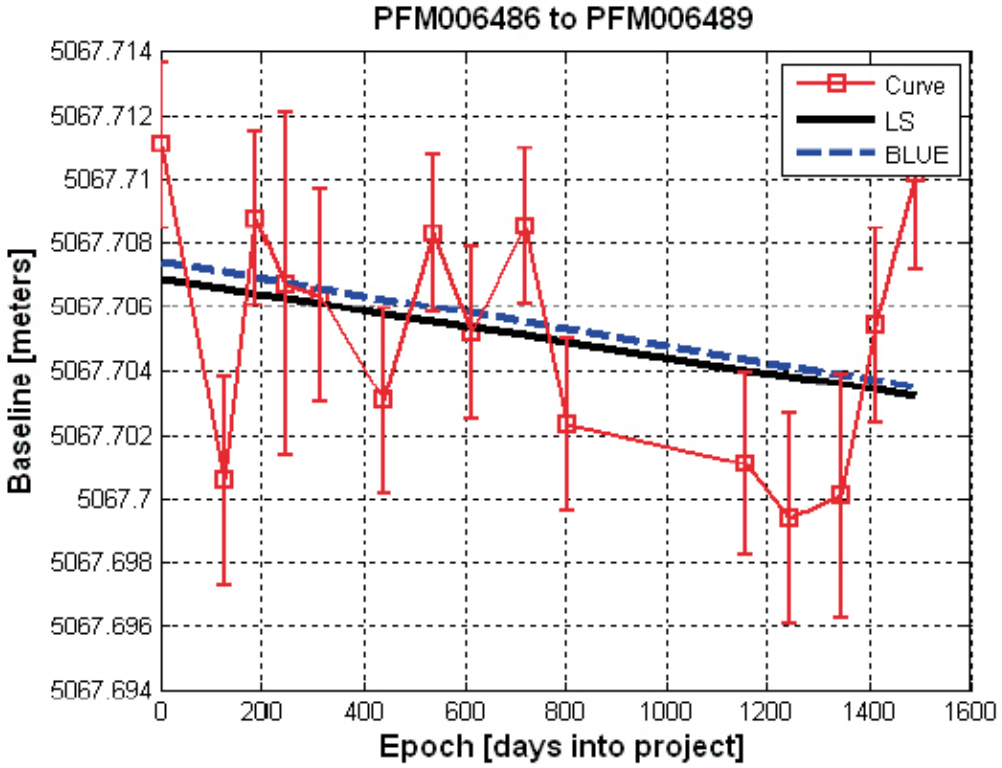

Figure A4-14. *Baseline variations between the stations PFM006486 and PFM006489. For the linear trends the black solid line is the LS estimate and the dashed-blue is the BLUE using Bernese formal errors.*

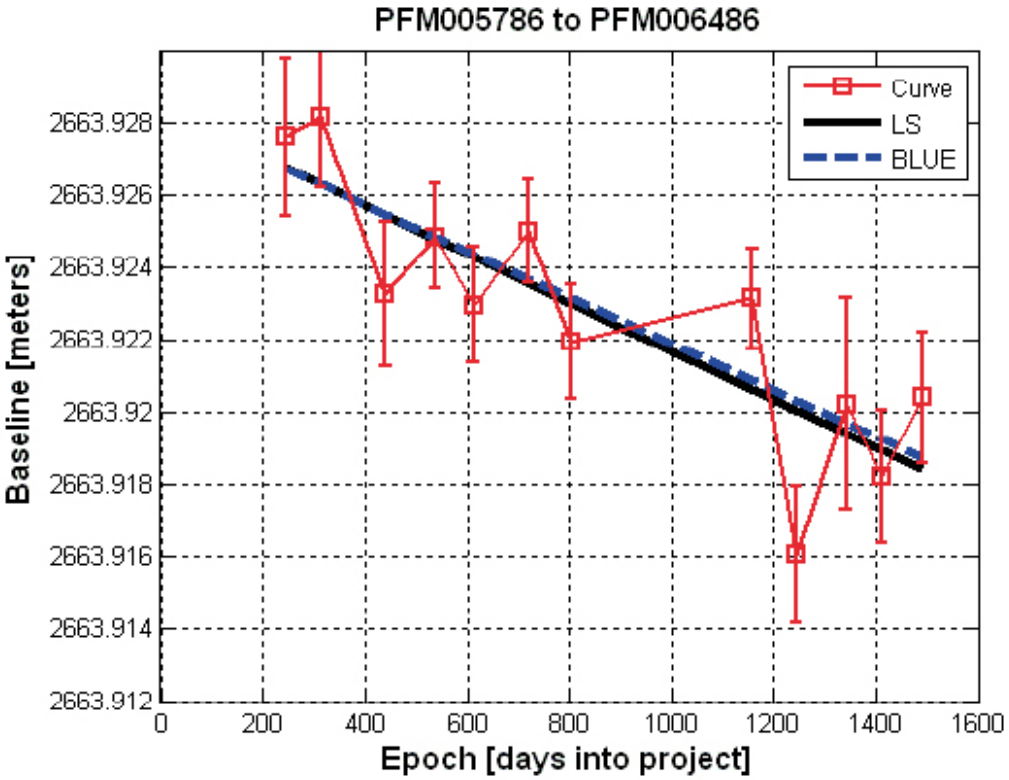

Figure A4-15. *Baseline variations between the stations PFM006486 and PFM005786. For the linear trends the black solid line is the LS estimate and the dashed-blue is the BLUE using Bernese formal errors.*

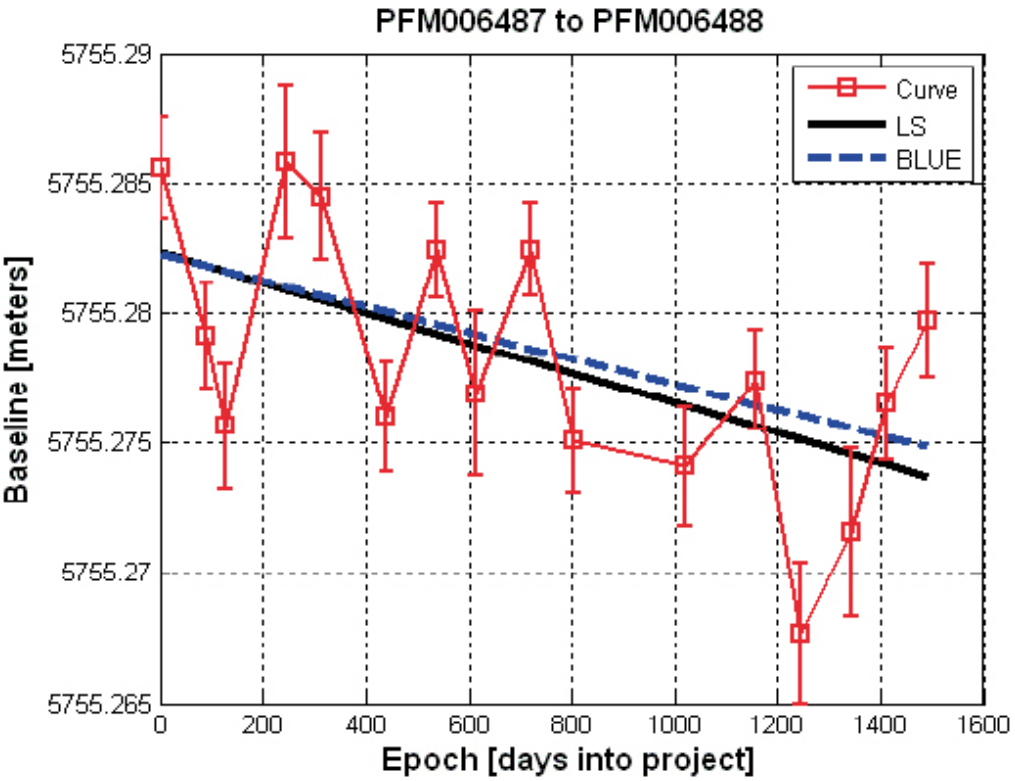

Figure A4-16. *Baseline variations between the stations PFM006487 and PFM006488. For the linear trends the black solid line is the LS estimate and the dashed-blue is the BLUE using Bernese formal errors.*

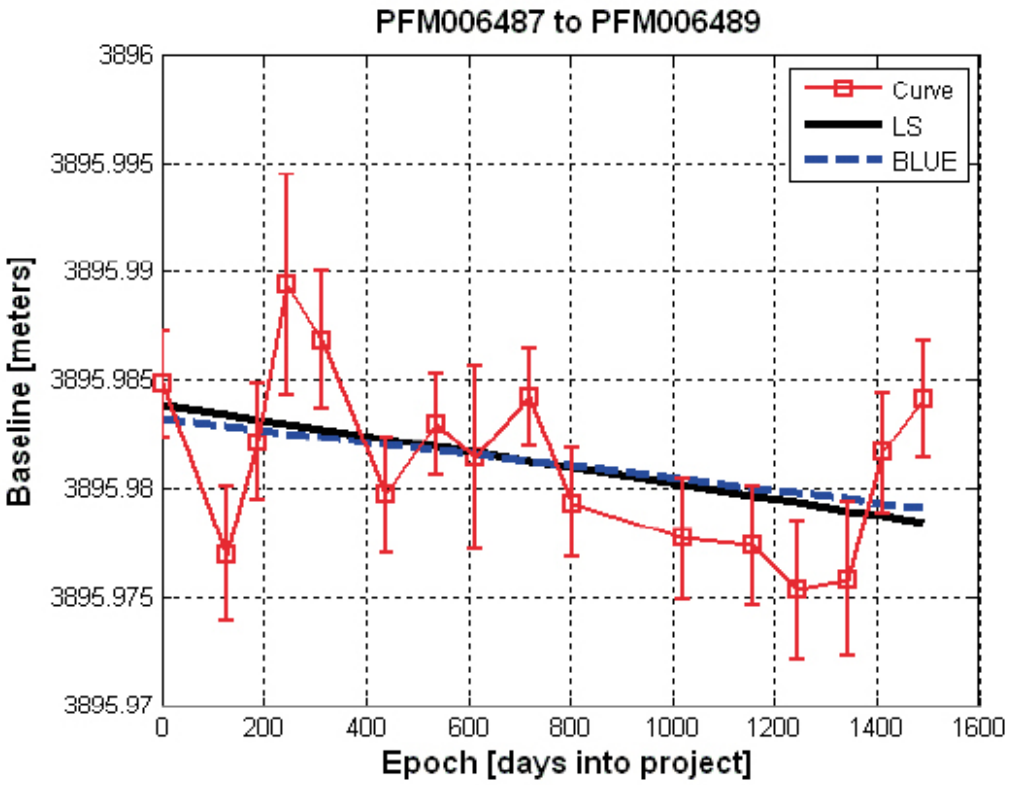

Figure A4-17. *Baseline variations between the stations PFM006487 and PFM006489. For the linear trends the black solid line is the LS estimate and the dashed-blue is the BLUE using Bernese formal errors.*

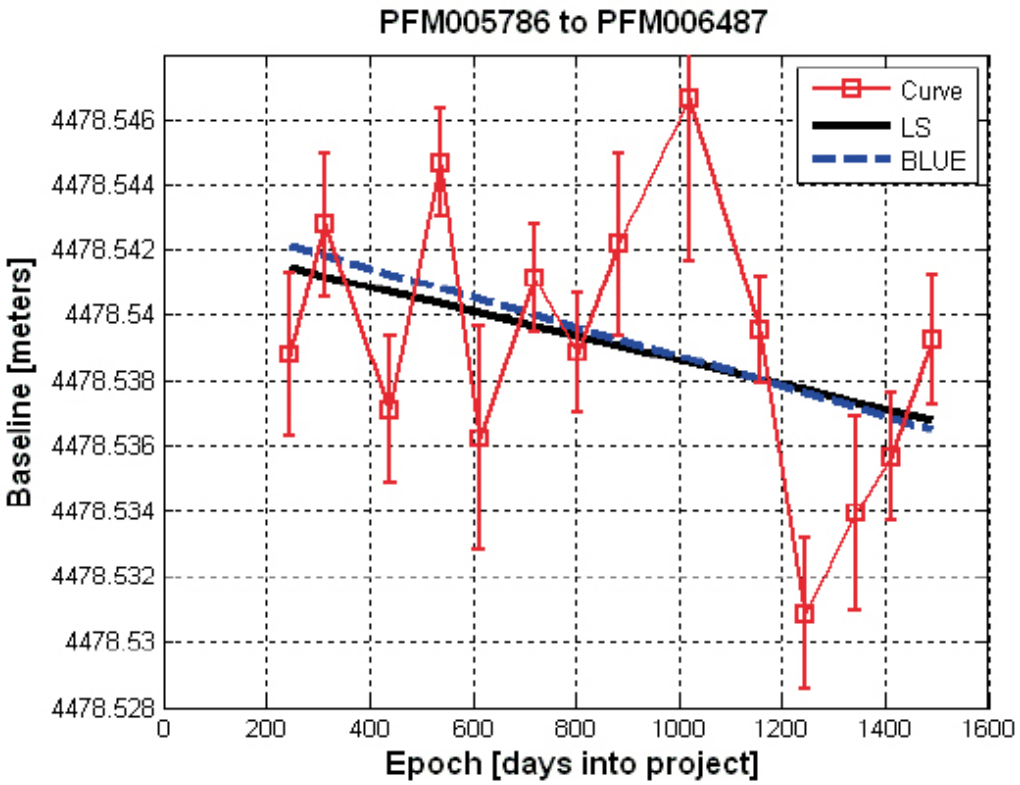

Figure A4-18. *Baseline variations between the stations PFM006487 and PFM005786. For the linear trends the black solid line is the LS estimate and the dashed-blue is the BLUE using Bernese formal errors.*

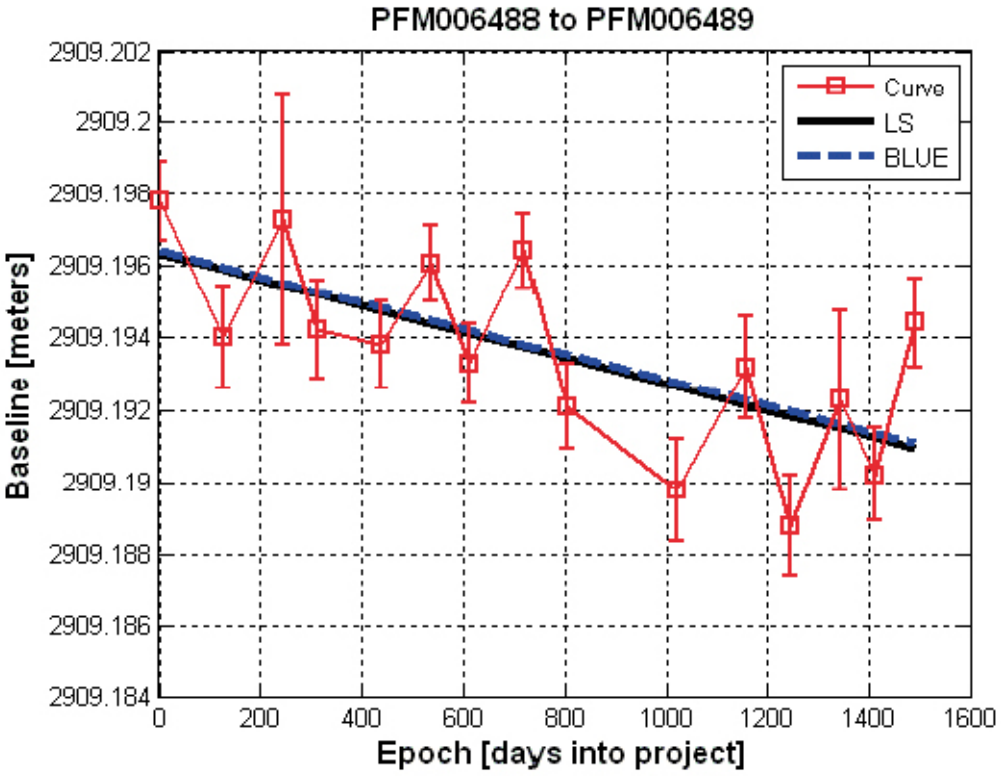

Figure A4-19. *Baseline variations between the stations PFM006488 and PFM006489. For the linear trends the black solid line is the LS estimate and the dashed-blue is the BLUE using Bernese formal errors.*

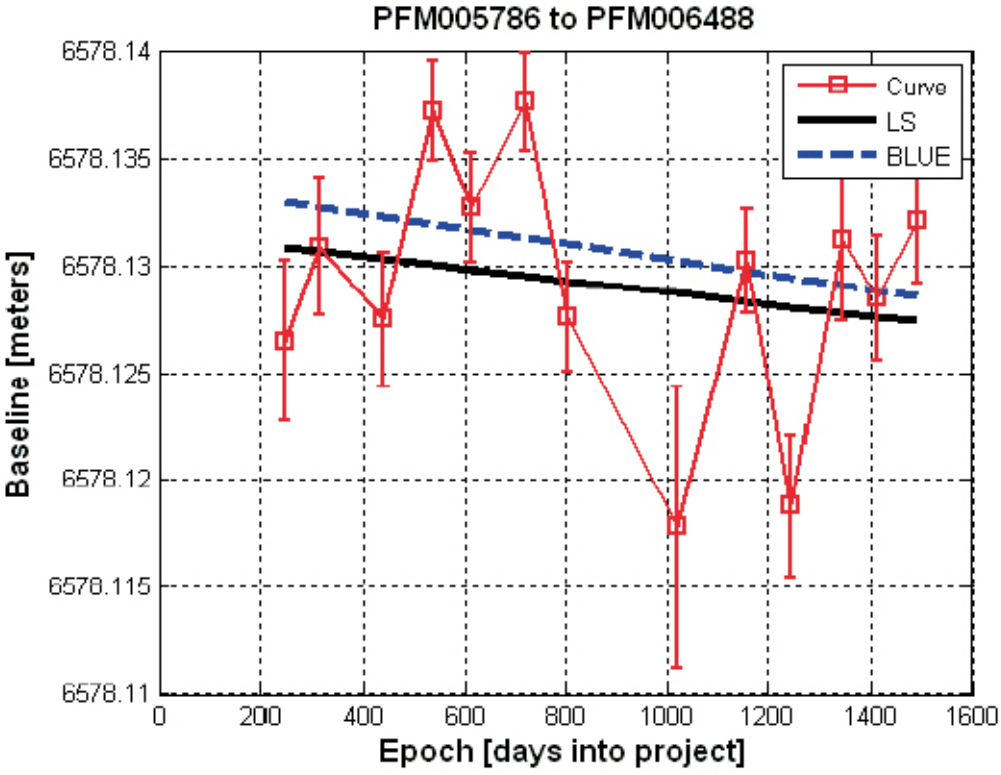

Figure A4-20. *Baseline variations between the stations PFM006488 and PFM005786. For the linear trends the black solid line is the LS estimate and the dashed-blue is the BLUE using Bernese formal errors.*

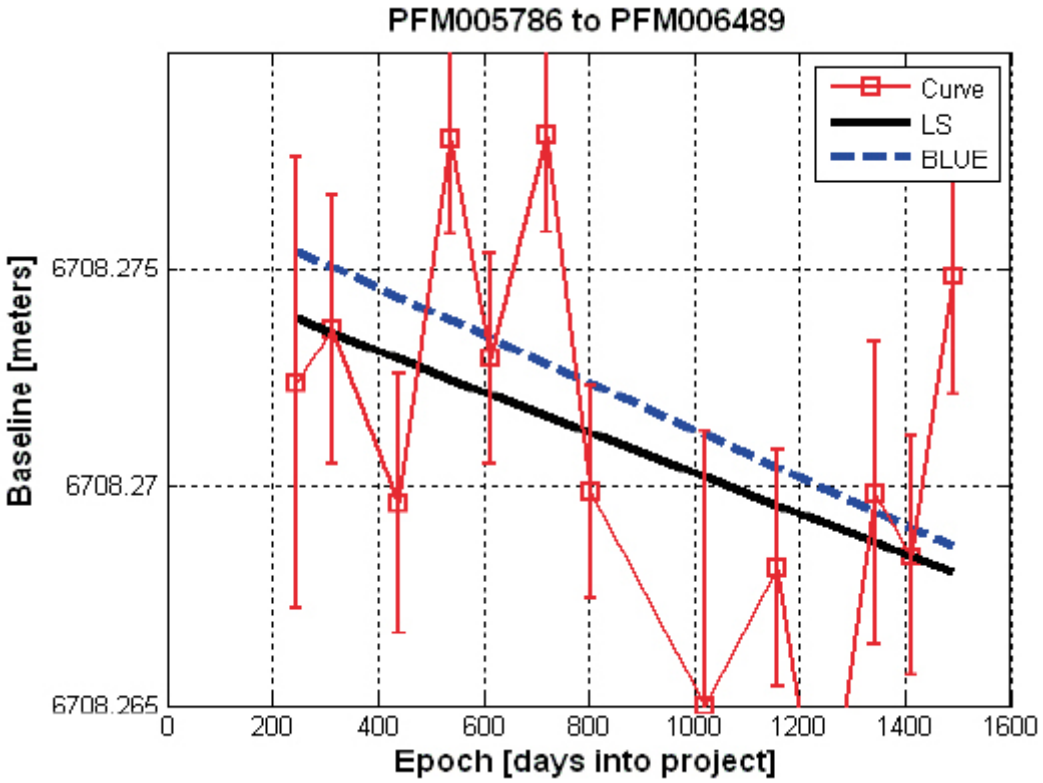

Figure A4-21. *Baseline variations between the stations PFM006489 and PFM005786. For the linear trends the black solid line is the LS estimate and the dashed-blue is the BLUE using Bernese formal errors.*

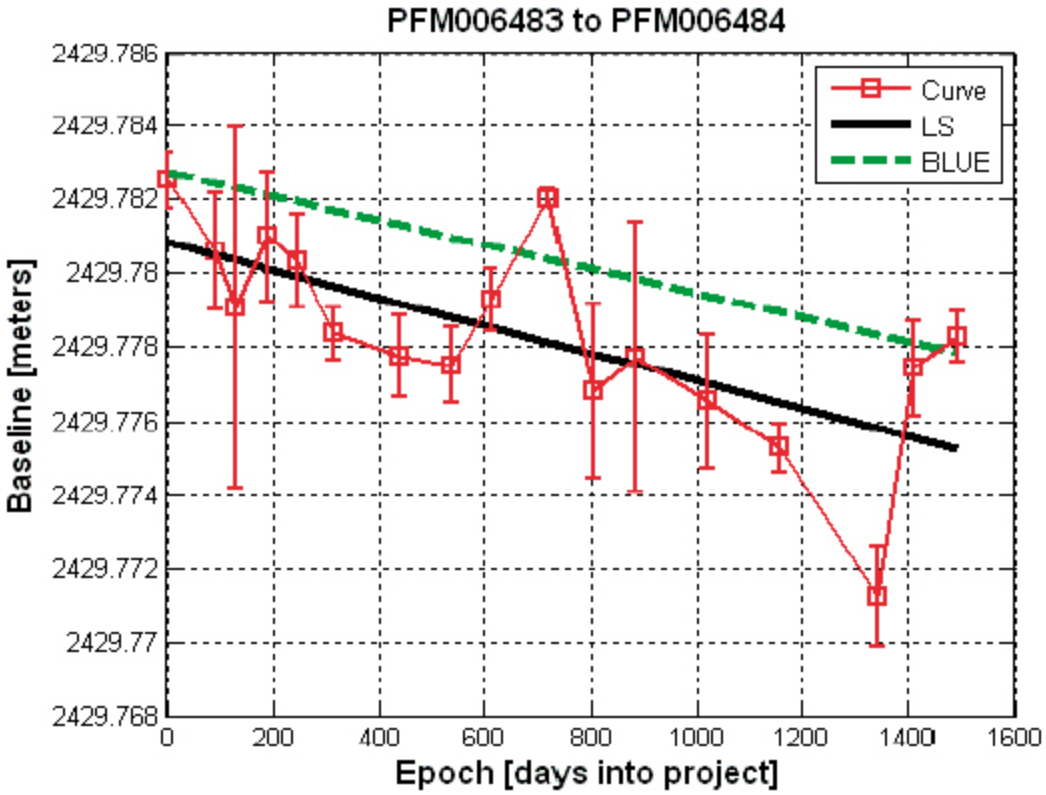

Figure A4-22. *Baseline variations between the stations PFM006483 and PFM006484. For the linear trends the black solid line is the LS estimate and the dashed-green is the BLUE using RMS.*

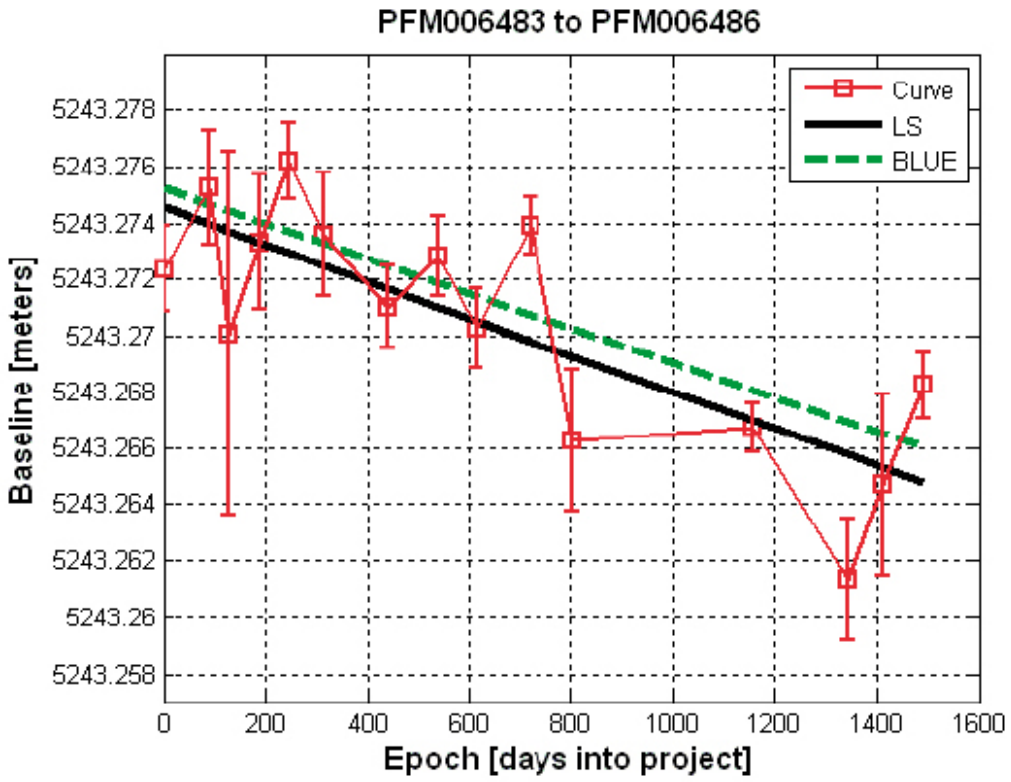

Figure A4-23. *Baseline variations between the stations PFM006483 and PFM006486. For the linear trends the black solid line is the LS estimate and the dashed-green is the BLUE using RMS.*

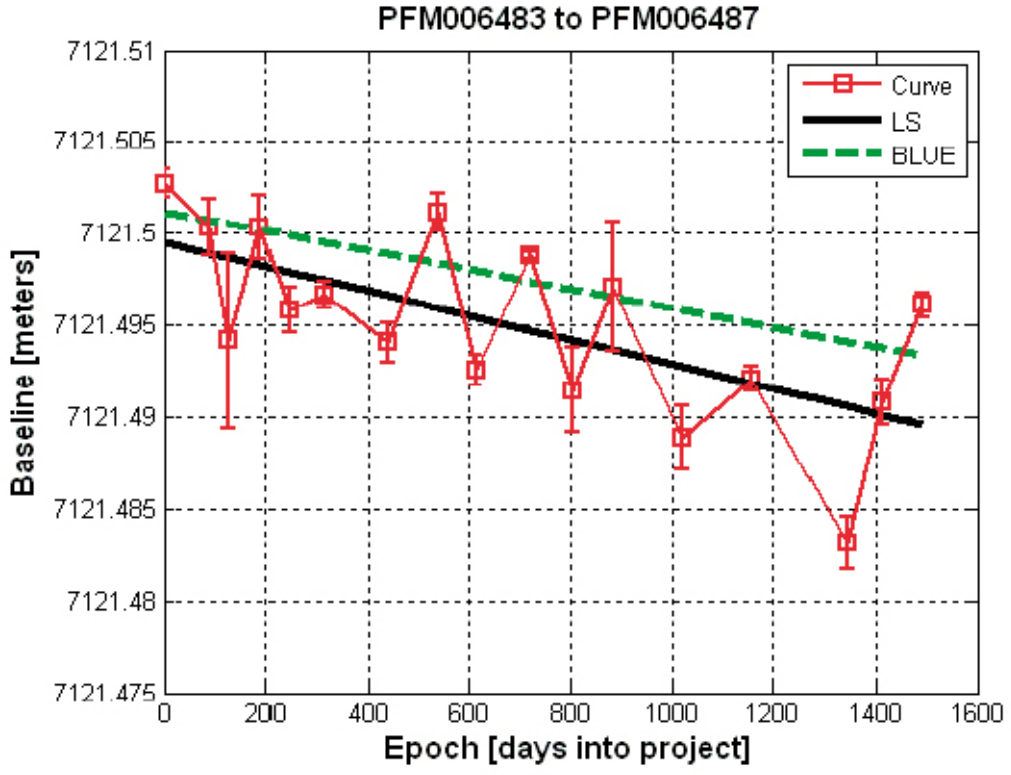

Figure A4-24. *Baseline variations between the stations PFM006483 and PFM006487. For the linear trends the black solid line is the LS estimate and the dashed-green is the BLUE using RMS.*

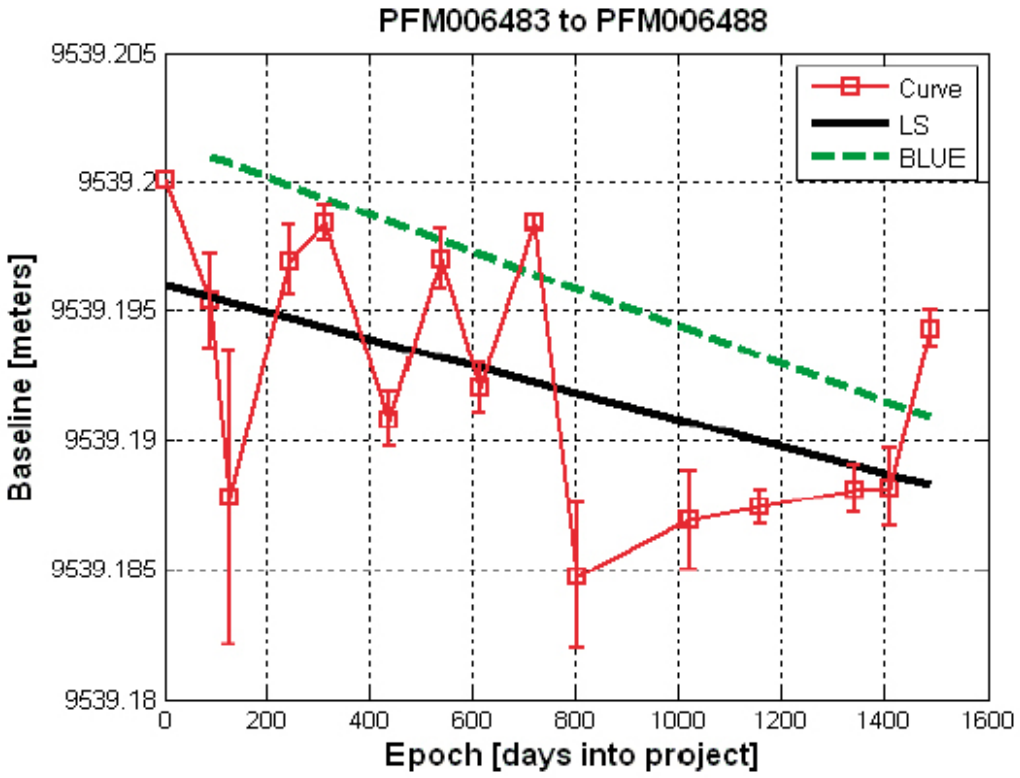

Figure A4-25. *Baseline variations between the stations PFM006483 and PFM006488. For the linear trends the black solid line is the LS estimate and the dashed-green is the BLUE using RMS.*

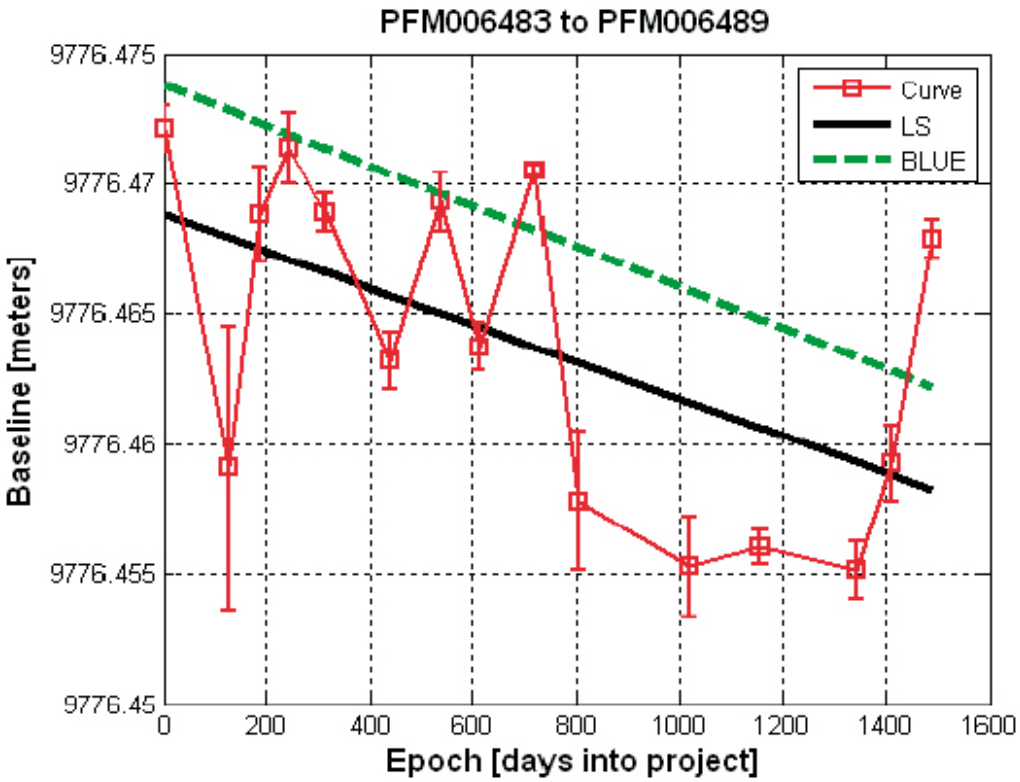

Figure A4-26. *Baseline variations between the stations PFM006483 and PFM006489. For the linear trends the black solid line is the LS estimate and the dashed-green is the BLUE using RMS.*

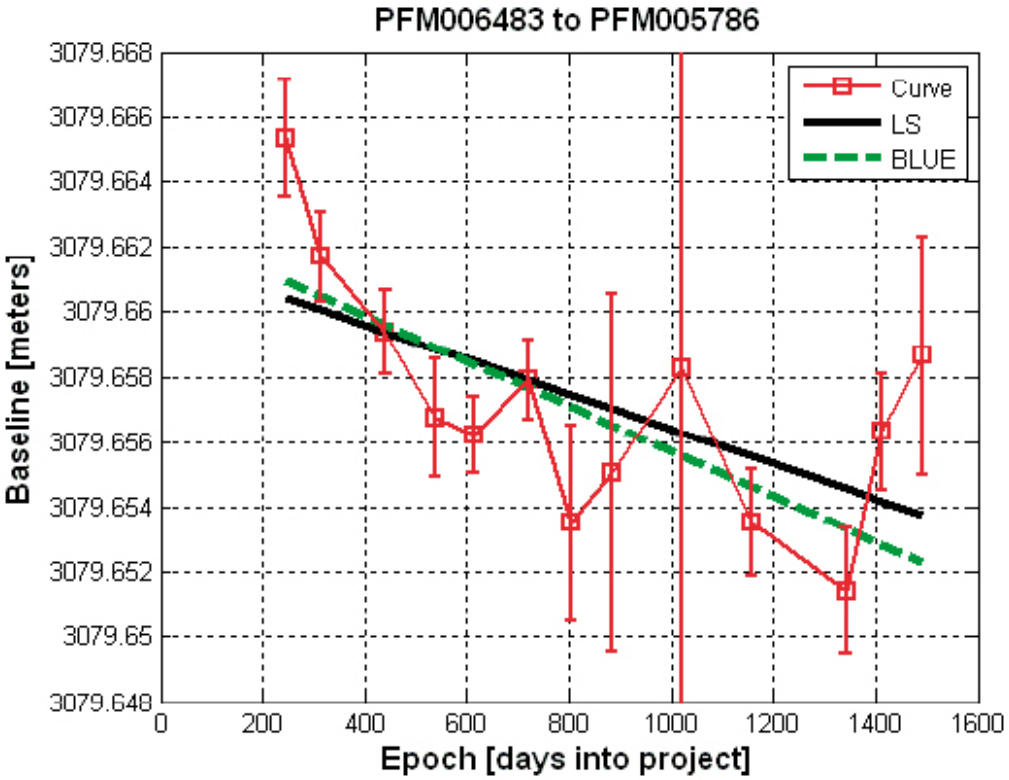

Figure A4-27. *Baseline variations between the stations PFM006483 and PFM005786. For the linear trends the black solid line is the LS estimate and the dashed-green is the BLUE using RMS.*

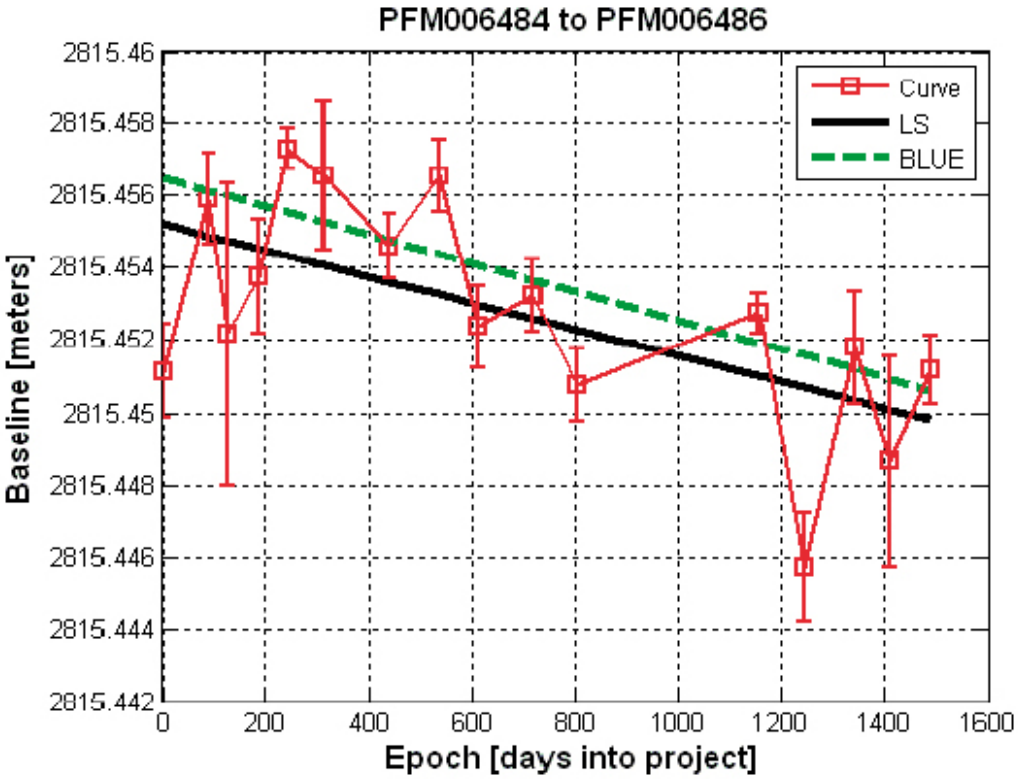

Figure A4-28. *Baseline variations between the stations PFM006484 and PFM006486. For the linear trends the black solid line is the LS estimate and the dashed-green is the BLUE using RMS.*

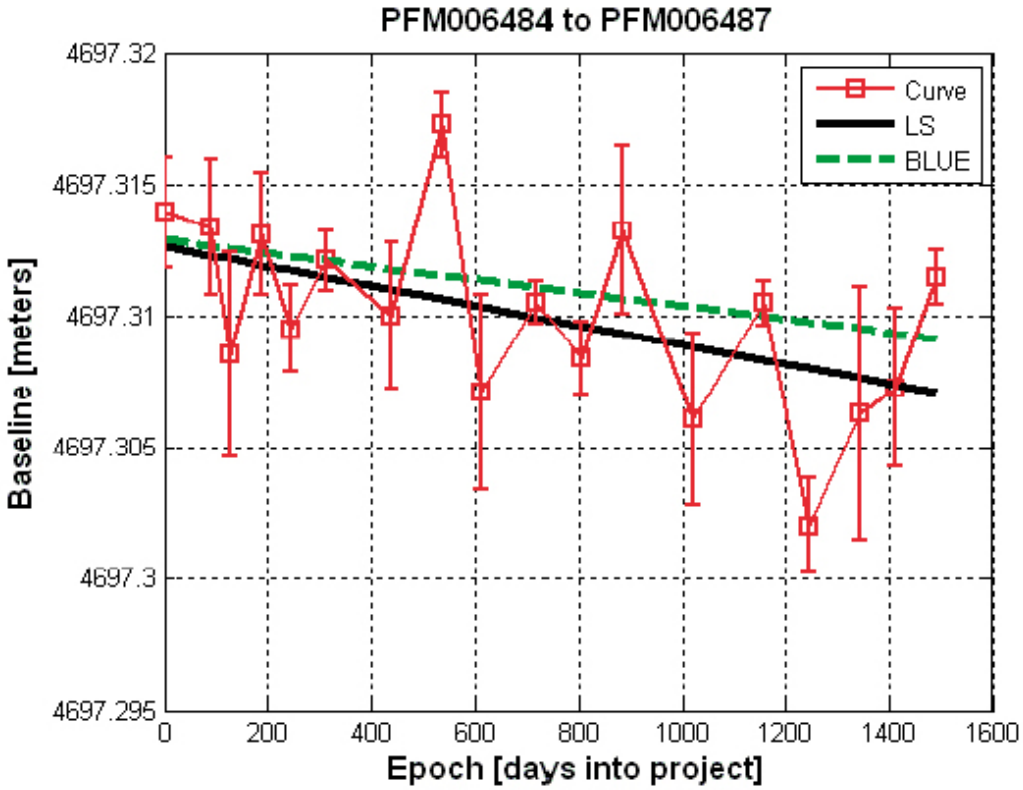

Figure A4-29. *Baseline variations between the stations PFM006484 and PFM006487. For the linear trends the black solid line is the LS estimate and the dashed-green is the BLUE using RMS.*

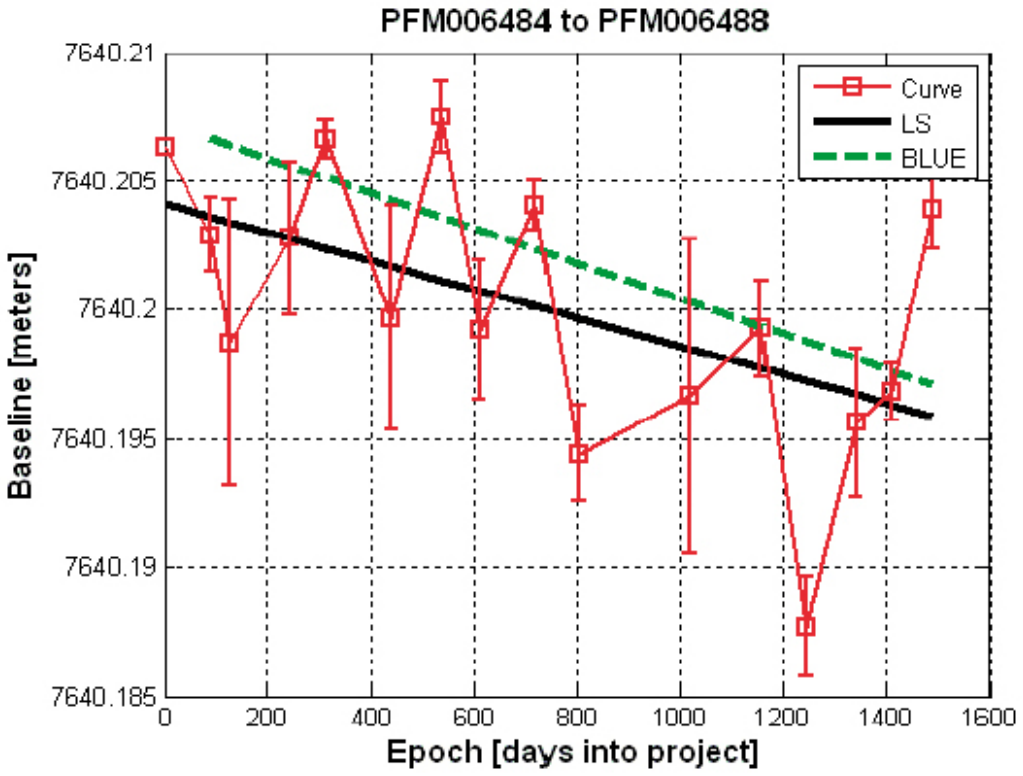

Figure A4-30. *Baseline variations between the stations PFM006484 and PFM006488. For the linear trends the black solid line is the LS estimate and the dashed-green is the BLUE using RMS.*

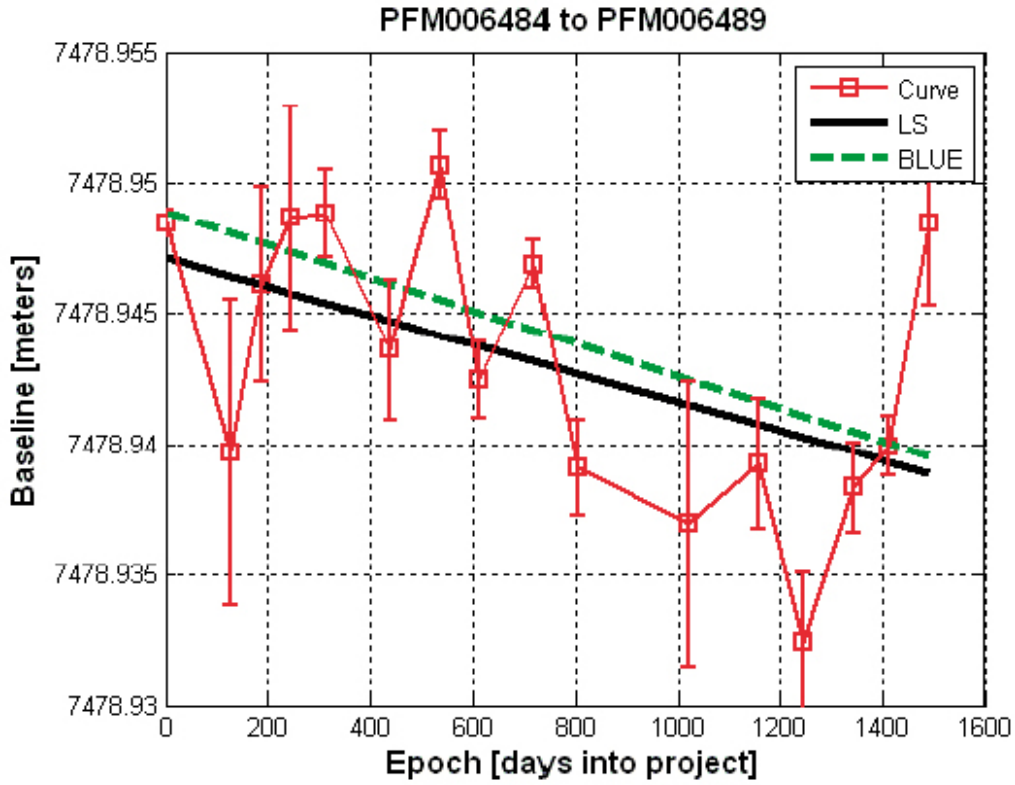

Figure A4-31. *Baseline variations between the stations PFM006484 and PFM006489. For the linear trends the black solid line is the LS estimate and the dashed-green is the BLUE using RMS.*

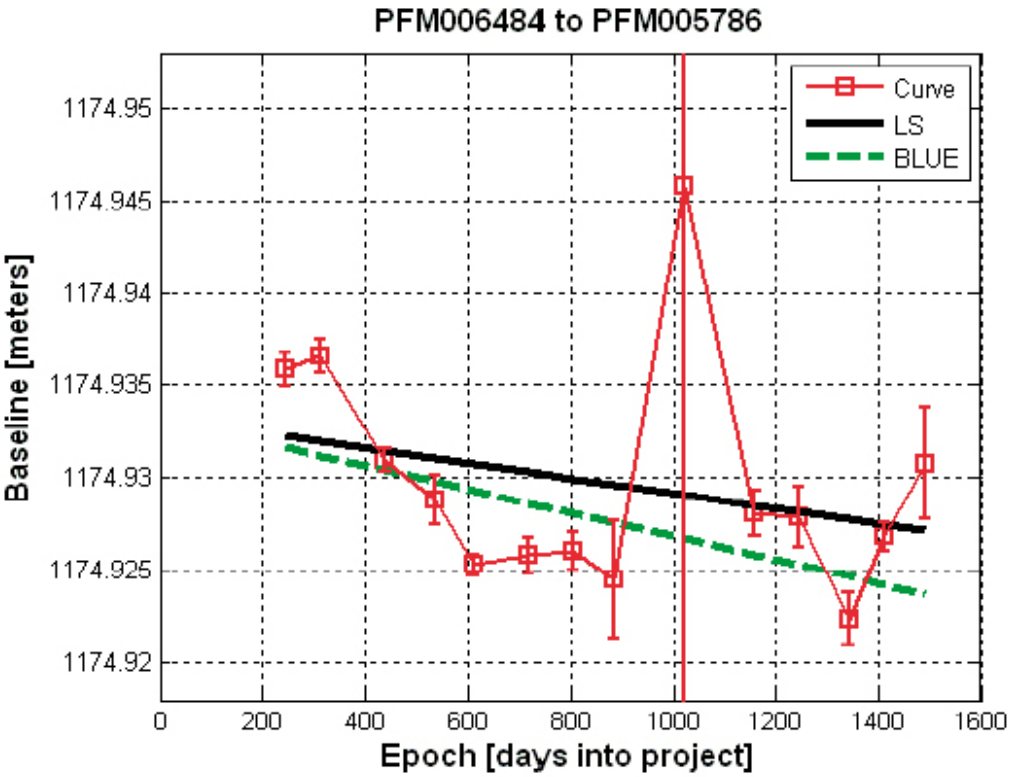

Figure A4-32. *Baseline variations between the stations PFM006484 and PFM005786. For the linear trends the black solid line is the LS estimate and the dashed-green is the BLUE using RMS.*

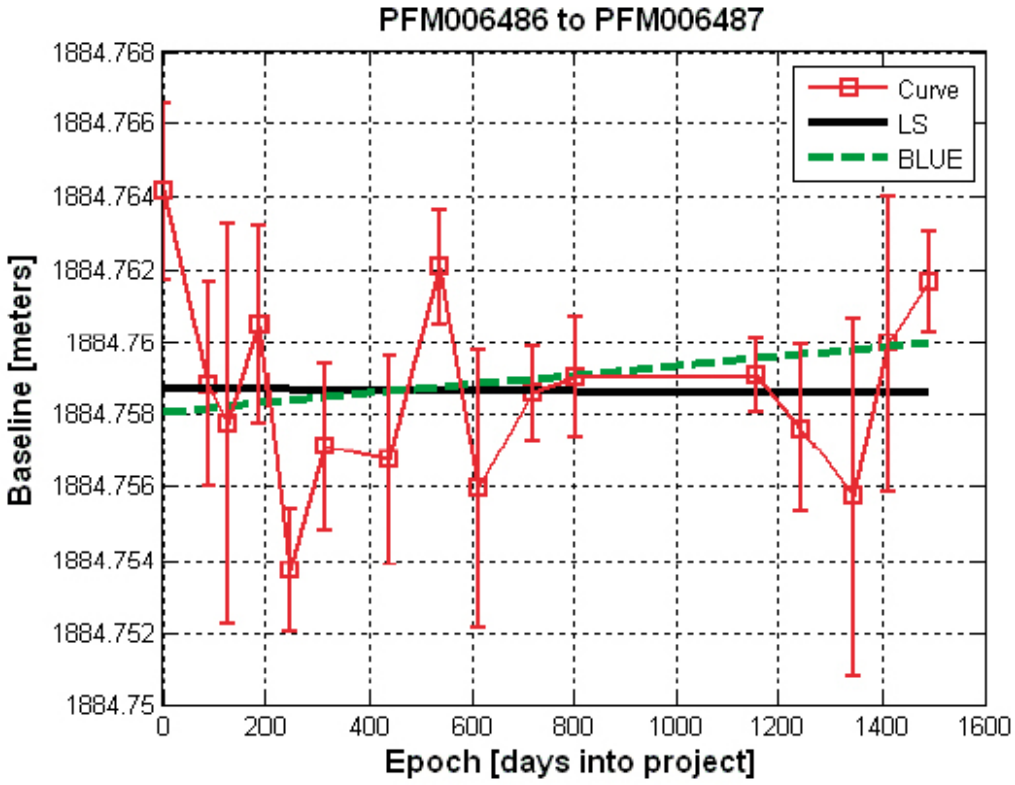

Figure A4-33. *Baseline variations between the stations PFM006486 and PFM006487. For the linear trends the black solid line is the LS estimate and the dashed-green is the BLUE using RMS.*

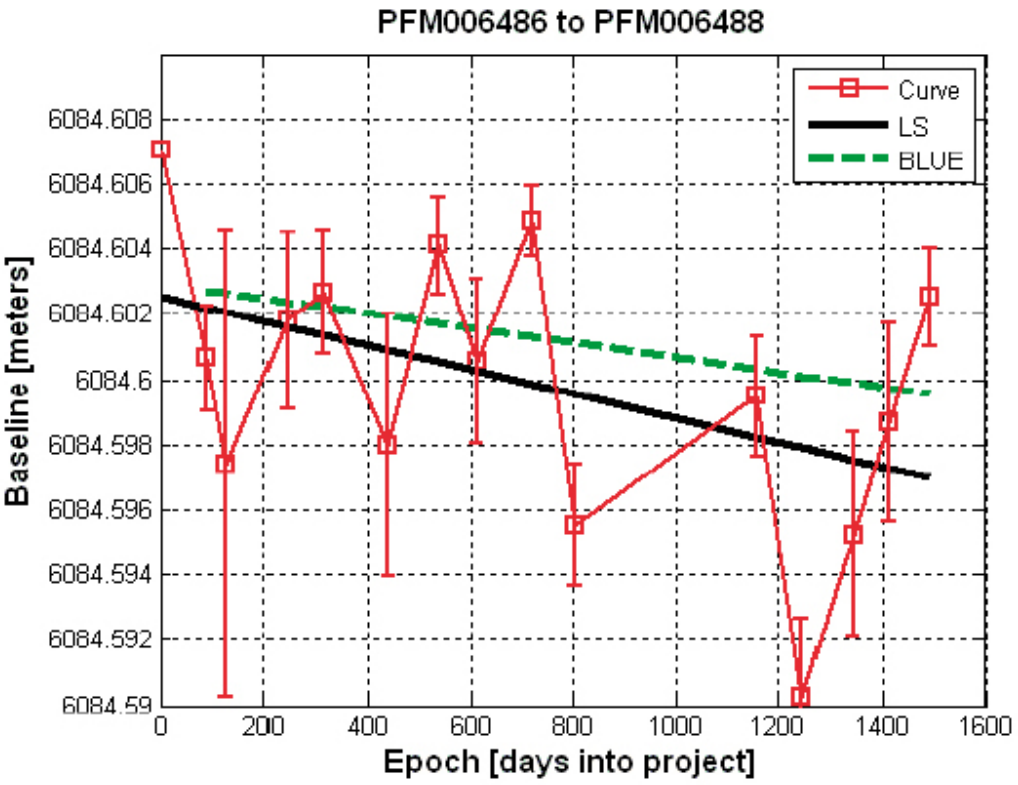

Figure A4-34. *Baseline variations between the stations PFM006486 and PFM006488. For the linear trends the black solid line is the LS estimate and the dashed-green is the BLUE using RMS.*

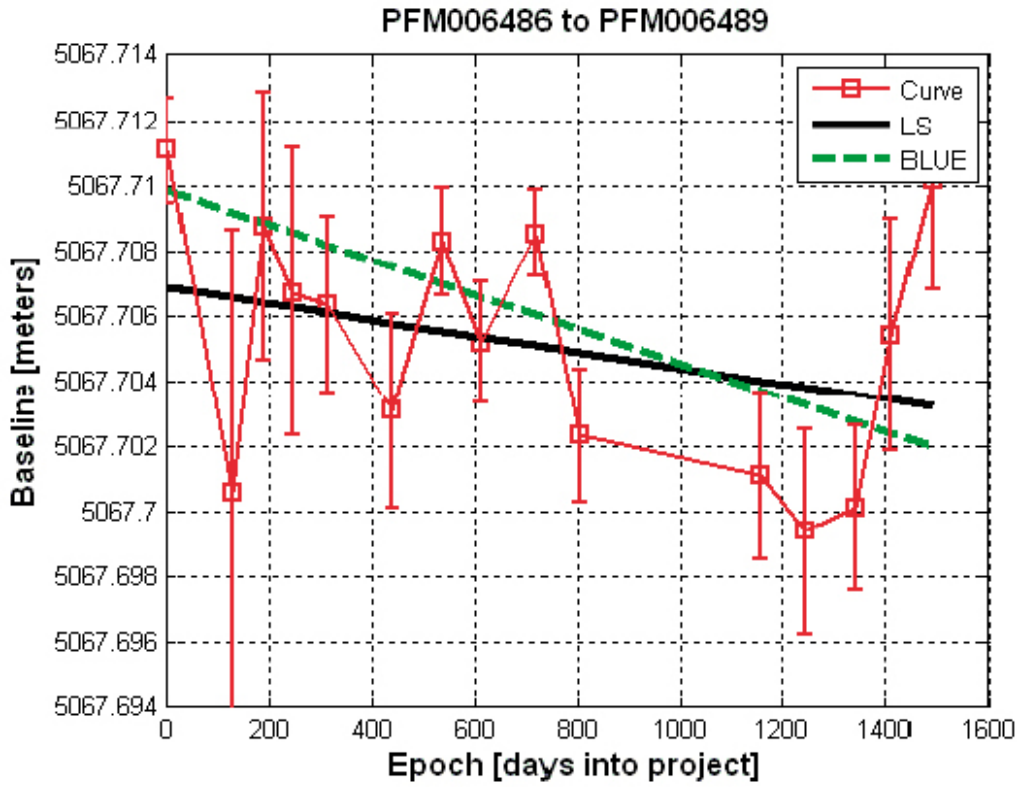

Figure A4-35. *Baseline variations between the stations PFM006486 and PFM006489. For the linear trends the black solid line is the LS estimate and the dashed-green is the BLUE using RMS.*

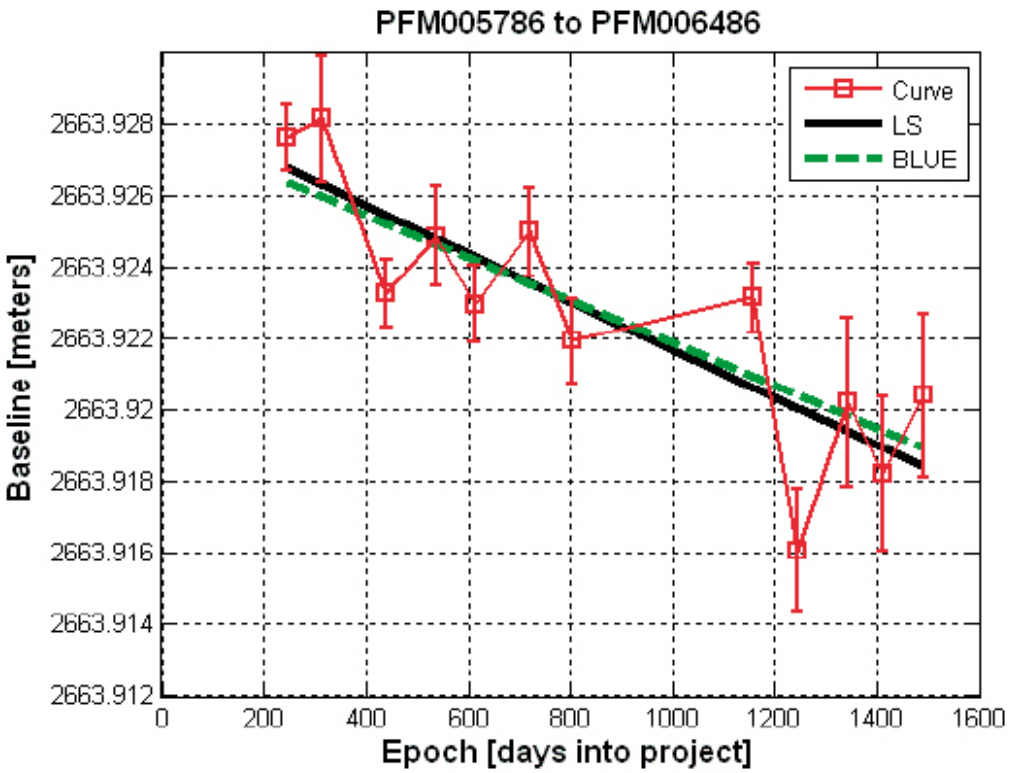

Figure A2-36. *Baseline variations between the stations PFM006486 and PFM005786. For the linear trends the black solid line is the LS estimate and the dashed-greenis the BLUE using RMS.*

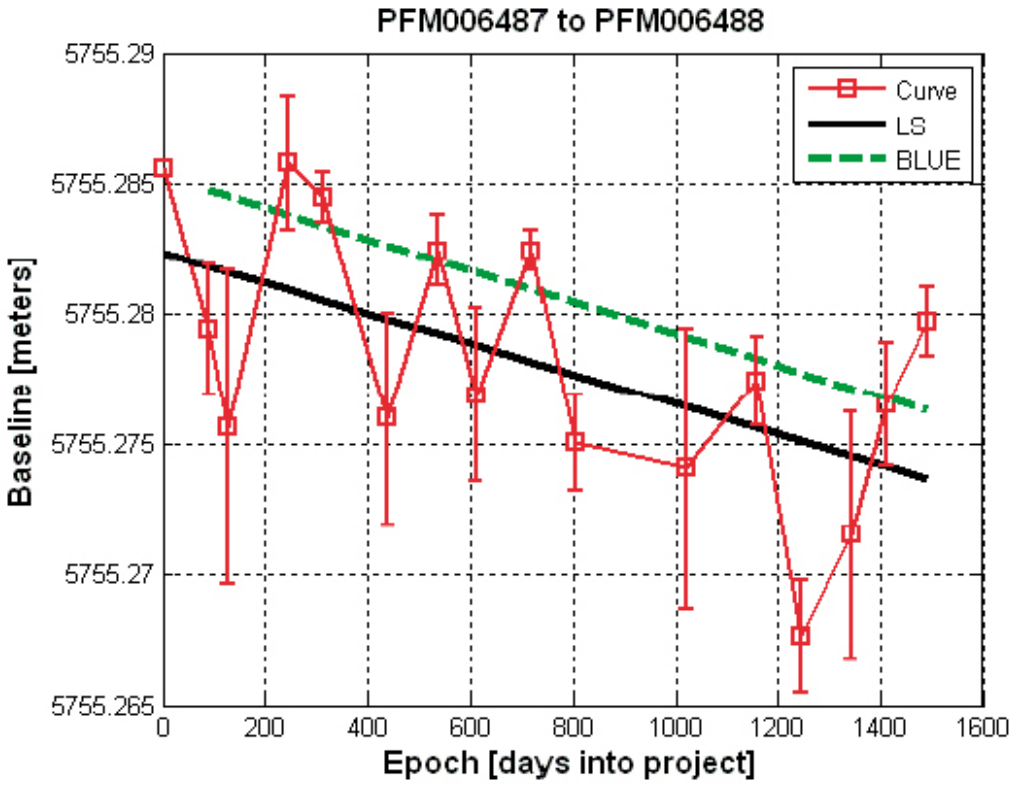

Figure A4-37. *Baseline variations between the stations PFM006487 and PFM006488. For the linear trends the black solid line is the LS estimate and the dashed-green is the BLUE using RMS.*

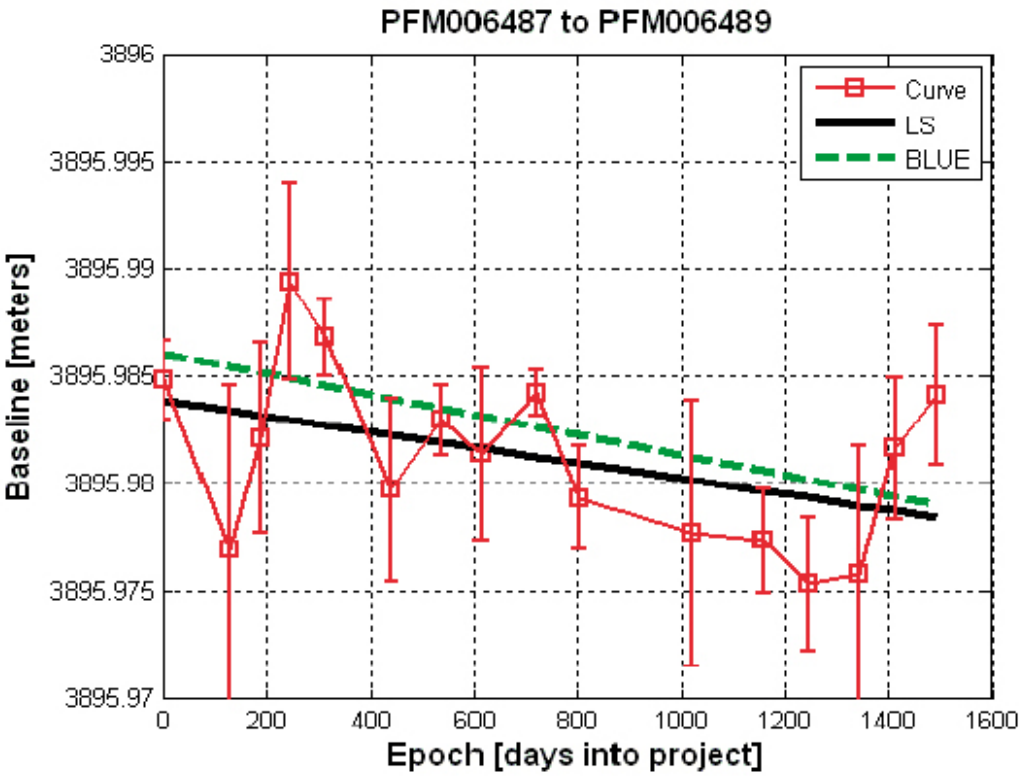

Figure A4-38. *Baseline variations between the stations PFM006487 and PFM006489. For the linear trends the black solid line is the LS estimate and the dashed-green is the BLUE using RMS.*

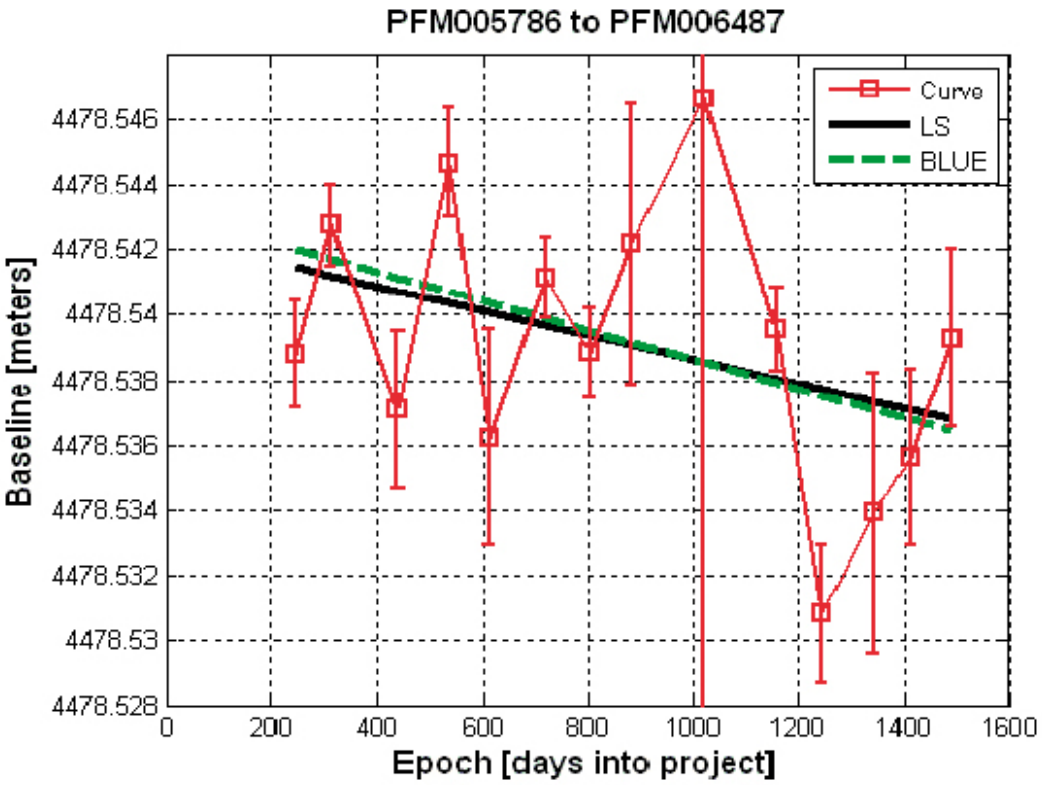

Figure A2-39. *Baseline variations between the stations PFM006487 and PFM005786. For the linear trends the black solid line is the LS estimate and the dashed-green is the BLUE using RMS.*

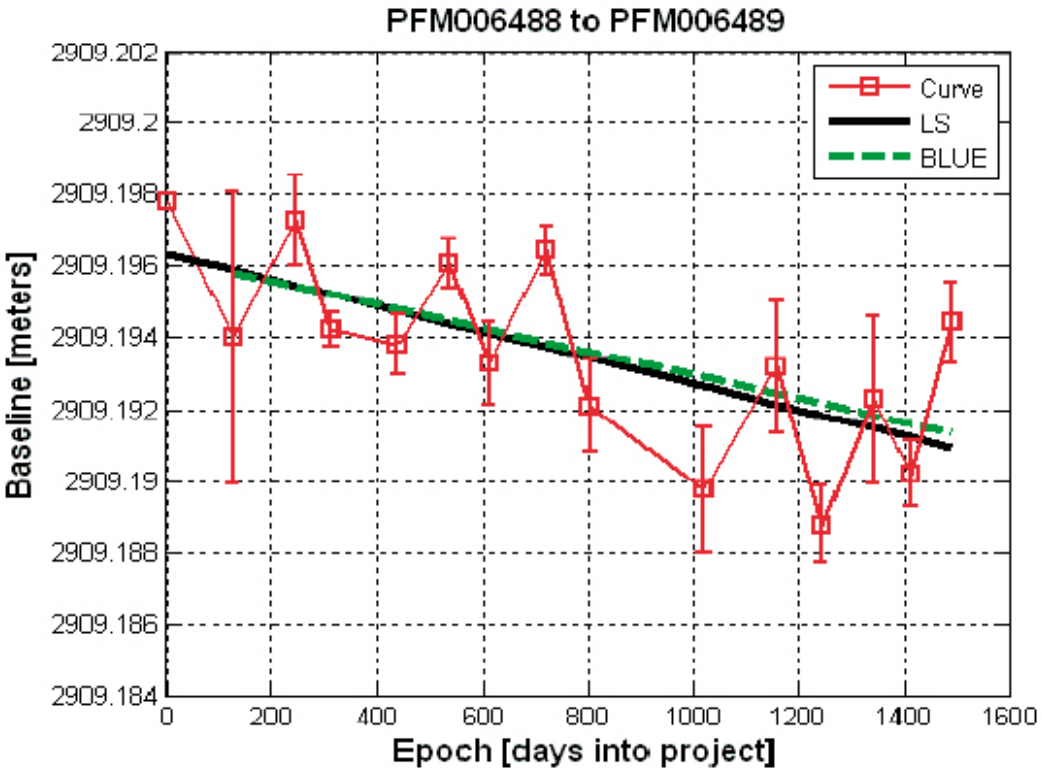

Figure A4-40. *Baseline variations between the stations PFM006488 and PFM006489. For the linear trends the black solid line is the LS estimate and the dashed-green is the BLUE using RMS.*

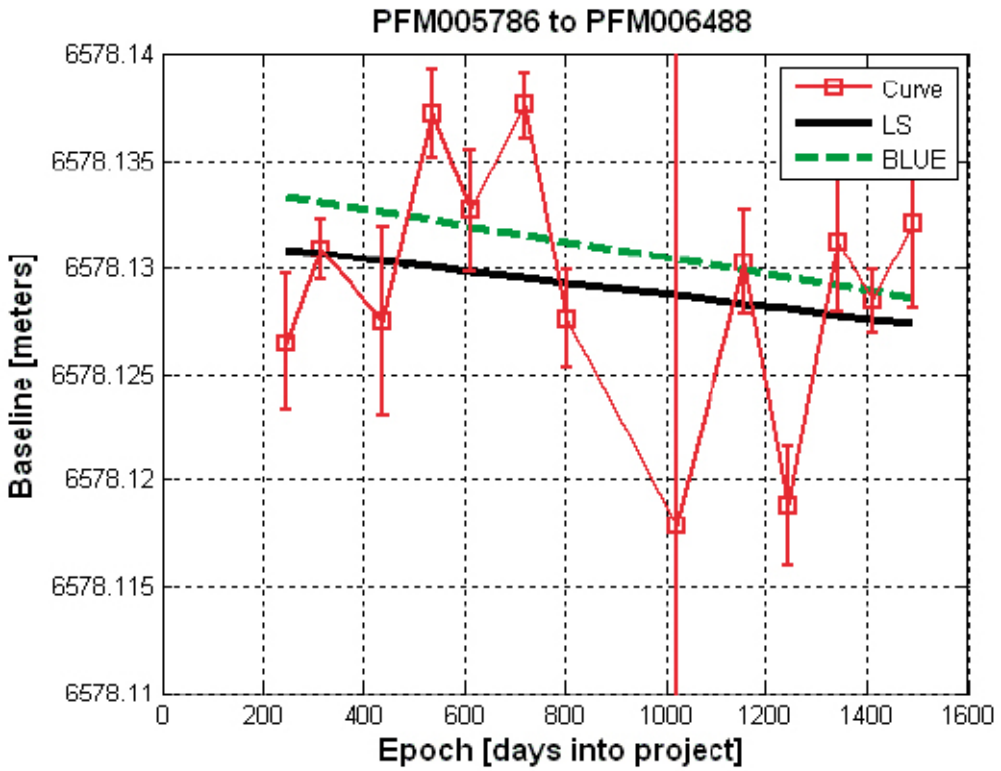

Figure A4-41. *Baseline variations between the stations PFM006488 and PFM005786. For the linear trends the black solid line is the LS estimate and the dashed-green is the BLUE using RMS.*

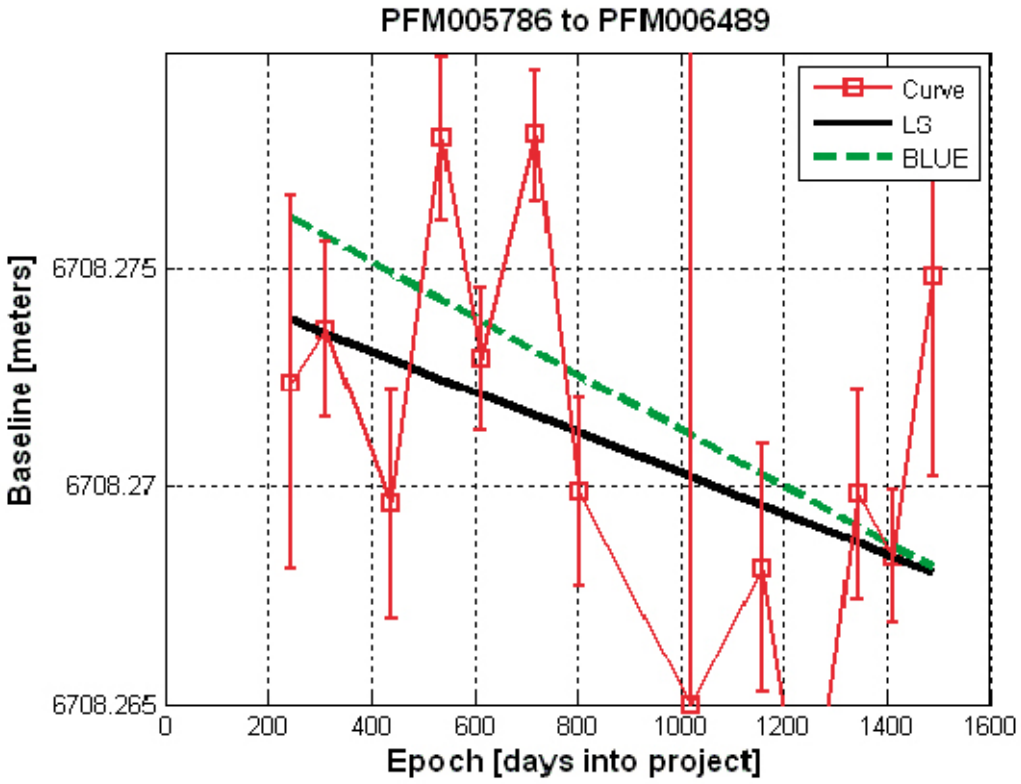

Figure A4-42. *Baseline variations between the stations PFM006489 and PFM005786. For the linear trends the black solid line is the LS estimate and the dashed-green is the BLUE using RMS.*

Appendix 5

Comparison of true data and AR predictions for the baseline variations

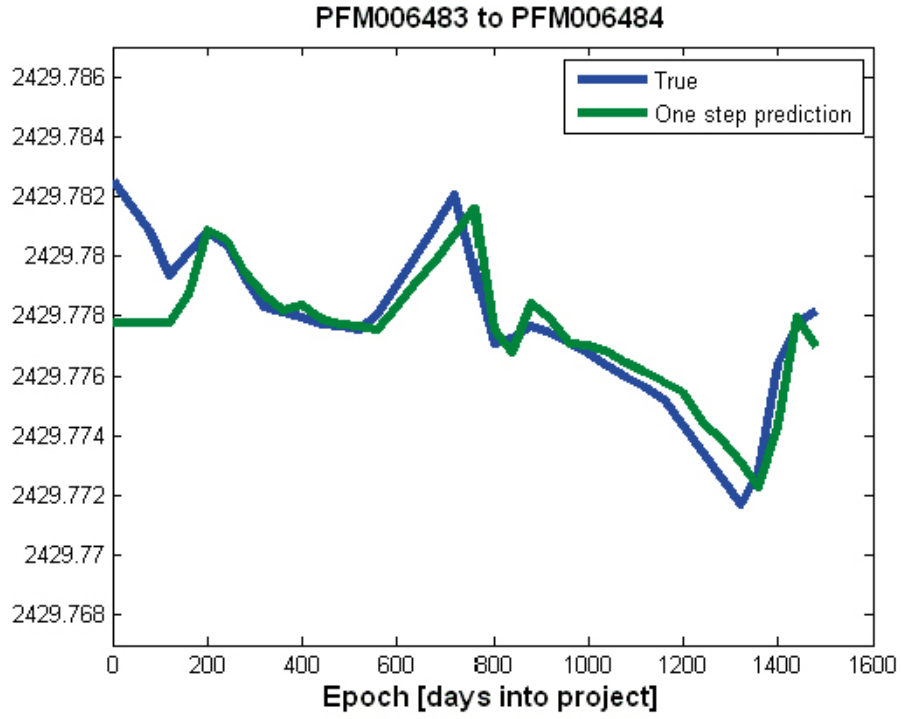

Figure A5-1. *Comparison of true data and AR predictions for the baseline variations between the stations PFM006483 and PFM006484.*

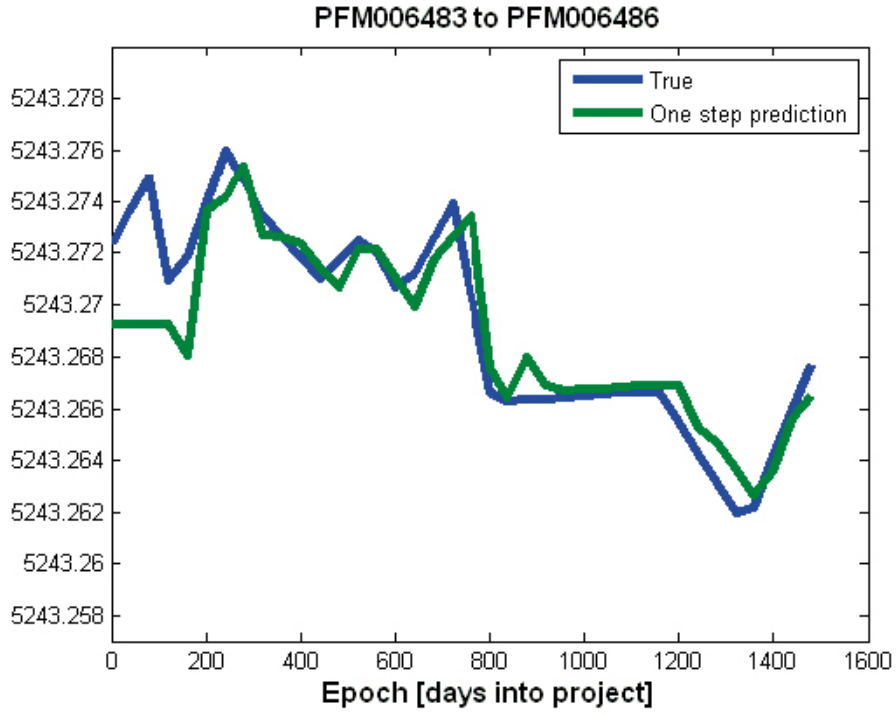

Figure A5-2. *Comparison of true data and AR predictions for the baseline variations between the stations PFM006483 and PFM006486.*

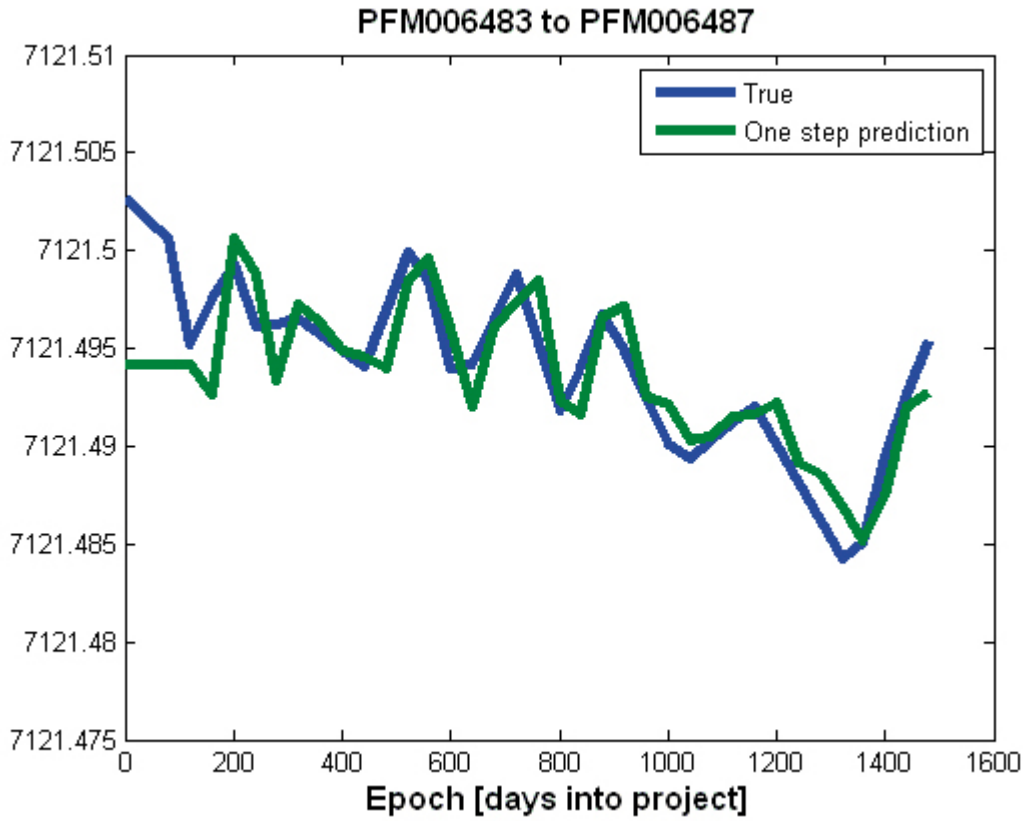

Figure A5-3. *Comparison of true data and AR predictions for the baseline variations between the stations PFM006483 and PFM006487.*

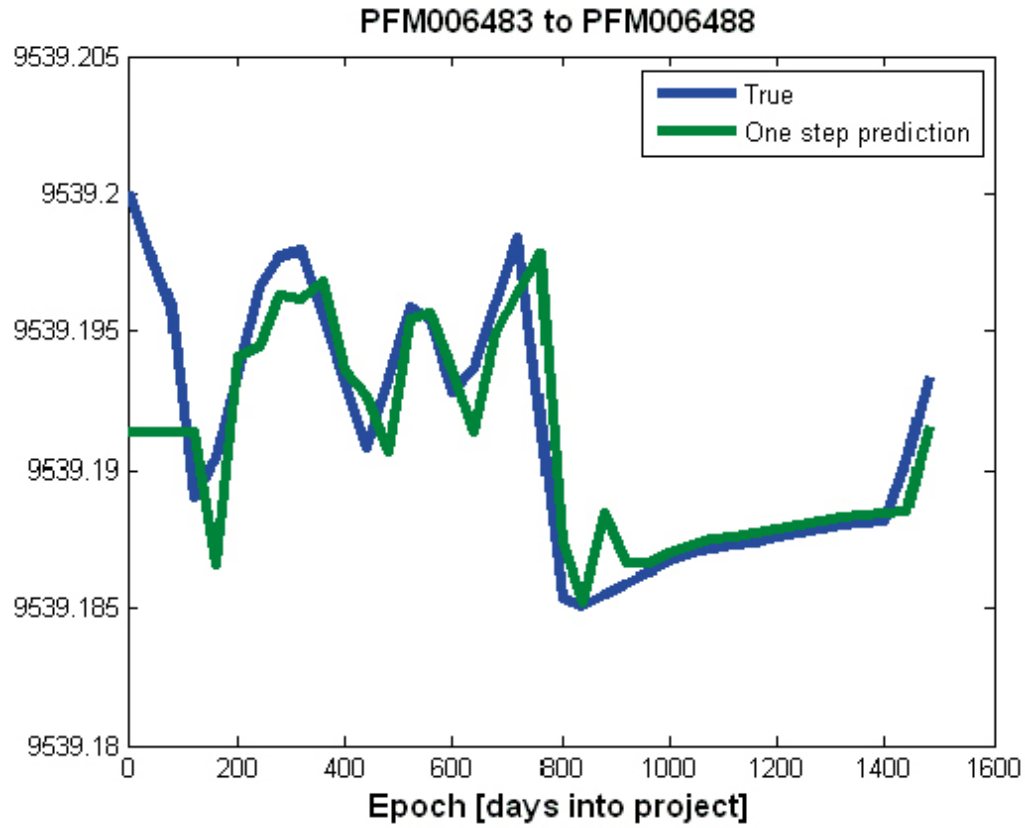

Figure A5-4. *Comparison of true data and AR predictions for the baseline variations between the stations PFM006483 and PFM006488.*

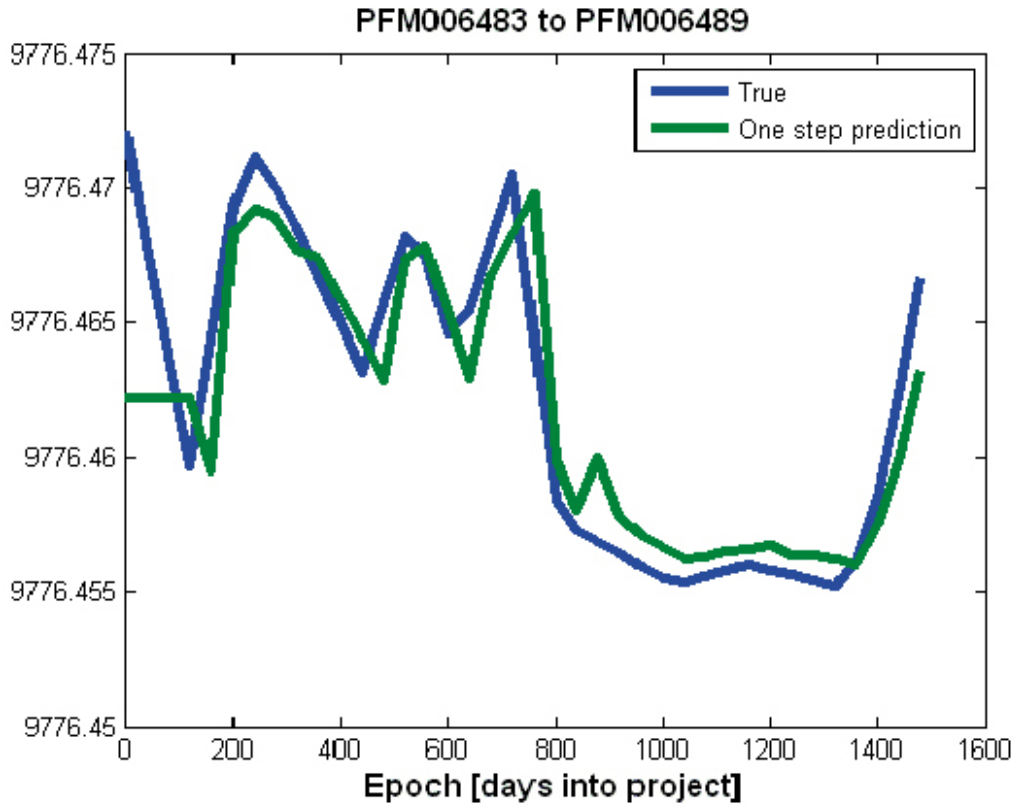

Figure A5-5. *Comparison of true data and AR predictions for the baseline variations between the stations PFM006483 and PFM006489.*

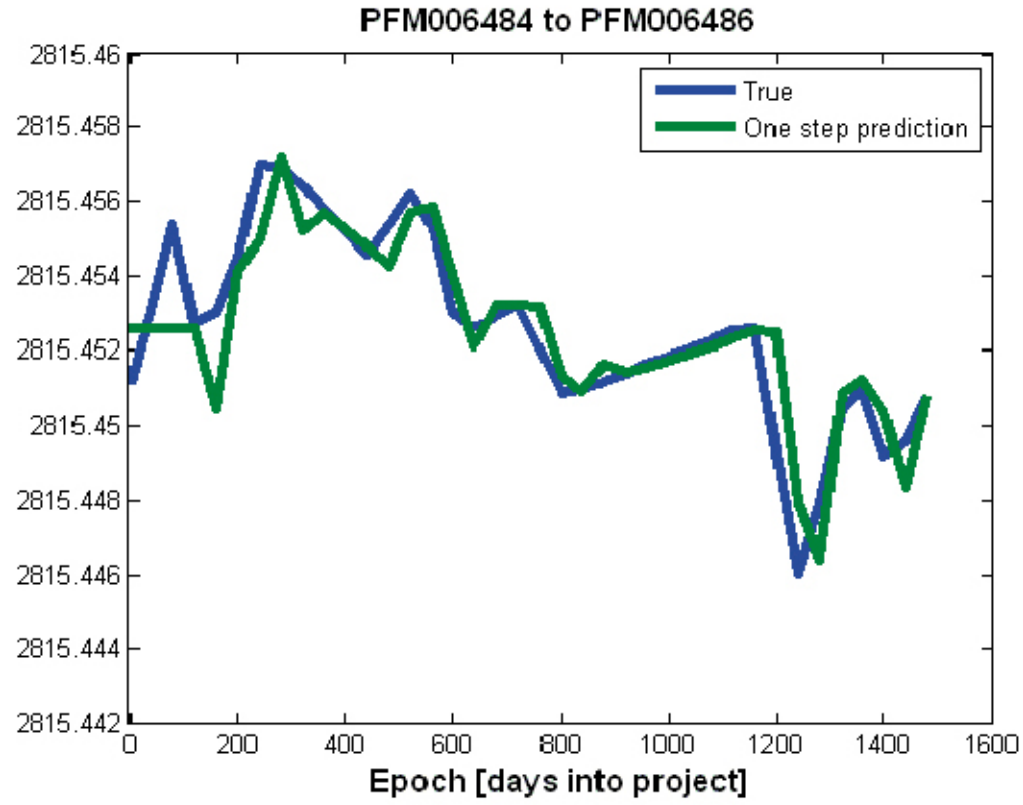

Figure A5-6. *Comparison of true data and AR predictions for the baseline variations between the stations PFM006484 and PFM006486.*

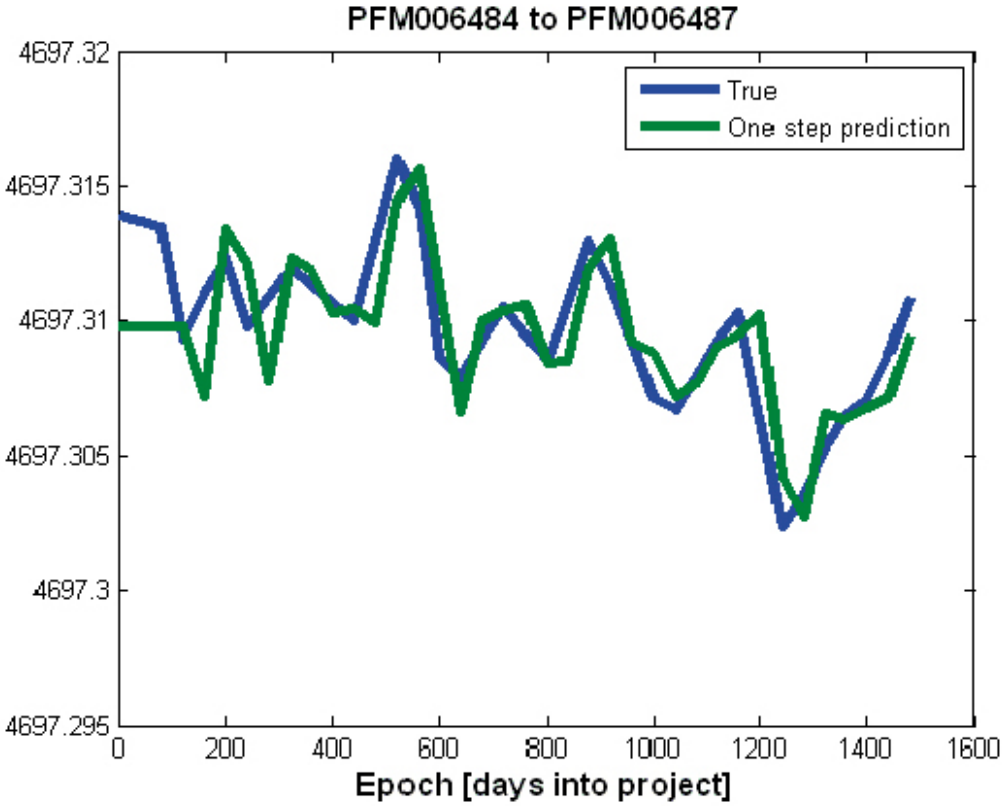

Figure A5-7. *Comparison of true data and AR predictions for the baseline variations between the stations PFM006484 and PFM006487.*

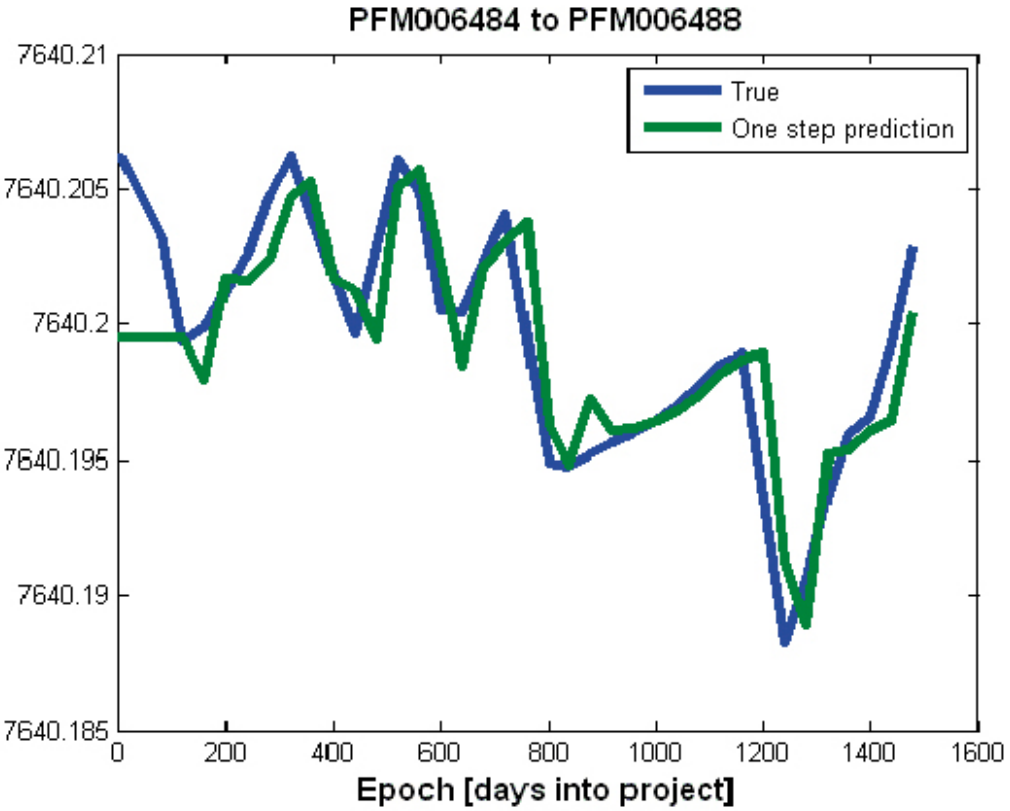

Figure A5-8. *Comparison of true data and AR predictions for the baseline variations between the stations PFM006484 and PFM006488.*

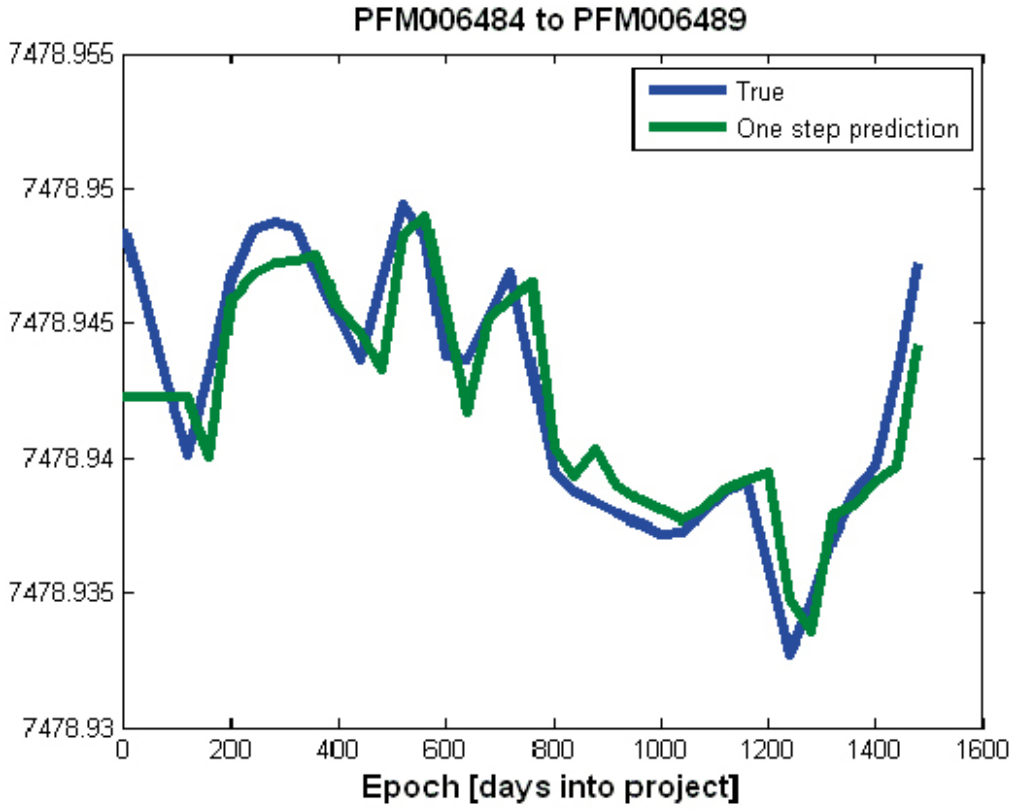

Figure A5-9. *Comparison of true data and AR predictions for the baseline variations between the stations PFM006484 and PFM006489.*

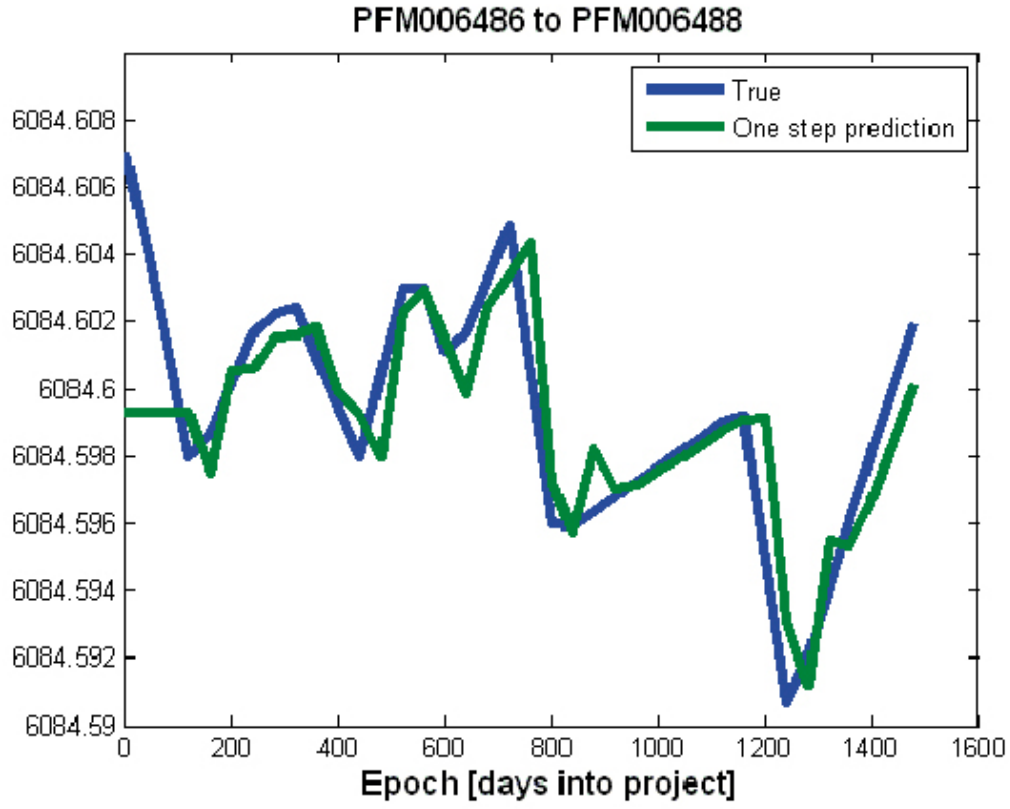

Figure A5-10. *Comparison of true data and AR predictions for the baseline variations between the stations PFM006486 and PFM006488.*

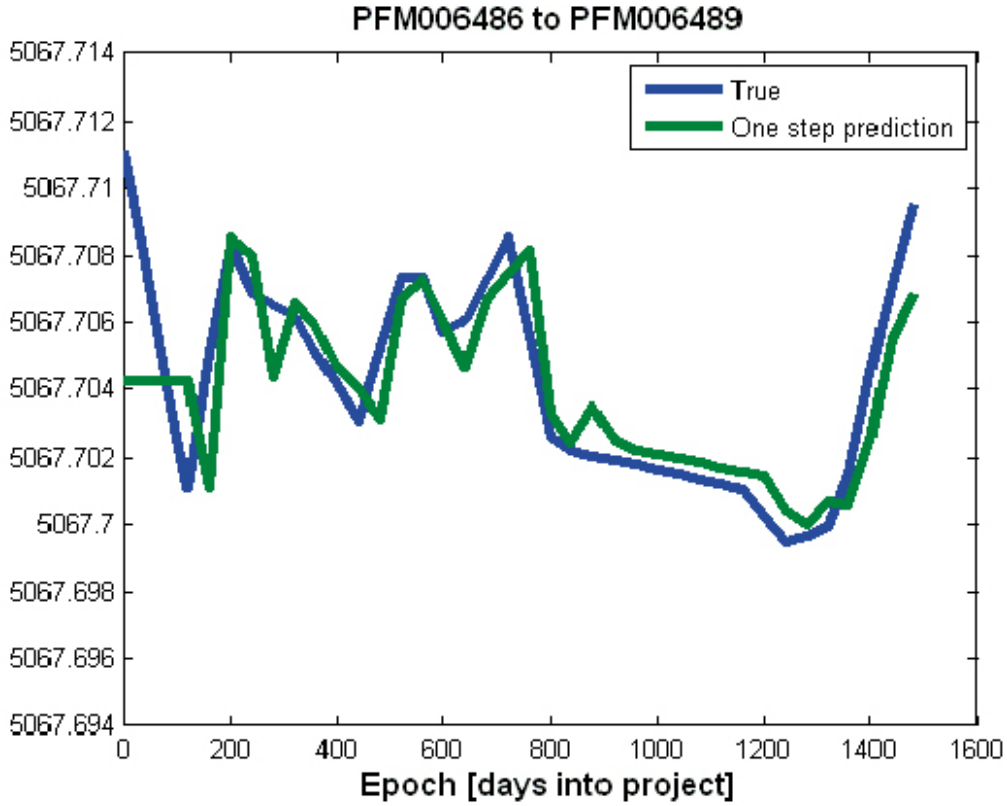

Figure A5-11. *Comparison of true data and AR predictions for the baseline variations between the stations PFM006486 and PFM006489.*

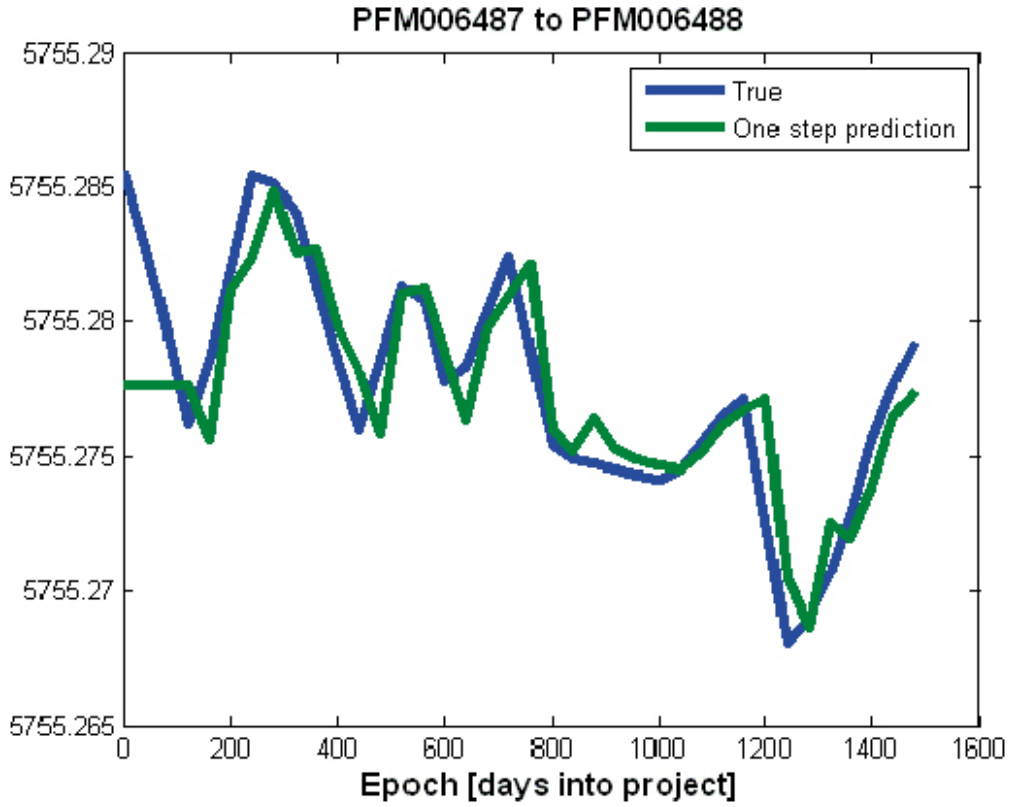

Figure A5-12. *Comparison of true data and AR predictions for the baseline variations between the stations PFM006487 and PFM006488.*

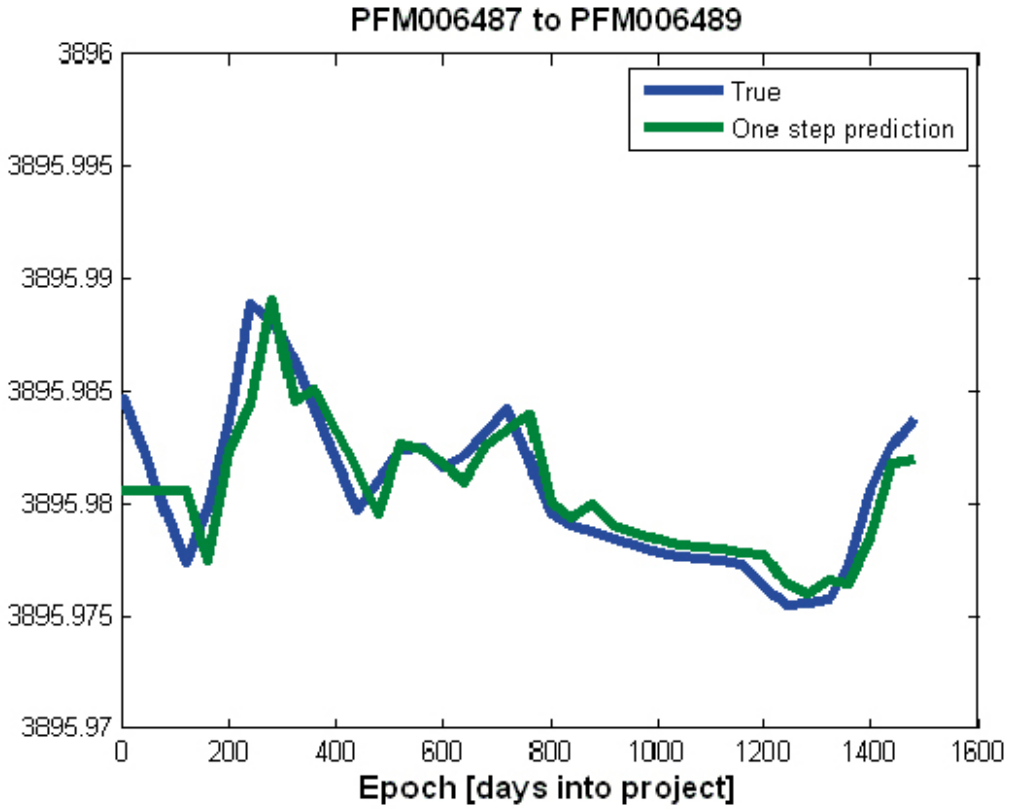

Figure A5-13. *Comparison of true data and AR predictions for the baseline variations between the stations PFM006487-PFM006489.*

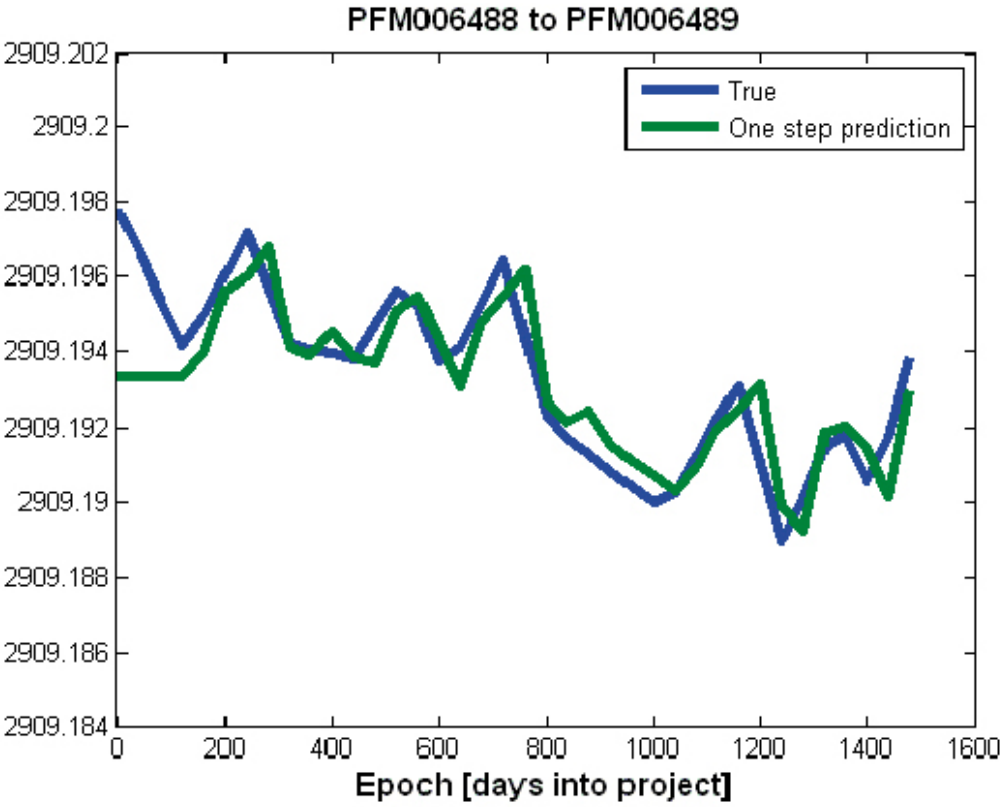

Figure A5-14. *Comparison of true data and AR predictions for the baseline variations between the stations PFM006488-PFM006489.*

Appendix 6

Comparison of the true data and ARMA predictions for the baseline variations

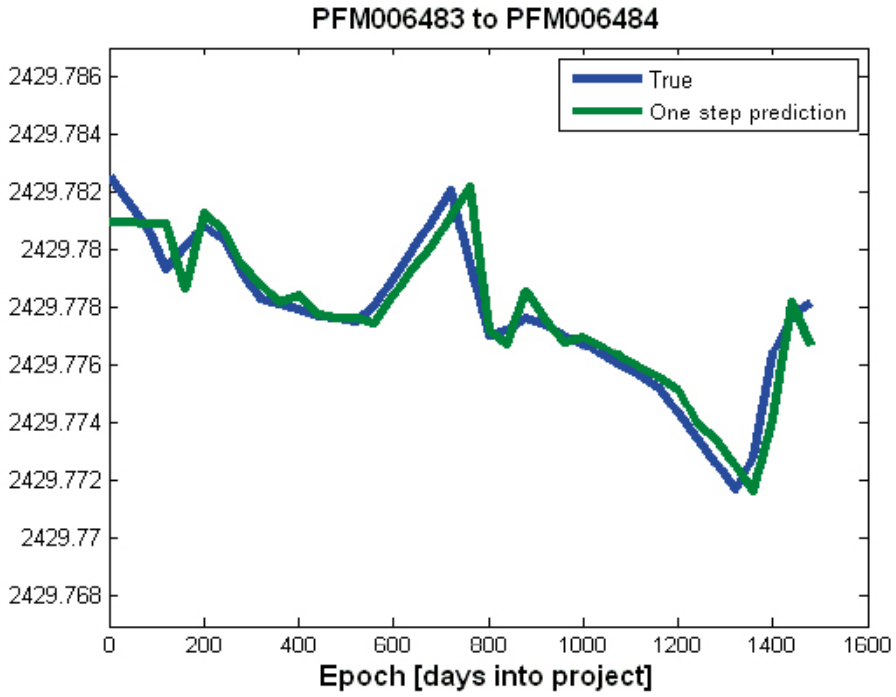

Figure A6-1. *Comparison of true data and ARMA predictions for the baseline variations between the stations PFM006483 and PFM006484.*

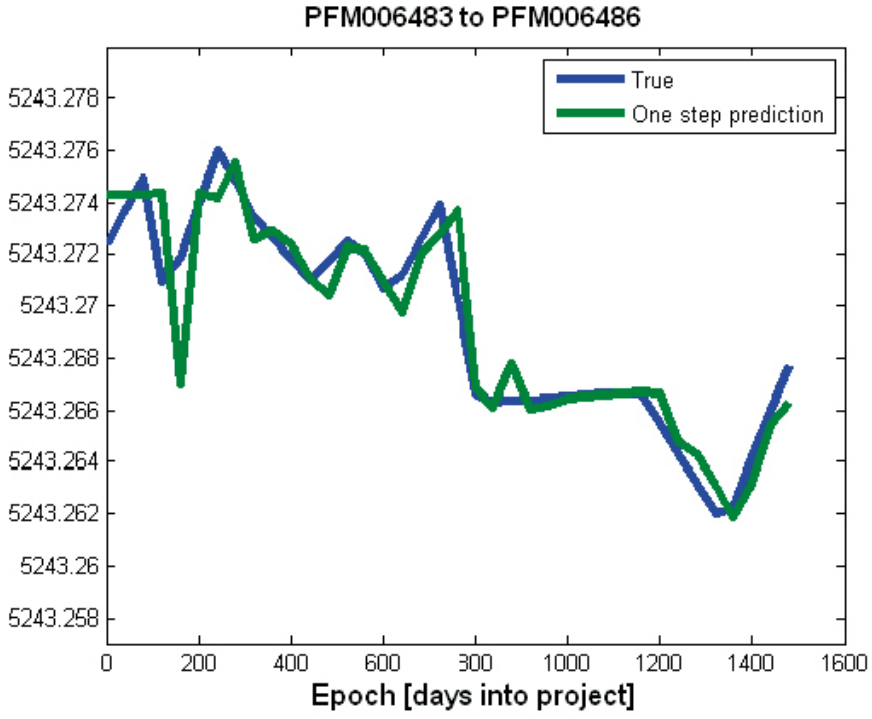

Figure A6-2. *Comparison of true data and ARMA predictions for the baseline variations between the stations PFM006483 and PFM006486.*

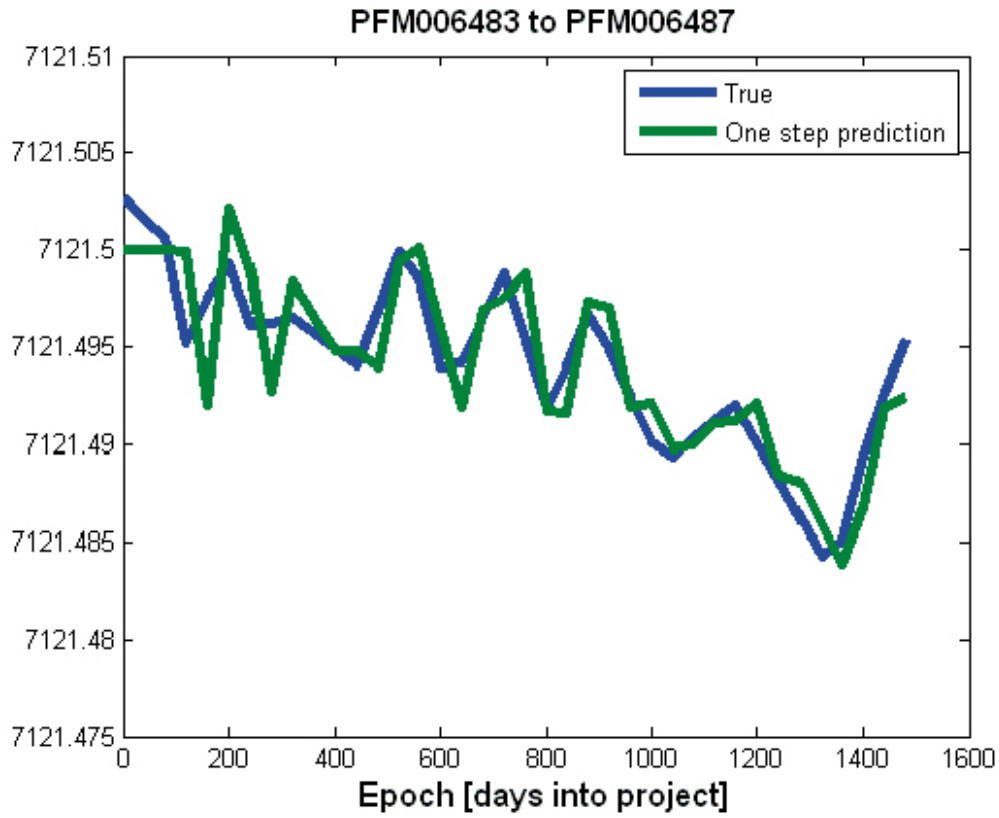

Figure A6-3. *Comparison of true data and ARMA predictions for the baseline variations between the stations PFM006483 and PFM006487.*

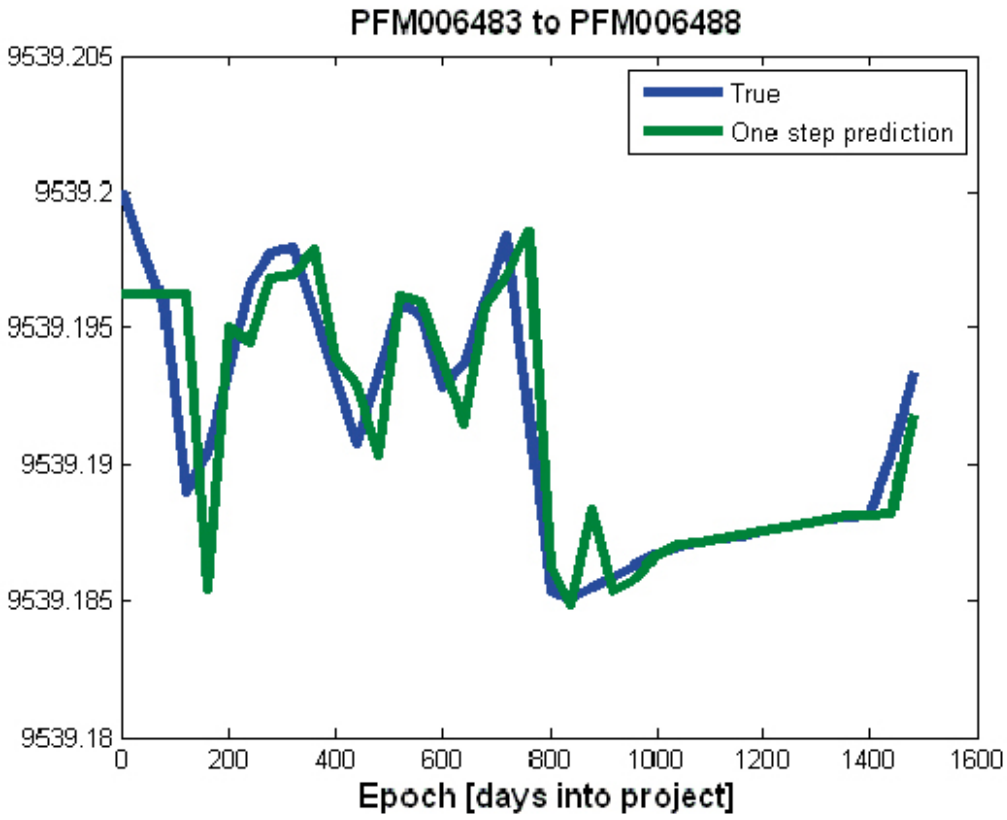

Figure A6-4. *Comparison of true data and ARMA predictions for the baseline variations between the stations PFM006483 and PFM006488.*

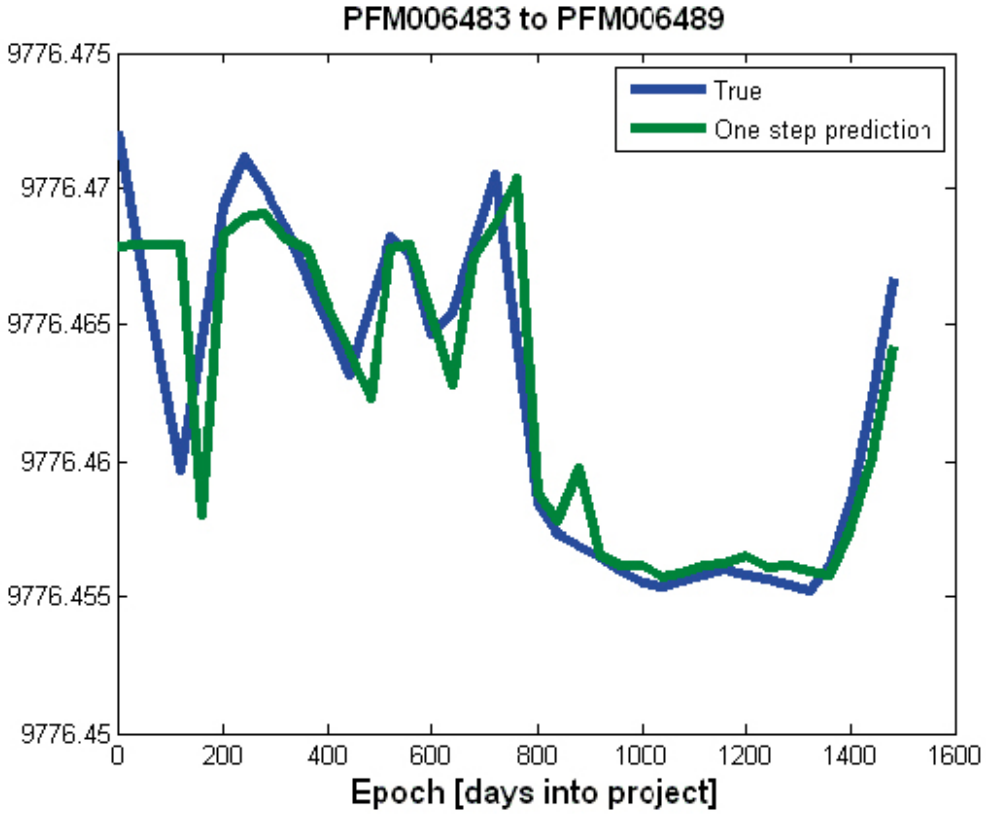

Figure A6-5. *Comparison of true data and ARMA predictions for the baseline variations between the stations PFM006483 and PFM006489.*

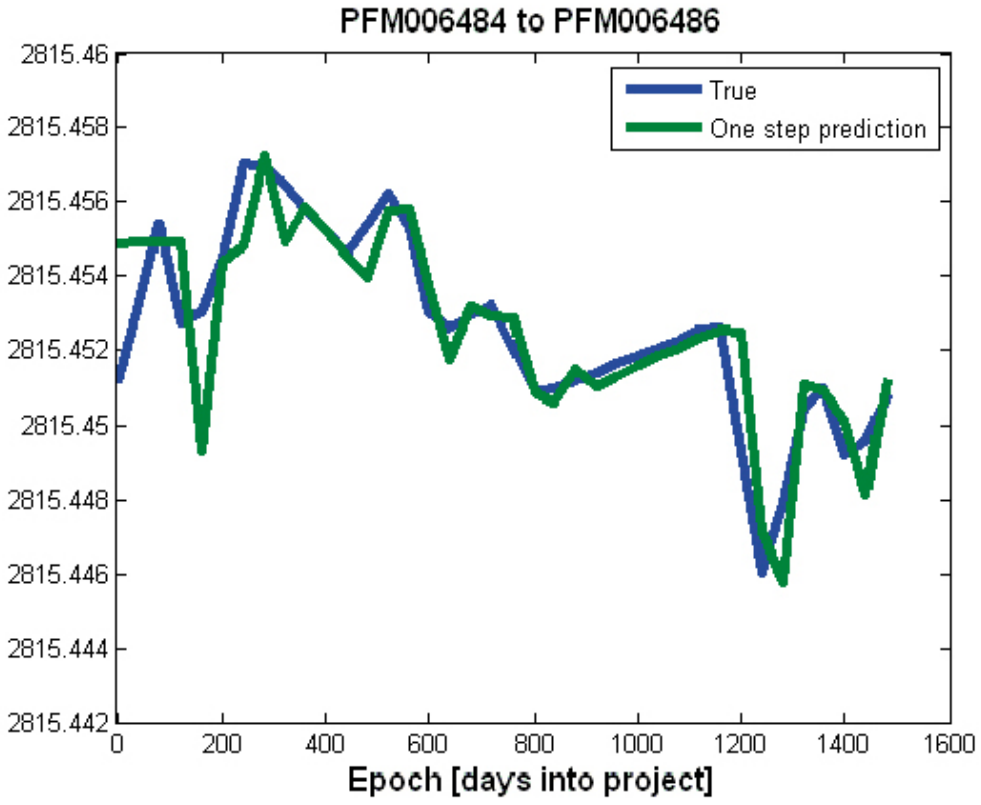

Figure A6-6. *Comparison of true data and ARMA predictions for the baseline variations between the stations PFM006484 and PFM006486.*

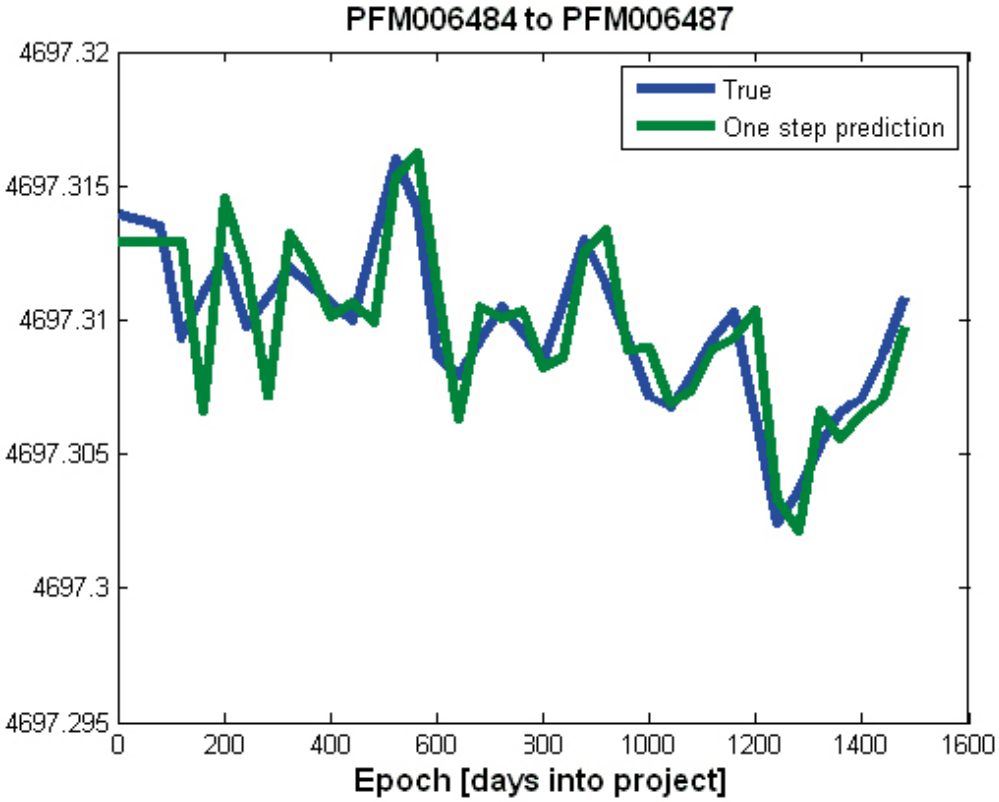

Figure A6-7. *Comparison of true data and ARMA predictions for the baseline variations between the stations PFM006484 and PFM006487.*

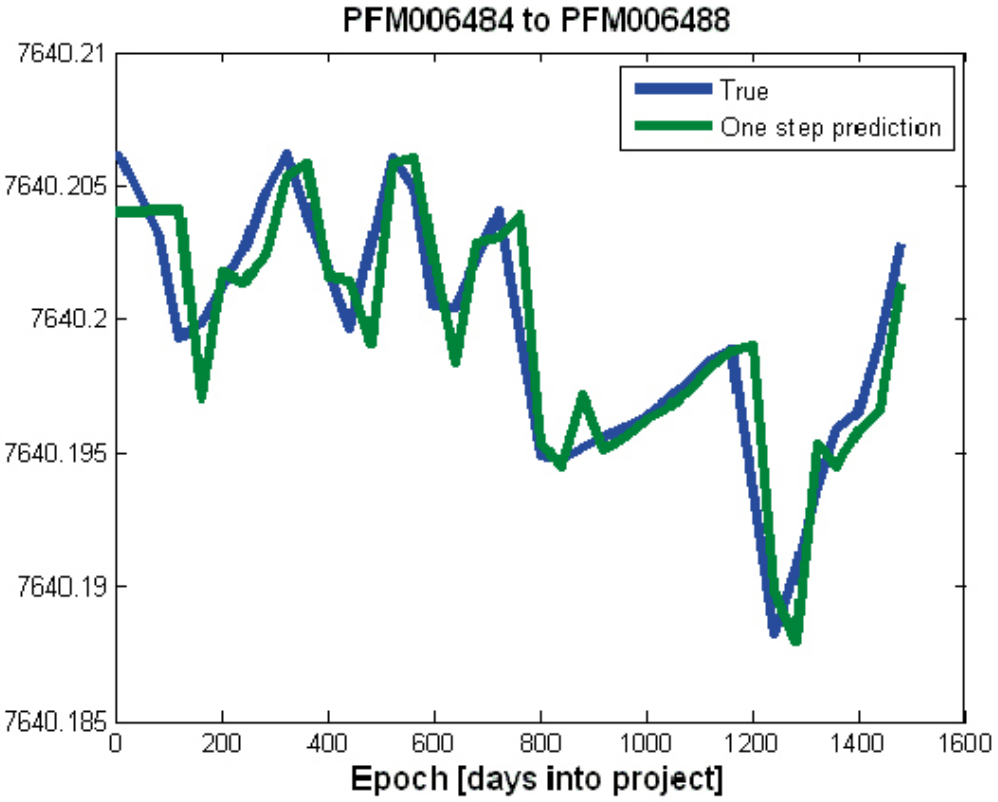

Figure A6-8. *Comparison of true data and ARMA predictions for the baseline variations between the stations PFM006484 and PFM006488.*

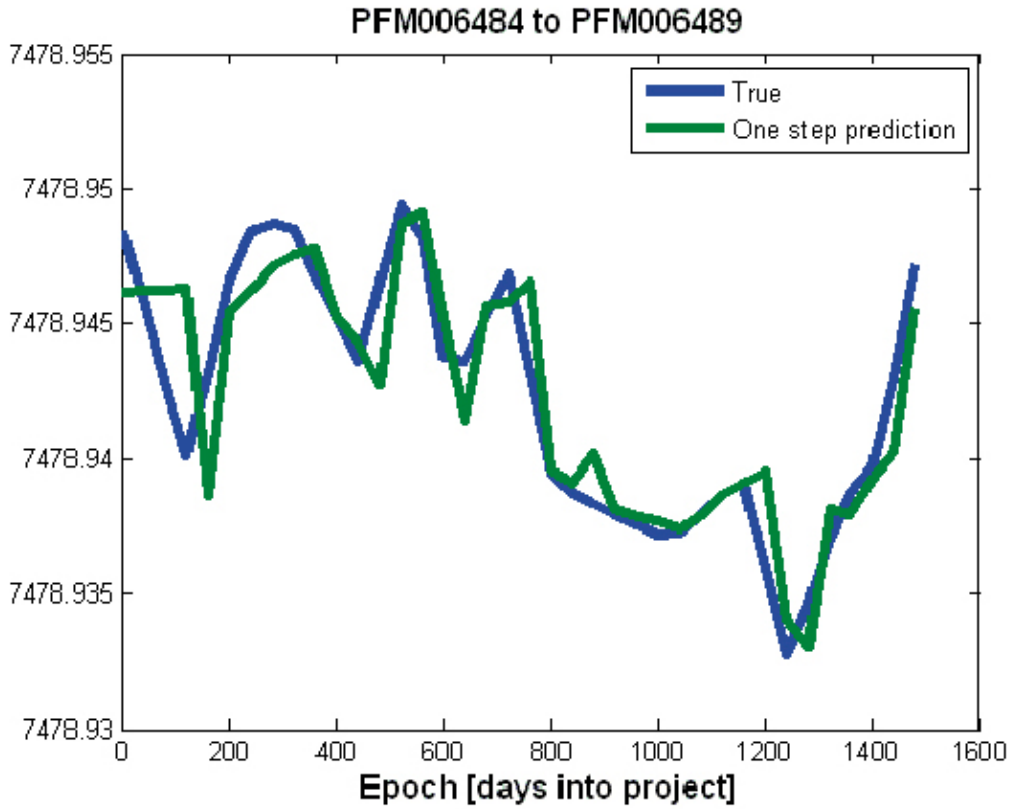

Figure A6-9. *Comparison of true data and ARMA predictions for the baseline variations between the stations PFM006484 and PFM006489.*

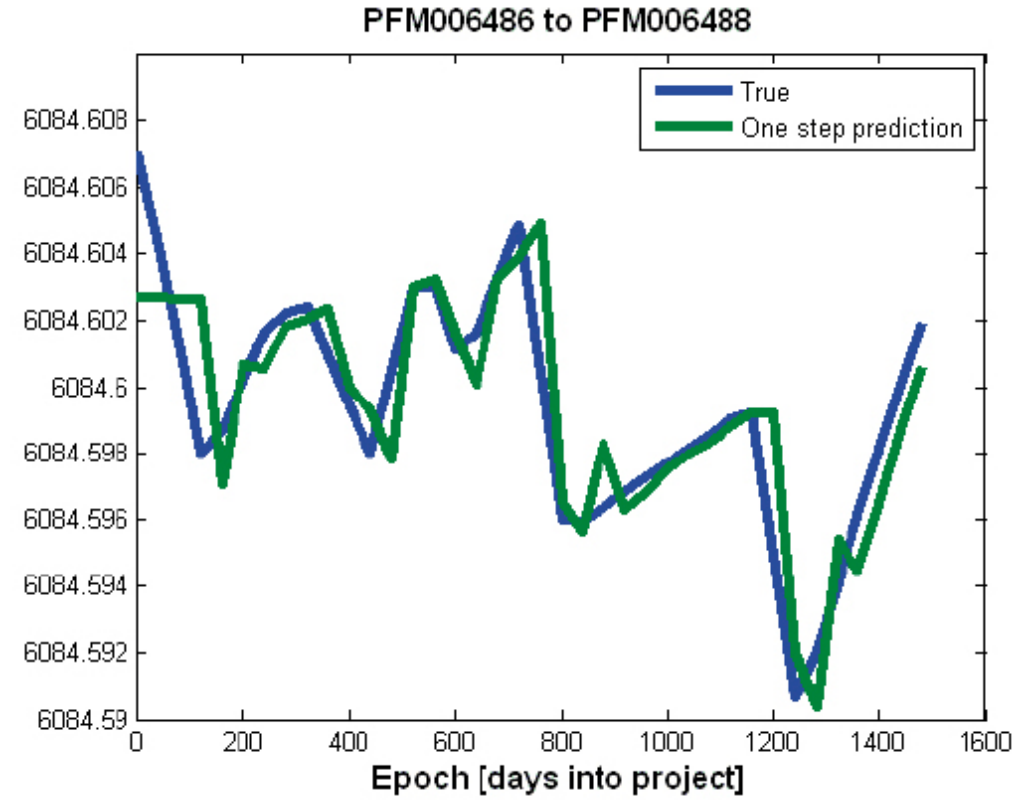

Figure A6-10. *Comparison of true data and ARMA predictions for the baseline variations between the stations PFM006486 and PFM006488.*

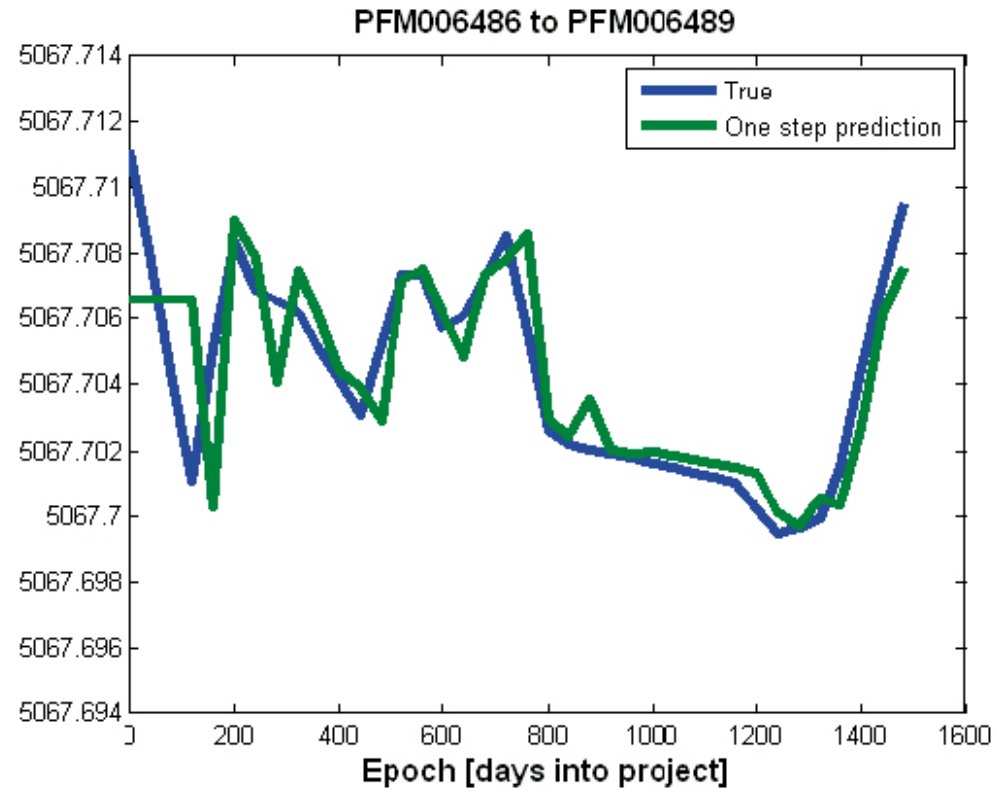

Figure A6-11. *Comparison of true data and ARMA predictions for the baseline variations between the stations PFM006486 and PFM006489.*

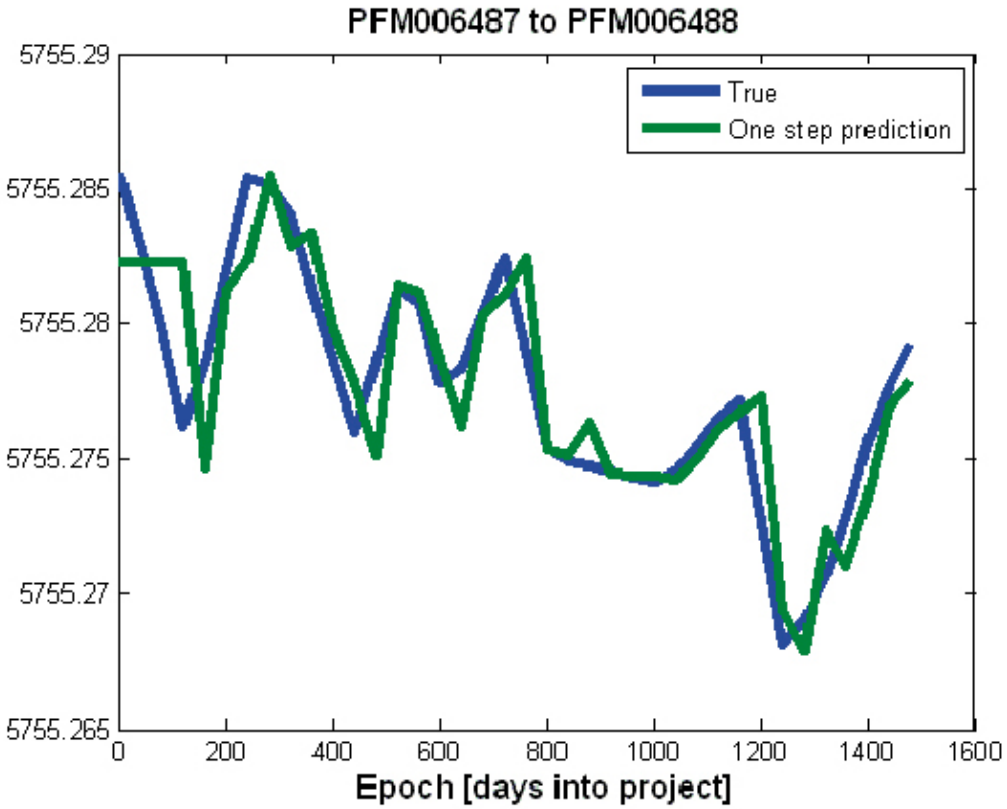

Figure A6-12. *Comparison of true data and ARMA predictions for the baseline variations between the stations PFM006487 and PFM006488.*

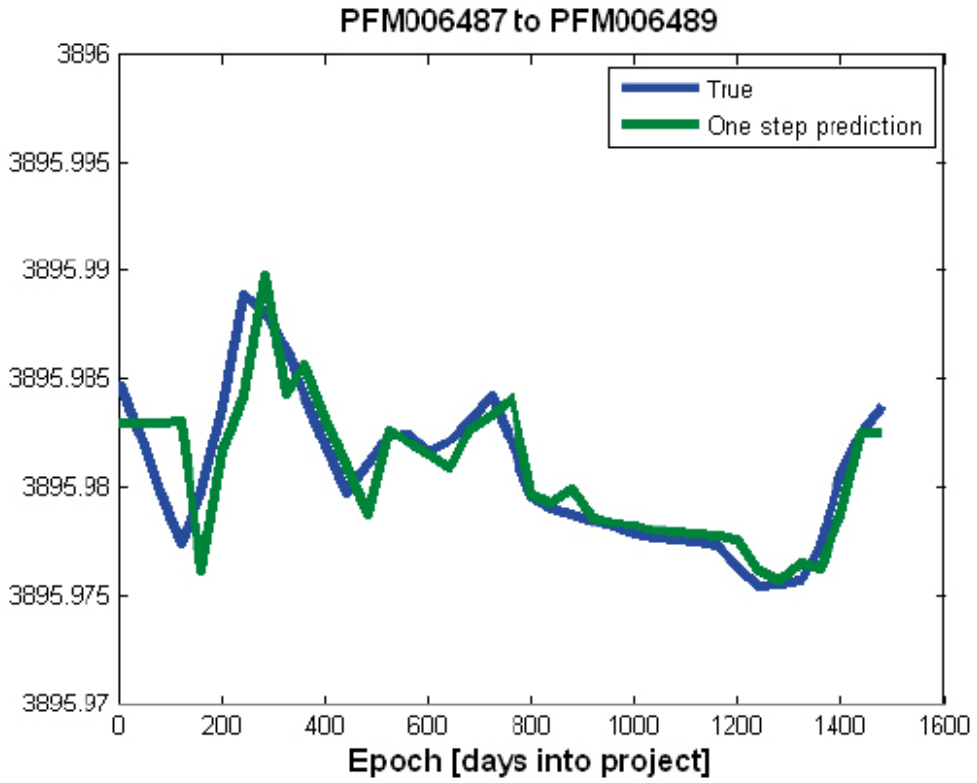

Figure A6-13. *Comparison of true data and ARMA predictions for the baseline variations between the stations PFM006487 and PFM006489.*

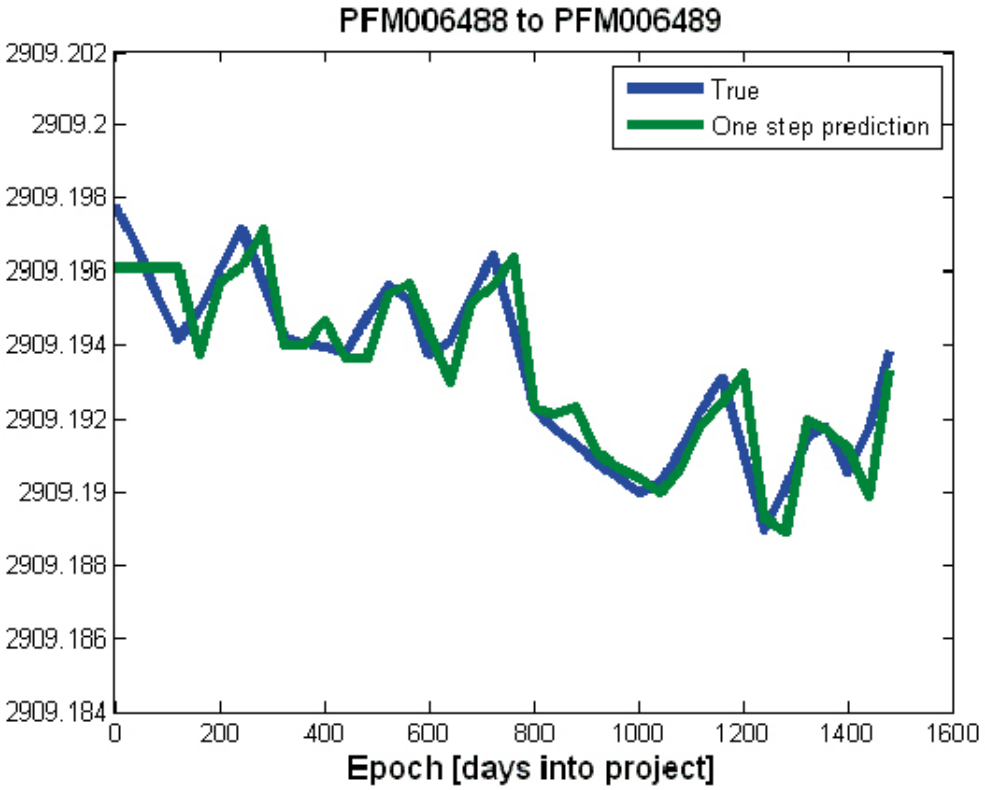

Figure A6-14. *Comparison of true data and ARMA predictions for the baseline variations between the stations PFM006488 and PFM006489.*